

NASA TECHNICAL
REPORT



NASA TR R-428

NASA TR R-428

EXTENSION OF LEADING-EDGE-SUCTION
ANALOGY TO WINGS WITH SEPARATED FLOW
AROUND THE SIDE EDGES AT SUBSONIC SPEEDS

by John E. Lamar

*Langley Research Center
Hampton, Va. 23665*



1. Report No. NASA TR R-428	2. Government Accession No.	3. Recipient's Catalog No.	
4. Title and Subtitle EXTENSION OF LEADING-EDGE-SUCTION ANALOGY TO WINGS WITH SEPARATED FLOW AROUND THE SIDE EDGES AT SUBSONIC SPEEDS		5. Report Date October 1974	
		6. Performing Organization Code	
7. Author(s) John E. Lamar		8. Performing Organization Report No. L-9460	
		10. Work Unit No. 501-06-04-01	
9. Performing Organization Name and Address NASA Langley Research Center Hampton, Va. 23665		11. Contract or Grant No.	
		13. Type of Report and Period Covered Technical Report	
12. Sponsoring Agency Name and Address National Aeronautics and Space Administration Washington, D.C. 20546		14. Sponsoring Agency Code	
		15. Supplementary Notes	
16. Abstract <p>This paper presents a method for determining the lift, drag, and pitching moment for wings which have separated flow at the leading and side edges with subsequently reattached flow downstream and inboard. Limiting values of the contribution to lift of the side-edge reattached flow are determined for rectangular wings. The general behavior of this contribution is computed for rectangular, cropped-delta, cropped-diamond, and cropped-arrow wings. Comparisons of the results of the method and experiment indicate reasonably good correlation of the lift, drag, and pitching moment for a wide planform range. The agreement of the method with experiment was as good as, or better than, that obtained by other methods. The procedure is computerized and is available from COSMIC as NASA Langley computer program A0313.</p>			
17. Key Words (Suggested by Author(s)) Suction analogy Reattached flow Vortex flow Cropped wings		18. Distribution Statement Unclassified - Unlimited STAR Category 01	
19. Security Classif. (of this report) Unclassified	20. Security Classif. (of this page) Unclassified	21. No. of Pages 71	22. Price* \$3.75

CONTENTS

	Page
SUMMARY	1
INTRODUCTION	1
SYMBOLS	2
THEORETICAL DEVELOPMENT	5
BEHAVIOR OF $K_{v,se}$	11
Unswep Wings	11
Straight trailing edge	11
Notched trailing edge	13
Swept Wings	14
Cropped deltas	14
Cropped diamonds and arrows	15
MODELS AND TEST CONDITIONS	16
EFFECT OF EDGE SHAPING ON RECTANGULAR-WING RESULTS	16
COMPARISONS WITH EXPERIMENTS	17
Unswep Wings	17
Straight trailing edge	17
Notched trailing edge	18
Swept Cropped Wings	18
Taper-ratio variation (deltas)	18
Trailing-edge sweep variation (diamond and arrow)	19
Arrow wing	19
COMPARISONS WITH OTHER THEORIES	19
Other Theories	19
General	19
Bollay	20
Flax	20
Gersten	20
Belotserkovskii	21
Bradley	21
Comparisons	21
Zero Aspect-Ratio Limit	22
CONCLUSIONS	22

	Page
REFERENCES	24
TABLE	26
FIGURES.	27

EXTENSION OF LEADING-EDGE-SUCTION ANALOGY TO WINGS
WITH SEPARATED FLOW AROUND THE SIDE EDGES
AT SUBSONIC SPEEDS

By John E. Lamar
Langley Research Center

SUMMARY

This paper presents a method of determining the lift, drag, and pitching moment for wings which have reattached flow around the leading and side edges. The method is an extension of the leading-edge-suction analogy of Polhamus applied to the side edges. The value of the term associated with the lift contribution of the reattached flow from the side edges $K_{v,se}$ has been found to exceed that of the leading edge for rectangular wings of aspect ratio less than 2. Limiting values of $K_{v,se}$ have been determined for rectangular wings. Comparisons of the results of this method with experiment indicate reasonably good correlation of the lift, drag, and pitching moment for a wide planform range. The agreement of the method with experiment was as good as, or better than, that obtained by other methods.

INTRODUCTION

Many current and proposed aircraft and missiles designed for high-speed flight employ highly sweptback and tapered low-aspect-ratio wings with sharp or thin edges. These planforms exhibit flow separation along the leading and side edges followed by subsequent reattachment downstream or inboard, respectively, over a large angle-of-attack and Mach number range. However, the effect of this separated-flow (commonly termed vortex flow) phenomenon is more important at subsonic speeds because of its larger contribution to the total aerodynamic characteristics. Polhamus in references 1, 2, and 3 has shown that, for a variety of pointed-tips planforms and Mach numbers, the contribution of the leading-edge vortex to the lift and drag can be accounted for by what is termed the leading-edge-suction analogy. The application of this analogy requires only that the attached-flow leading-edge suction, available from inviscid theory, be known accurately.

It is evident that the separated flow around the tips or side edges of swept and unswept lifting surfaces has essentially the same behavior as that around the highly swept leading edge. Consequently, it should be possible to predict the effect of side-edge

vortices on the aerodynamic characteristics of low-aspect-ratio planforms by an analysis similar to those used to treat the leading edge. The purpose of the present paper will be to detail how one such extension to the leading-edge-suction analogy can be effected. The one new element required in this extension is the attached-flow side-edge suction force and its derivation is presented.

Total-force and total-moment predictions, including both the leading- and side-edge suction-force contributions, have been made for a variety of planform shapes and are compared with previously published data and new subsonic wind-tunnel data. Also, a discussion of some other methods which attempt such predictions (refs. 4 to 11) will be given and comparisons with the present technique are made where possible.

SYMBOLS

Values are given in both SI Units and U.S. Customary Units. The measurements and calculations were made in U.S. Customary Units.

\mathcal{AR}	aspect ratio
$B_j(x_i)$	coefficient of $\eta^{2(j-1)}$ at x_i of the spanwise curve fit of equation (12)
b	span, cm (in.)
C_D	drag coefficient, $\frac{\text{Drag}}{q_\infty S_{\text{ref}}}$
$C_{D,0}$	experimental value of drag coefficient at $C_L = 0$
ΔC_D	drag coefficient due only to lift, $C_D - C_{D,0}$
C_L	lift coefficient, $\frac{\text{Lift}}{q_\infty S_{\text{ref}}}$
$C_{L\alpha} = \frac{\partial C_L}{\partial \alpha}$	
C_m	pitching-moment coefficient about the reference point, unless otherwise stated it is located at $\frac{c_{\text{ref}}}{4}$, $\frac{\text{Pitching moment}}{q_\infty S_{\text{ref}} c_{\text{ref}}}$
C_N	normal-force coefficient, $\frac{\text{Normal force}}{q_\infty S_{\text{ref}}}$

- c streamwise chord, cm (in.)
- $c(\eta)$ streamwise half chord at η , cm (in.)
- $d(\eta)$ x-location of local midchord with respect to half root chord, cm (in.)
- F tip suction force from one side edge, N (lbf)
- $G(x)$ defined by equation (2), $m^{3/2}/\text{sec}$ ($\text{ft}^{3/2}/\text{sec}$)
- j index ranging from 1 to p
- $$K_p = \frac{\partial(C_{N,p})}{\partial(\sin \alpha \cos \alpha)}$$
- $$K_{v,le} = \frac{\partial \left(\frac{2 \text{ Leading-edge suction force from one side}}{q_\infty S_{ref}} \right)}{\partial \sin^2 \alpha}$$
- $$K_{v,se} = \frac{\partial \left(\frac{2 \text{ Tip suction force from one side edge}}{q_\infty S_{ref}} \right)}{\partial \sin^2 \alpha}$$
- $$K_{v,tot} = \beta K_{v,le} + K_{v,se}$$
- M Mach number of free stream
- N maximum number of chord loadings in modified Multhopp solution
- n index ranging from 0 to N - 1
- $$\frac{q_n(\eta)}{q_\infty}$$
- coefficient of chordal loading function in modified Multhopp solution, m (ft)
- q_∞ free-stream dynamic pressure, N/m^2 (lbf/ft^2)
- R Reynolds number
- S_{ref} reference area, m^2 (ft^2)

$s(x)$	distributed edge suction force (see eq. (1)), N/m (lbf/ft)
U	free-stream velocity, m/sec (ft/sec)
u	induced velocity in the X-direction at a point (x,y), m/sec (ft/sec)
v	induced velocity in the Y-direction of a point (x,y), m/sec (ft/sec)
x,y	distances from a coordinate origin located at the leading-edge apex; x positive downstream and y positive toward right wing tip
Δx	distance along tip chord, cm (in.)
α	angle of attack, degrees
$\beta = \sqrt{1 - M^2}$	
Γ	accumulated circulation at a point (x,y) (see eq. (5)), m ² /sec (ft ² /sec)
γ	distributed bound vorticity at a point (x,y) (see eq. (6)), m/sec (ft/sec)
δ	distributed trailing vorticity at a point (x,y) (see eq. (4)), m/sec (ft/sec)
η	nondimensional spanwise variable, $2y/b$
θ	chordwise angular variable (see eq. (9)), degrees
θ_{x_i}	θ value which yields x_i in equation (9)
Λ	leading-edge sweep angle, positive for sweepback, degrees
λ	taper ratio, c_t/c_r
ξ	fraction of local chord
ρ	density, kg/m ³ (slugs/ft ³)
Ω	trailing-edge sweep angle, positive for sweepback, degrees

Subscripts:

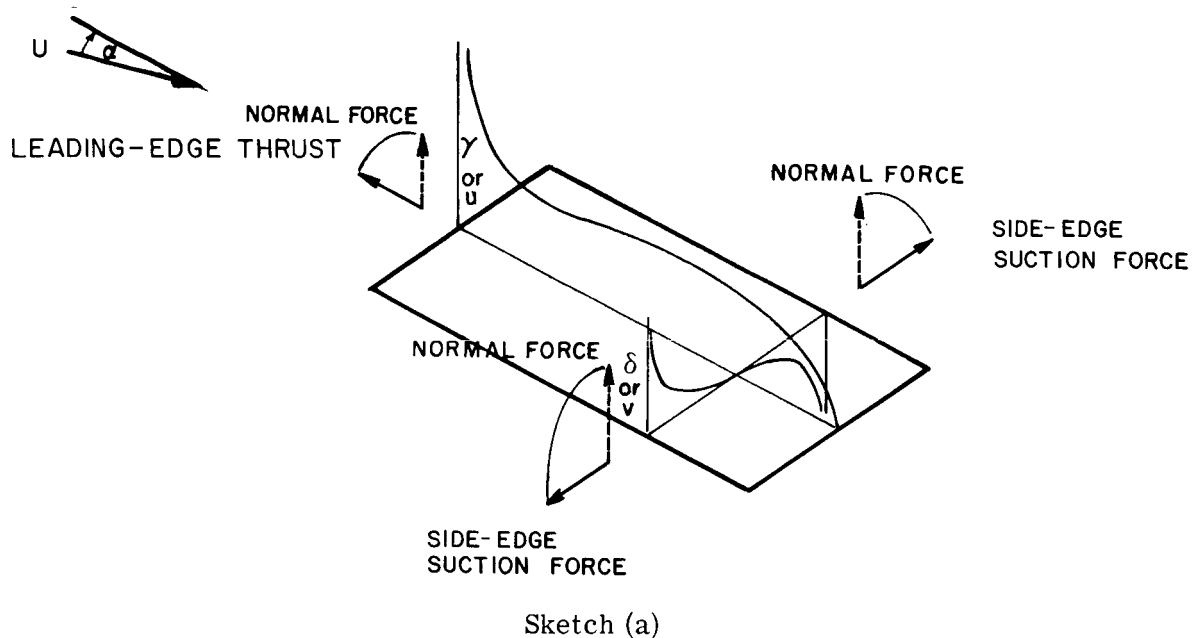
c	centroid
i	particular item of location
le	leading edge
n	notch
p	potential or attached flow
r	root
ref	reference
se	side edge
t	tip
te	trailing edge
tot	total
vle	vortex effect at the leading edge
vse	vortex effect at the side edge

THEORETICAL DEVELOPMENT

The concept embodied in the leading-edge-suction analogy of Polhamus is developed in reference 1. However, to aid in illustrating the application to other edges, the primary ideas are briefly reviewed.

Wings which have attached flows develop suction forces along their leading edges if the stagnation surface does not lie along that edge. This suction force can be envisioned as arising by either of two processes: (1) the pressure near the leading edge acting over the edge thickness or (2) the product of the square of the induced tangential velocity and the distance to the edge. For a wing of infinitesimal thickness the induced

tangential velocity approaches an infinite value of $u(x,y)$ as shown in sketch (a); however, its product (described above) is still finite.



If the flow separates from the wing in going around the leading edge due to its sharpness or thinness, or due to a combination of thickness and angle of attack, the suction force in the chord plane is lost. However, if this separated flow forms into a shed vortex which causes the flow to reattach to the leeward surface of the wing, then the energy redistributes on the upper surface near the leading edge and consequently the force acts in the normal-force direction. By making the edge sharp this additional normal force can be generated at almost all angles of attack.

According to the analogy, the reattached line or details of the pressure field need not be known in advance in order to determine the reattached-flow force. However, if pitching-moment estimates are needed the distribution of the reattached force must be known. The centroid of the leading-edge suction has been used as the longitudinal location of this force. This assumption does not have provision for angle-of-attack effects on the location of the reattachment line or vortex core, hence the core is assumed to remain stationary near the wing leading edge.

From the above outlined ideas it can be seen that the conditions which lead to this additional normal force would not necessarily be limited to wings with separated flows around the leading edge but could be applied to any similar situation where, in potential flow, an edge suction force would be produced. Sketch (a) also shows, for example, that along the side edge of a finite streamwise tip chord large values of $v(x,y)$ are produced

due to flow around the side edges. These in combination with the infinitesimal thickness that lead to them would produce a finite suction force in the Y-direction (side-edge suction force, plus or minus depending on the edge). Hence, all that is required to employ a generalized suction analogy to the side edges is to determine the attached-flow side-edge suction force.

A mathematical procedure for computing this side force is developed in the following steps. Figure 1 illustrates graphically selected steps for a typical wing at a particular chordwise and spanwise location.

(1) The suction distribution along an edge per unit length is obtained from reference 12 to be of the form

$$s(x) = \rho\pi G(x)^2 \quad (1)$$

where for side-edge or tip suction the term $G(x)$ is interpreted as

$$G(x) = \sqrt{\frac{b}{2}} \lim_{\eta \rightarrow 1} \sqrt{1 - \eta} v(x, y) \quad (2)$$

where $v(x, y)$ is the perturbation velocity in the Y-direction.

(2) The velocity $v(x, y)$ is related to the trailing vorticity by

$$v(x, y) = \frac{1}{2} \delta(x, y) \quad (3)$$

(3) The trailing vorticity of a particular x-position x_i is determined by

$$\delta(x_i, y) = \frac{\partial \Gamma(x_i, y)}{\partial y} = \frac{2}{b} \frac{\partial \Gamma(x_i, \eta)}{\partial \eta} \quad (4)$$

where

$$\Gamma(x_i, y) = \int_{x_{1e}}^{x_i} \gamma(x, y) dx = 2 \int_{x_{1e}}^{x_i} u(x, y) dx \quad (5)$$

See figure 1.

(4) The subsonic bound-vorticity distribution is represented herein by

$$\gamma(x, y) = \frac{U}{2} \frac{1}{c(\eta)} \frac{2}{\pi} \sum_{n=0}^{N-1} \frac{\cos n\theta + \cos(n+1)\theta}{\sin \theta} \frac{q_n(\eta)}{q_\infty} \quad (6)$$

which is employed in a new version of the modified Multhopp lifting surface solution of reference 13.

(5) Upon obtaining solutions for the $\frac{q_n(\eta)}{q_\infty}$ terms from the method of reference 13, equation (5) becomes

$$\frac{\Gamma(x_i, y)}{U} = \frac{1}{\pi c(\eta)} \int_{x_{1e}}^{x_i} \sum_{n=0}^{N-1} \frac{\cos n\theta + \cos(n+1)\theta}{\sin \theta} \frac{q_n(\eta)}{q_\infty} dx \quad (7)$$

or

$$\frac{\Gamma(x_i, y)}{U} = \frac{1}{\pi} \int_0^{\theta x_i} \sum_{n=0}^{N-1} [\cos n\theta + \cos(n+1)\theta] \frac{q_n(\eta)}{q_\infty} d\theta \quad (8)$$

where

$$x = \frac{c_r}{2} - c(\eta) \cos \theta + d(\eta) \quad (9)$$

and

$$dx = c(\eta) \sin \theta d\theta \quad (10)$$

Upon integrating, the result of equation (8) is

$$\frac{\Gamma(x_i, y)}{U} = \frac{1}{\pi} \left\{ \sum_{n=1}^{N-1} \frac{q_n(\eta)}{q_\infty} \left[\frac{\sin n\theta}{n} + \frac{\sin(n+1)\theta}{n+1} \right] \Big|_0^{\theta x_i} + \frac{q_0(\eta)}{q_\infty} [\theta + \sin \theta] \Big|_0^{\theta x_i} \right\} \quad (11)$$

(6) Knowledge of the $\Gamma(x_i, y)$ distribution at discrete points is not sufficient for the present analysis since it is the $\frac{\partial \Gamma(x_i, y)}{\partial \eta}$ variation which is needed. This requires a knowledge of the continuous variation of the $\frac{q_n(\eta)}{q_\infty}$ terms. In the Multhopp solution the spanwise distributions of these terms are assumed to be composed of a sine series, which is expressible as an even power series in η . Hence, the $\frac{\Gamma(x_i, \eta)}{U}$ values computed by equation (11) will be curve fitted at each x_i location with

$$\frac{\Gamma(x_i, \eta)}{U} = \frac{b}{2} \sqrt{1 - \eta^2} \left[B_1(x_i) + B_2(x_i)\eta^2 + \dots + B_p(x_i)\eta^{2(p-1)} \right] \quad (12)$$

where the $B_j(x_i)$ values are determined in the fitting process. Four terms in the series were determined to represent adequately the $\frac{\Gamma(x_i, \eta)}{U}$ distribution in a least-squared sense.

(7) Hence, the differentiation of equation (12) with respect to η leads to

$$\frac{\partial \Gamma(\mathbf{x}_i, \eta)}{\partial \eta} = \frac{b}{2} U \left\{ \sqrt{1 - \eta^2} \left[2B_2(\mathbf{x}_i)\eta + 4B_3(\mathbf{x}_i)\eta^3 + 6B_4(\mathbf{x}_i)\eta^5 \right] - \frac{\eta}{\sqrt{1 - \eta^2}} \left[B_1(\mathbf{x}_i) + B_2(\mathbf{x}_i)\eta^2 + B_3(\mathbf{x}_i)\eta^4 + B_4(\mathbf{x}_i)\eta^6 \right] \right\} \quad (13)$$

As $\eta \rightarrow 1$ the first group of terms $\rightarrow 0$ and the second group $\rightarrow -\infty$. Therefore, it is only these last terms in combination with their multiplier which can contribute to the suction. Setting $\eta = 1$ in all the terms except those multiplied by $\frac{1}{\sqrt{1 - \eta^2}}$ results in

$$\lim_{\eta \rightarrow 1} \frac{\partial \Gamma(\mathbf{x}_i, \eta)}{\partial \eta} = \lim_{\eta \rightarrow 1} \left\{ - \frac{bU\eta}{2\sqrt{1 - \eta^2}} \left[B_1(\mathbf{x}_i) + B_2(\mathbf{x}_i)\eta^2 + B_3(\mathbf{x}_i)\eta^4 + B_4(\mathbf{x}_i)\eta^6 \right] \right\} \quad (14)$$

(8) Substituting equation (14) into equations (4) and (2) results in

$$G(\mathbf{x}_i) = -\sqrt{\frac{b}{2}} \frac{U}{2} \lim_{\eta \rightarrow 1} \frac{\sqrt{1 - \eta}}{\sqrt{1 - \eta^2}} \left[B_1(\mathbf{x}_i) + B_2(\mathbf{x}_i) + B_3(\mathbf{x}_i) + B_4(\mathbf{x}_i) \right] \quad (15)$$

Squaring and simplifying leads to

$$G(\mathbf{x}_i)^2 = \frac{bU^2}{16} \left[\sum_{j=1}^4 B_j(\mathbf{x}_i) \right]^2 \quad (16)$$

(9) Combining equations (1) and (16) yields

$$s(\mathbf{x}_i) = \frac{\rho U^2 b \pi}{16} \left[\sum_{j=1}^4 B_j(\mathbf{x}_i) \right]^2 \quad (17)$$

or

$$s(\mathbf{x}_i) = \frac{q_\infty b \pi}{8} \left[\sum_{j=1}^4 B_j(\mathbf{x}_i) \right]^2 \quad (18)$$

(10) The magnitude of the tip suction force from one edge can be found by

$$F = \int_{x_{le,t}}^{x_{te,t}} s(x_i) dx \quad (19)$$

or, in coefficient form

$$\frac{F}{q_\infty S_{ref}} = \frac{b\pi}{8S_{ref}} \int_{x_{le,t}}^{x_{te,t}} \left[\sum_{j=1}^4 B_j(x_i) \right]^2 dx \quad (20)$$

(11) Inasmuch as $s(x_i)$ depends on $[v(x,y)]^2$ and since $v(x,y)$ is linearly dependent on the values of $\frac{q_n(\eta)}{q_\infty}$, which are dependent on $\sin \alpha$ or α (in radians) for small angles of attack, then $s(x_i)$ depends on $\sin^2 \alpha$. Hence, the partial derivative with respect to $\sin^2 \alpha$ can be taken of $\frac{F}{q_\infty S_{ref}}$ to determine a K_V -type term analogous to that obtained for the leading-edge-suction force in reference 1. Therefore the equation defining $K_{V,se}$ may be written

$$K_{V,se} = \frac{\partial \left[\frac{2F}{q_\infty S_{ref}} \right]}{\partial \sin^2 \alpha} \quad (21)$$

With the determination of the attached-flow side force and by use of the generalized suction analogy, the magnitude of the additional normal force associated with the separated flow around the side edge can be found and its contribution to the static longitudinal aerodynamic characteristics can be taken into account. For example:

$$C_L = K_p \sin \alpha \cos^2 \alpha + (K_{V,le} + K_{V,se}) \sin^2 \alpha \cos \alpha \quad (22)$$

or

$$C_L = K_p \sin \alpha \cos^2 \alpha + K_{V,tot} \sin^2 \alpha \cos \alpha \quad (23)$$

$$\Delta C_D = C_L \tan \alpha = K_p \sin^2 \alpha \cos \alpha + K_{V,tot} \sin^3 \alpha \quad (24)$$

and

$$C_m = K_p \sin \alpha \cos \alpha \frac{\bar{x}_p}{c_{ref}} + K_{V,le} \sin^2 \alpha \frac{\bar{x}_{le}}{c_{ref}} + K_{V,se} \sin^2 \alpha \frac{\bar{x}_{se}}{c_{ref}} \quad (25)$$

where the particular \bar{x} -terms equal

$$x_{\text{ref}} - x_{c,i}$$

Appropriate simplifications can be made if only the leading or side edges are sharp.

The procedure is computerized and is available from COSMIC as NASA Langley computer program A0313.

BEHAVIOR OF $K_{v,se}$

The behavior of $K_{v,se}$ will be studied by examining the important parameters which affect its variation. They must include planform variables along with Mach number since both affect the span loading and, consequently, $K_{v,se}$. The planform variables associated with unswept or swept wings having streamwise side edges will be considered.

Unswept Wings

Straight trailing edge.- The geometric parameter defining rectangular wings is, of course, the aspect ratio. Values of $K_{v,se}$ were computed based on the described procedure and the results are presented in figure 2 as a function of this parameter. The figure shows a rapid decrease of $K_{v,se}$ (solid curve) with increasing βAR to the extent that for $\beta AR = 2$ the value of $K_{v,se}$ was only approximately one-half of the value at $\beta AR = 0$. The procedure by which the limiting values of $K_{v,se}$ are determined is presented next.

The $K_{v,se}$ limit as $AR \rightarrow \infty$ is easy to establish because with the reference area also $\rightarrow \infty$ and the side edge forces remaining finite, $K_{v,se} \rightarrow 0$. However, in order to establish the $K_{v,se}$ limit as $AR \rightarrow 0$ it is necessary to refer to reference 14 where certain stipulations are given for wings of very low aspect ratio. They are: (1) no chordwise loading past the point of maximum span and (2) the span loadings are elliptical. For a wing with an unswept leading edge and streamwise tips the maximum span occurs at the leading edge which according to the first stipulation would require the chord loading to be impulsive. With the form of the loadings now specified a procedure similar to that already detailed can be used to determine this $K_{v,se}$ value. By employing the C_L expression consistent with the prescribed loadings, $C_L = \frac{\pi AR \alpha}{2}$, then $K_{v,se} = \pi$.¹ If the C_L expression of Helmbold (ref. 15) which is

¹It should be noted that for $AR = 0$ this is the same value as for the delta wing $K_{v,le}$ given in reference 1. That they are the same is not surprising since the delta wing has its sweep angle $\rightarrow 90^\circ$ as $AR \rightarrow 0$. Hence, the leading edges are becoming like side edges and with $K_{v,le} \rightarrow 0$ for unswept wings, their totals are identical.

$$C_L = \frac{2\pi AR\alpha}{\sqrt{AR^2 + 4} + 2}$$

was used instead, then the values of $K_{v,se}$ are weighted by an expression which is valid over a wider aspect-ratio range. The results of these computations yield the long dashed curve in figure 2 which in comparison with the solid curve shows mostly the effect of going from an impulsive-type chord loading to a finite-aspect-ratio-wing chord loading.

To demonstrate the reduction in $K_{v,se}$ which occurs in going from an impulsive chord loading to one that is either of the $\cot \frac{\theta}{2}$ type or constant (see fig. 3), while keeping the span loading elliptical and the aspect ratio near zero, computations were made using the same procedure as before and resulted in

$$K_{v,se} = 1.93$$

for the $\cot \frac{\theta}{2}$ loading, and

$$K_{v,se} = 1.33$$

for the constant chord loading.

Figure 4 shows some of the results of a numerical experiment designed to determine the aspect-ratio limit of the present method as $AR \rightarrow 0$. From this experiment there are several important points to be made in this regard which follow:

(1) The three-dimensional span loadings of wings in this aspect-ratio range are found numerically to be nearly elliptical, hence the effects seen here are primarily associated with the change in chord loadings.

(2) The validity of the tip-suction distributions associated with the $AR = 0.05$ and $AR = 0.0001$ wings is suspect since these wings are outside the aspect-ratio range where the attached-flow method employed would yield reliable results. The validity is questioned because the near- and far-field drag results did not agree well indicating an inability of the method to get good chord loadings at these AR values.

(3) The $AR = 0.1, 0.2, 0.3,$ and 0.5 wings had acceptable agreement between the two induced drag results, hence the chord-loading solutions can be assumed to be theoretically correct. Because of the above points the present theoretical prediction of the $K_{v,se}$ shown in figure 2 has been adjusted between $\beta AR = 0.10$ and 0 to fair into π at $\beta AR = 0$ by extrapolating the theoretical curve to the $\beta AR = 0$ value from slender-wing theory.

Figure 5 presents the variation of βK_p , $\beta K_{v,le}$, and $K_{v,tot}$ with βAR . The βK_p curve is well known (as $\beta C_{L\alpha}$) and will not be discussed. It is interesting to note that at $\beta AR = 2$ the value of $\beta K_{v,le}$ is about equal to the computed value of $K_{v,se}$

in figure 2, and with increasing βAR , the value of $\beta K_{v,le}$ becomes larger than $K_{v,se}$. The total of $\beta K_{v,le}$ and $K_{v,se}$ stays within a ± 10 -percent band about π for the βAR range considered; consequently, to a good approximation, $K_{v,se} = \pi - \beta K_{v,le}$ in this βAR range.

Notched trailing edge. - The discussion so far about the general behavior of $\beta K_{v,se}$ with βAR and its limits for rectangular wings is applicable to wings with notched trailing edges. Some variations occur in between the limits reflecting the changes in side- and trailing-edge geometry. A reason for considering wings of this type was to determine if more side-edge vortex lift could be obtained for a given span and area.

The major difference in the computation of the tip suction for these wings, as compared with those having straight trailing edges (although different, it poses no problem), is that these wings can accumulate all of the chord load at the inboard span stations (due to shortened chord) ahead of the tip trailing edge. This makes $\Gamma(x,\eta)$ constant for all chord stations aft of the notch in the spanwise curve fitting of $\Gamma(x,\eta)$ - a part of the tip-suction computational process - and is illustrated in figure 6. (Because the potential-flow solution uses only a continuous chord description, the inner streamwise edge of the notch is not treated streamwise but at some sweep angle. This causes, in figure 6, the $\frac{\Gamma(\eta)}{U}$ not to be totally unchanged aft and inboard of the notch.)

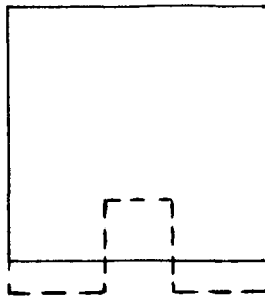
One aspect of the notched-wing edge suction that tends to be confusing is the lack of edge suction along the inner edge. To understand this lack of suction it must be remembered that for a suction force to be present along an infinitesimally thin edge the

tangential flow at the edge must approach an infinite value. This means that $\frac{\partial \Gamma(x_1, \eta)}{\partial \eta}$

or $v(x_1, \eta) \rightarrow \pm \infty$ along the inner edge, but figure 6 clearly shows that $\frac{\partial \Gamma(x_1, \eta)}{\partial \eta}$ only $\rightarrow -\infty$ as $\eta \rightarrow 1$. Hence, no inner edge suction is produced for the notched wing examined.

In order to show an example of the changes which can occur in $K_{v,se}$ and $K_{v,tot}$ as a result of forming a notched wing (see sketch (b)) from a rectangular one by extending the side edge 10 percent and removing area at the trailing edge to keep the same aspect ratio the following table was prepared for $M = 0$:

Planform: $AR = 1$	$K_{v,se}$	$K_{v,tot}$
Rectangular	2.1255	2.9071
Notched	2.3863	3.1650
Percent change	12.3	8.9



Sketch (b). - Rectangular and notched wings. $\mathcal{AR} = 1$.

For this aspect ratio K_p and $K_{v,le}$ fall off slightly in going from a rectangular to a notched wing, however, for $\alpha > 6^\circ$ the larger $K_{v,tot}$ of the notched wing is sufficient to cause its C_L value to exceed that of the rectangular wing and thereafter remain larger.

Swept Wings²

The $K_{v,se}$ variations for wings with leading-edge sweepback, streamwise tip chords, and unswept or swept trailing edges called cropped deltas and either cropped diamonds or arrows, respectively, are considered.

Cropped deltas. - Cropped-delta wings are defined in terms of aspect ratio, leading-edge sweep, and taper ratio. The effect of varying these geometric parameters and Mach number on $K_{v,se}$ and $K_{v,le}$ is given in figure 7 and their sum at $M = 0$ appears in figure 8. From figure 7 the following effects were noted for three separate sets of independent variables:

Set	λ	Λ	\mathcal{AR}	M	$K_{v,se}$	$K_{v,le}$
1	Constant	Increasing	Decreasing	Constant	Increasing	Decreasing
2	Increasing	Constant	Decreasing	Constant	Increasing	Decreasing
3	Constant	Constant	Constant	Increasing	Increasing	Increasing

Although there is a wide variation of $K_{v,se}$ and $K_{v,le}$ with the geometric parameters, shown in figure 7, their sums fall within a 10-percent band around π (see fig. 8).

²Reference 16 found two separate vortex systems for a rectangular wing, but for swept cropped wings the tip-vortex system merges with that from the leading edge to form only one system at a low angle of attack.

It is interesting to note that the number π keeps appearing in suction analogy considerations – as a limiting value at $AR = 0$ ($K_{v,se}$ for unswept-leading-edge wings and $K_{v,le}$ for delta wings), as an approximate total of $K_{v,se}$ and $K_{v,le}$ for the unswept-leading-edge wings and cropped deltas over a range of aspect ratio, or as half the two-dimensional value of $K_{v,le}$.

Cropped diamonds and arrows. - The cropped-diamond or cropped-arrow wings are defined by the same geometric parameters as the cropped deltas with the addition of trailing-edge sweep. In order to isolate the trailing-edge-sweep effect on $K_{v,se}$ the following study was performed. The wing leading-edge sweep and tip-chord length were fixed for four different combinations of these parameters and the trailing-edge sweep angle Ω was generally varied from 60° to -60° . The actual tip chord was held constant rather than λ since $K_{v,se}$ has been shown in the section on unswept leading edges and notched trailing edges to be almost directly related to changes in tip-chord length. Furthermore, with Ω varying, the taper ratio defined in terms of c_r would be varying for a fixed c_t . Hence, the taper ratio is only used at $\Omega = 0^\circ$ to fix the c_t . The total of $K_{v,se}$ and $K_{v,le}$ is presented in figure 9 rather than the separate coefficients since, along any one of the three curves with a nonzero tip chord, both $K_{v,se}$ and $K_{v,le}$ have the same general behavior with aspect ratio. This is because the reference area used to determine the coefficients is the true area which varies widely over the Ω -range. In fact with the leading-edge sweep and tip chord fixed as $\Omega \rightarrow -90^\circ$ the reference area $\rightarrow \infty$ which causes $K_{v,tot} \rightarrow 0$ as $AR \rightarrow 0$. Thus, any finite tip or leading-edge-suction force will yield a zero coefficient.

The variations of $K_{v,tot}$ with three separate sets of geometric parameters are given in the following table:

Set	AR	Λ	c_t	Ω	$K_{v,tot}$
1	Increasing	Constant	Constant	Increasing	Increasing
2	Constant	Constant	Increasing	Increasing	Increasing
3	Constant	Increasing	Increasing ^a	Increasing	Increasing

^aAlthough c_t is increasing, λ is constant for unswept trailing edge.

As an exercise $K_{v,tot}$ values were recomputed for wings with $\Lambda = 63^\circ$ and $\lambda_{\Omega=0} = 0.4$ over the Ω -range using as a reference area that of the $\Omega = 0^\circ$ wing. The resultant variation of $K_{v,tot}$ was less than 10 percent.

MODELS AND TEST CONDITIONS

In order to provide needed data for comparison with the present method, an experimental investigation was conducted. A total of 10 thin flat wings were tested, each having streamwise tips and symmetrical beveling along the leading and side edges. Six of the wings had unswept leading edges along with symmetrically beveled trailing edges. Geometrical descriptions of the models are given in table I. Figures 10 and 11 are photographs of the models and typical model installations are shown in figures 12 and 13.

The models were tested in the Langley high-speed 7- by 10-foot tunnel at $M \approx 0.20$, $q_\infty \approx 2394 \text{ N/m}^2$ (50 psf), and $R \approx 4.265 \times 10^6/\text{m}$ ($1.30 \times 10^6/\text{ft}$). Number 80 transition grit at a density of ≈ 1 particle/2 mm was added to both sides of each model approximately 2.54 cm (1 in.) behind the wing leading edges and extending to the tips. A bolt-on balance housing was mounted on one side of the model with a dummy housing mounted symmetrically on the other side. (See figs. 12(b), 13(a), and 13(b).) The drag data have been corrected to a condition of free-stream static pressure acting on the base of the balance and dummy housings and in the chamber. No blockage or wall-interference corrections were made due to the small models employed at a low test Mach number.

EFFECT OF EDGE SHAPING ON RECTANGULAR-WING RESULTS

The results predicted by the generalized suction analogy (present method) will be compared with experimental data for the various models of the investigation. However, before these comparisons are presented the results of a limited study concerned with the agreement which can be obtained with wings having different edge conditions will be discussed. Also, the effect of separation occurring primarily at the side edges and not the leading edges will also be discussed.

Figure 14 shows the effect of edge shaping on the variation of C_N with α for an $AR = 2$ rectangular wing. There is not much effect noted (probably due to the low test Reynolds numbers) except for the unsymmetrical beveled edges which exhibit a camber contribution to C_N . (Some of the data were converted to C_N from C_L values at zero leading-edge thrust.) The best agreement between the present method and previous experimental data is achieved with the thin rounded-plate model until the leading-edge flow no longer reattaches to the wing. Reference 16 considers this to occur at $\alpha > 15^\circ$. The symmetrically beveled wing achieved the highest test C_N values and was well predicted even at $\alpha > 15^\circ$.

Reference 17 shows that for an $AR = 0.2$ rectangular wing the higher values of C_L are obtained for $\alpha < 37^\circ$ with a thin flat plate. Hence the best agreement with the

present method is expected when applied to thin flat wings with symmetrical beveling along the leading and side edges. (It should be noted that the models constructed for the purpose of providing data for comparison with the present method had these features.)

Wings with well-rounded leading edges but having separation vortices along the side edges (due either to symmetrical beveling or attached-flow breakdown due to exceeding a critical Reynolds number) provide interesting data for comparison with the present method. This is because all nonlinear effects, which tend to increase the curve of C_L plotted against α at a rate faster than that for the attached flow, must be attributed to the side-edge suction for angles of attack below leading-edge separation. Such data was found in reference 6 for rectangular wings of various aspect ratio and compared in figure 15 with the present method. In general, the agreement is good until the leading-edge flow separates and consequently affects the side-edge vortex effects.

Not only does edge shaping affect C_N and C_L but the drag coefficient due only to lift ΔC_D as well. Figure 16 shows the variation of ΔC_D with aspect ratio for different edge conditions at four different values of C_L . As expected, for $AR > 1.0$ all the curves for $C_L^2/\pi AR$ and attached flow are slightly lower than those for wings with round leading edges and sharp side edges. They also show that over the entire AR and C_L ranges values of ΔC_D due to the round-leading-edge, sharp-side-edge configurations, which retain their leading-edge suction, are lower than those for the configurations with sharp leading and side edges. In general, at any C_L for $AR < 1$ the value of ΔC_D for the round-leading-edge, sharp-side-edge configuration is lower than either attached-flow drag value due to the nonlinear contribution of C_L from the tip. Furthermore, for $C_L = 0.05, 0.20,$ and 0.35 there are aspect ratios for which the values of ΔC_D for the configurations with sharp leading and side edges are lower than those for attached flow, reflecting again the increasing contribution of the side edges as AR decreases.

COMPARISONS WITH EXPERIMENTS

Unswep Wings

Straight trailing edge.- Figure 17 presents some static longitudinal aerodynamic characteristics plotted against C_L for five rectangular wings ranging in aspect ratio from 0.2 to 3.0 at a Mach number of 0.2.

In figures 17 to 21 the curves of C_D for zero percent leading-edge suction are computed by $C_D = C_{D,0} + C_L \tan \alpha$ with $C_L = C_{L,tot}$ and the 100-percent-suction curves are determined by $C_{D,0} + C_L^2/\pi AR$. For these five models some observations can be made. They are:

(1) The predicted C_L variation with α is in reasonable agreement with the experimental data. If the tip-suction contribution to C_L had not been included in the theory, the agreement would have been poor except at $AR = 3$.

(2) The C_D data are well predicted by the zero percent leading-edge suction and show the reduction in C_D below that for attached flow at $AR = 0.2, 0.3,$ and 0.4 , which is consistent with the results of figure 16.

(3) The C_m trends are reasonably well predicted for the $AR = 0.2, 0.3, 0.4,$ and 1.0 wings although the predicted values for all except $AR = 1.0$ show more nose-down moment than measured. However, it can also be seen that if it were not for the C_m contribution from the side edge, the predicted moment would go the wrong way.

(4) At $AR = 3.0$ both the C_L variation with α and C_m data show that for $C_L > 0.4$ the leading-edge vortex lift is being lost and also, of course, its contribution to C_m . This occurs, as for the $AR = 2$ wing discussed earlier, because the leading-edge flow no longer reattaches to the wing for $\alpha \approx 8^\circ$. With the loss in $C_{L,vle}$ the C_m data now show primarily the effect of the side-edge separated flow.

Notched trailing edge.- The data (again static longitudinal aerodynamic characteristics plotted against C_L) for the notched rectangular wing presented in figure 18 are predicted well by the present method and illustrate again the significant contribution that tip suction makes for wings in this aspect-ratio range. In comparing the data for the $AR = 1$ rectangular wing with these data it can be seen that (as discussed in the section on the behavior of $K_{v,se}$) the values of C_L are generally higher for the notched wing although the lift distributions produce approximately the same C_m variation. The predicted C_m for the notched wing is more negative than that for the rectangular wing (see fig. 17(d)) and only slightly overpredicts the experimental nose-down moment.

Swept Cropped Wings

Taper-ratio variation (deltas).- Figure 19 presents static longitudinal aerodynamic characteristics as a function of C_L for a series of cropped delta wings with variable λ at $M = 0.6$ and $\Lambda = 63^\circ$. The experimental data are for models which did not have sharp edges (ref. 18). However, the comparison shows generally good agreement between the data and the present method. The airfoil employed was the NACA 63A002 which at low Reynolds number develops separated flow due to the small leading-edge radius. At the higher angles of attack vortex breakdown must be occurring ahead of the trailing edge to account for the decrease in C_L and increase in C_D . The curves of the various contributions of C_L plotted against α show that with increasing λ the $C_{L,vse}$ contribution increases, as it should. The underprediction of C_L at the higher angles of attack and taper ratios, before the occurrence of vortex breakdown, can be

attributed to the actual shed-vortex system which produces additional induced effects above that predicted for an assumed core lying in the vicinity of the leading and side edges. An underprediction of C_L was also found for sharp-edged diamond wings in reference 19.

For delta wings of $AR \leq 2$, the centroids of leading-edge suction and attached-flow lift are approximately the same (ref. 20); hence using the attached-flow lift centroid to concentrate all of the lift for the moment prediction was an acceptable procedure. This is no longer true if the delta-type wing has a cropped tip for then each individual loading centroid must be used.

Trailing-edge sweep variation (diamond and arrow).- Figure 20 presents some static longitudinal aerodynamic characteristics plotted against C_L for a family of cropped wings all having $\Lambda = 63^\circ$ and the same tip-chord length and tested at $M = 0.2$. The models differ in their Ω -values which vary from -40° to 40° . For $\Omega = 0^\circ$ and -40° C_L is under predicted, as for the cropped deltas which causes the predicted C_D values (zero percent leading-edge suction) to be much higher than those experimentally measured. The C_D data do follow $C_{D,0} + C_L \tan \alpha$ (zero percent leading-edge suction) where C_L is the experimental value. The C_m data are well predicted especially at $\Omega = -40^\circ$. For $\Omega = 40^\circ$ the extra induced effect to lift is lost, as in reference 19 for the arrow wing, bringing the predictions of the C_L variations with α and C_D into good agreement with the data. The C_m data are well predicted for lift coefficients up to ≈ 0.5 , after which the data are more positive.

Flow pictures of the leading-edge shed vortex showed that breakdown occurs ahead of the trailing edge for the cropped-diamond, cropped-delta, and cropped-arrow wings at $\alpha \approx 25^\circ$, 24° , and 22° , respectively. The C_L variation with α shows for the respective models that, above these values of α , C_L increases at a slower rate than before.

Arrow wing.- Figure 21 presents static longitudinal aerodynamic characteristics plotted against C_L for a cropped-arrow wing. In general, the data are very well predicted up to $C_L = 0.7$, after which C_L falls off slightly and from the C_m data it appears that some or all of the contribution from the side edge is being lost. This also shows up in the C_L variation with α . Around $C_L = 1.0$ the leading-edge-vortex breakdown occurs ahead of the trailing edge resulting in additional loss in C_L .

COMPARISONS WITH OTHER THEORIES

Other Theories

General.- Theoretical estimates for the effects of separated flow along streamwise side edges on the aerodynamic characteristics of swept and unswept wings have been

made by various authors (refs. 4 to 11). Of these the ones most commonly referenced are Bollay, Flax, and Gersten (refs. 4, 6, and 8, respectively). These along with the more recent methods of Belotserkovskii (ref. 10) and Bradley (ref. 11) will be briefly reviewed after which comparisons will be made with the present method and with experimental data.

Bollay. - Bollay's flow model (ref. 4) is associated with a rectangular wing and assumes attached flow around the leading edge with the flow around the side edge separating and trailing off at some angle, nominally $\alpha/2$, to the free stream. A further assumption, which agrees well with experiment, is that the span loading is constant. The resultant formulation retains $\sin^2 \alpha$ and $\sin \alpha \cos \alpha$ terms in the C_N expression and appears adequate for the extremes of aspect ratio. However, for aspect ratios from 1 to 6 this method overpredicts the experimental C_N . Values of ΔC_D could be computed with Bollay's method but, due to the employment of the mean pressure, C_m cannot be determined with the same accuracy. This method was not intended to be used for wings with sharp leading edges.

Flax. - Flax and Lawrence (ref. 6) use a combination of attached- and cross-flow methods to arrive at procedures for calculating C_L and C_m in terms of the sum of α -contributions up through α^2 for delta and rectangular wings. The coefficient of α^2 in the C_L equation is taken to be the two-dimensional cross-flow drag coefficient. Its value is 2.0 for rectangular wings with separated flow around the side edges and attached flow around the leading edges. The same value is used for thin delta wings. For rectangular wings with sharp leading and side edges the value of the two-dimensional cross-flow drag coefficient is replaced by an empirically determined value of 3.0. Flax and Lawrence state that retaining the trigonometric term in the α^2 term to make it $\sin^2 \alpha$, "while more rigorously correct . . . does not always lead to results in better agreement with experiment." The C_m equation, which is empirically developed, has one linear term in α and two α^2 terms. The second α^2 term is added to contribute a moment from a force located at the half root chord, which is found in the present paper to be correct only for $AR = 0$. Values of ΔC_D could be computed with this model.

Gersten. - Gersten (ref. 8) employs Bollay's flow model in spanwise strips which allows him to represent a separated flow about the leading edge for rectangular and delta-type wings. The flow trails off the surface at half the wing angle of attack resulting in a full wake flow over the wing surface. Unfortunately, this does not represent well the physical flow model of wings with both sharp leading and side edges at least in the low-to-moderate angle-of-attack range where flow reattachment occurs. Gersten, like Flax and Lawrence, has equations for C_L and C_m which depend on α and α^2 (trigonometric terms neglected) where the coefficients are determined from two

contributions: (1) linear theory (attached flow) and (2) nonlinear theory (shed vorticity all across the wing surface). Values of ΔC_D can be calculated easily with this method.

Garner's method (ref. 9) was developed to be an extension of Gersten's but this effort was concerned primarily with establishing a similar technique having a different attached-flow solution.

Belotserkovskii. - Belotserkovskii (ref. 10) solves the separated side-edge problem by using a discrete vortex lattice which has no trailing leg at the tip but has the bound filaments trail across the tip and wrap up into a shed-vortex sheet. The effect of the strength and location of this rolled-up tip sheet is also taken into account, by iteration, in obtaining a solution. The leading-edge flow is assumed to be attached. Normal-force and pitching-moment results are computed.

Bradley. - Bradley's method (ref. 11) is based on computing the leading- and side-edge-suction forces and then employing the generalized suction analogy – similar to the present method³ – to predict C_L and ΔC_D for a variety of planforms. The major difference between the two methods is the potential-flow solutions employed to arrive at the suction forces. The present method uses a modified Multhopp approach with continuous pressure loadings, whereas Bradley's method uses the discrete loadings of the vortex-lattice procedure. Limited comparisons made with the two methods for wings having separated flows indicate that they are in excellent agreement. Pitching moments could be determined with this method but none were given in reference 11.

Comparisons

Comparisons of predictions – by the previously discussed theories and the present method – and experimental data are to be made for representative or the complete series of planforms which have been analyzed and results published.

Figure 22 presents results for $AR = 0.2$ and 1.0 rectangular wings at $M \approx 0$ from the present method and experiment and from the methods of Bollay and Belotserkovskii ($AR = 1.0$ only). The data for both wings are seen to be predicted better with the present method over the entire α -range than with the other methods.

Figure 23 shows static longitudinal aerodynamic characteristics plotted against α at $M \approx 0$ for an $AR = 1.0$ rectangular wing obtained from the present method and experiment along with those from Flax, Gersten, Garner, and Belotserkovskii. The C_L data are best predicted by the present method over the α -range, however, the $C_{m,le}$ data are only best predicted by the present method up to $\alpha \approx 16^\circ$. Around this value of α it appears that the leading-edge vortex core has moved enough to begin to

³Bradley references the original application of the present method to rectangular wings.

contribute a noticeable nose-down moment. In addition to this change it would be expected that the pitching moment from the side edge would be affected by the change in flow conditions. The present method predicted no pitching-moment contribution from the leading-edge vortex lift since the reference point was at the leading edge.

Figure 24 presents the C_L and C_m variations with α for two wings at $M \approx 0$ which have $\Lambda = 45^\circ$, $\lambda = 1.0$, and aspect ratios of 1 and 2. They were obtained from the present method and those of Gersten, Garner, and Belotserkovskii along with data from reference 8. At $AR = 1$ the present method with separated flow assumed at the leading and side edges predicts the C_L and C_m data more accurately than either of the other methods separately. For the $AR = 2$ wing no one method works well over the entire α -range, although up to $\alpha \approx 12^\circ$ the C_L and C_m data are slightly better predicted by the present and Gersten's methods. A comparison of $C_{L,p} + C_{L,vse}$ with wing data would indicate that the leading-edge vortex lift begins to fall off noticeably for $\alpha \approx 12^\circ$. This could occur for several reasons, the most likely is that the shed-vortex system is beginning to break down near or ahead of the wing trailing edge.

Zero Aspect-Ratio Limit

At $AR = 0.2$ the present method yields a value of $K_{v,se} = 2.8$ which results in a good estimation of C_L and C_N as a function of α . However, a comparison with C_N data found in reference 4 for $AR < 0.2$ shows that the method of Bollay (ref. 4) estimates more closely the experimental results and both Bollay's estimates and the experimental data are smaller than the present-method predictions. Evidently, for some aspect ratio between 0.134 and 0.20 the flow no longer reattaches on the upper surface over any significant angle-of-attack range, as required by the present method, which results in a pure wake flow and a sharp reduction in the actual value of $K_{v,se}$. (Note that if $K_{v,se} = 2.0$ for a $AR = 0$ wing a pure wake flow could be implied since this would be the same value as that for the cross-flow drag coefficient at this aspect ratio.) Gersten's results (ref. 8) indicate a nonlinear coefficient of ≈ 5.9 at $AR = 0$ which is almost twice the π -result from the present method.

CONCLUSIONS

An analysis of an extension of the leading-edge-suction analogy of Polhamus (NASA TN D-3767) to wings with separated flow around their side edges is presented. Comparisons of predicted and experimental data and other analytical methods have yielded the following conclusions:

(1) Based on slender-wing theory the value of the term associated with the lift from the separated flow at the side edges $K_{v,se}$ is π at zero aspect ratio.

(2) The infinite-aspect-ratio value of $K_{v,se}$ is zero.

(3) For rectangular wings with aspect ratio less than 2 the value of $K_{v,se}$ is larger than the value of the term associated with the lift at the leading edge $K_{v,le}$. Above an aspect ratio of 2, $K_{v,le}$ is larger than $K_{v,se}$ but for all aspect ratios below 2.8 the totals of $K_{v,se}$ and $K_{v,le}$ are very near π .

(4) For cropped-delta wings the totals of $K_{v,se}$ and $K_{v,le}$ for a wide range of sweep angle, taper, and aspect ratios varied less than ± 10 percent about π ; however, both $K_{v,se}$ and $K_{v,le}$ varied widely.

(5) For cropped wings with leading- and trailing-edge sweep the total of $K_{v,se}$ and $K_{v,le}$ increases with increasing aspect ratio, leading-edge sweep, trailing-edge sweep (becoming more arrow like), and tip chord.

(6) The lift variation was well predicted over an angle-of-attack range for four rectangular wings of aspect ratios 0.5, 1.0, 1.5, and 2.0 having round leading edges and vertical side edges using $K_{v,se}$ as the only separated-flow lift contributor.

(7) Experimental data of pitching moment, lift, and drag for rectangular, cropped-delta, cropped-diamond, and cropped-arrow wings were predicted reasonably well by the present method. Some drag correlations confirmed predicted drag values below those of 100-percent leading-edge suction.

(8) Without the side-edge contribution to separated-flow lift and moment, the value of predicted lift would, in general, be too low and the moments could be more positive.

(9) Sweptback wings which have large amounts of area behind the point of maximum span develop lift values in excess of those predicted due to additional induced effects associated with the actual shed-vortex system.

(10) It has been determined that the present method predicts wing static longitudinal aerodynamic data as well as, or better than, many other methods.

(11) The separated-flow model assumed by the present method is more nearly consistent with the real flow than that of some other methods.

Langley Research Center,
National Aeronautics and Space Administration,
Hampton, Va., July 23, 1974.

REFERENCES

1. Polhamus, Edward C.: A Concept of the Vortex Lift of Sharp-Edge Delta Wings Based on a Leading-Edge-Suction Analogy. NASA TN D-3767, 1966.
2. Polhamus, Edward C.: Charts for Predicting the Subsonic Vortex-Lift Characteristics of Arrow, Delta, and Diamond Wings. NASA TN D-6243, 1971.
3. Polhamus, Edward C.: Predictions of Vortex-Lift Characteristics by a Leading-Edge Suction Analogy. *J. Aircraft*, vol. 8, no. 4, Apr. 1971, pp. 193-199.
4. Bolland, William: A Theory for Rectangular Wings of Small Aspect Ratio. *J. Aeronaut. Sci.*, vol. 4, no. 7, May 1937, pp. 294-296.
5. Weinig, F.: Lift and Drag of Wings With Small Span. NACA TM 1151, 1947.
6. Flax, A. H.; and Lawrence, H. R.: The Aerodynamics of Low-Aspect-Ratio Wings and Wing-Body Combinations. Third Anglo-American Aeronautical Conference, Joan Bradbrooke and E. C. Pike, eds., Royal Aeronautical Soc., 1952, pp. 363-398.
7. Wadlin, Kenneth L.; Ramsen, John A.; and Vaughan, Victor L., Jr.: The Hydrodynamic Characteristics of Modified Rectangular Flat Plates Having Aspect Ratios of 1.00, 0.25, and 0.125 and Operating Near a Free Water Surface. NACA Rep. 1246, 1955. (Supersedes NACA TN's 3079 by Wadlin, Ramsen, and Vaughan and 3249 by Ramsen and Vaughan.)
8. Gersten, K.: Calculation of Non-Linear Aerodynamic Stability Derivatives of Aeroplanes. AGARD Rep. 342, Apr. 1961.
9. Garner, H. C.; and Lehrian, Doris E.: Non-Linear Theory of Steady Forces on Wings With Leading-Edge Flow Separation. NPL Aero Rep. 1059, Brit. A.R.C., Feb. 15, 1963.
10. Belotserkovskii, S. M. (J. W. Palmer, transl.): Calculation of the Flow About Wings of Arbitrary Planform at a Wide Range of Angles of Attack. Libr. Transl. No. 1433, Brit. R.A.E., Feb. 1970.
11. Bradley, R. G.; Smith, C. W.; and Bhateley, I. C.: Vortex-Lift Prediction for Complex Wing Planforms. *J. Aircraft*, vol. 10, June 1973, pp. 379-381.
12. Jones, Robert T.; and Cohen, Doris: Aerodynamics of Wings at High Speeds. Vol. VII of High Speed Aerodynamics and Jet Propulsion, A. F. Donovan and H. R. Lawrence, eds., Princeton Univ. Press, 1957, p. 24.
13. Lamar, John E.: A Modified Multhopp Approach for Predicting Lifting Pressures and Camber Shape for Composite Planforms in Subsonic Flow. NASA TN D-4427, 1968.

14. Jones, Robert T.: Properties of Low-Aspect-Ratio Pointed Wings at Speeds Below and Above the Speed of Sound. NACA Rep. 835, 1946.
15. Helmbold, H. B.: Der unvurwundene Ellipsenflügel als tragende Fläche. Jahrb. 1942 der Deutschen Luftfahrt-forschung, R. Oldenbourg (Munich), pp. I 111 – I 113.
16. Parkinson, G. V.; Sun, Y. C.; and Davis, H. R.: Observations on Low Aspect Ratio Wings at High Incidence. Canadian Aeronaut. & Space J., vol. 13, no. 3, Mar. 1967, pp. 111-116.
17. Martynov, A. K. (V. H. Brix, transl.): Practical Aerodynamics. MacMillan Co., 1965, p. 319.
18. Emerson, Horace F.: Wind-Tunnel Investigation of the Effect of Clipping the Tips of Triangular Wings of Different Thickness, Camber, and Aspect Ratio-Transonic Bump Method. NACA TN 3671, 1956. (Supersedes NACA RM A53L03.)
19. Davenport, Edwin E.; and Huffman, Jarrett K.: Experimental and Analytical Investigation of Subsonic Longitudinal and Lateral Aerodynamic Characteristics of Slender Sharp-Edge 74° Swept Wings. NASA TN D-6344, 1971.
20. Snyder, Melvin H., Jr.; and Lamar, John E.: Application of the Leading-Edge-Suction Analogy to Prediction of Longitudinal Load Distribution and Pitching Moments for Sharp-Edged Delta Wings. NASA TN D-6994, 1972.
21. Winter, H.: Flow Phenomena on Plates and Airfoils of Short Span. NACA TM-798, 1936.
22. Scholz, N.: Kraft- und Druckverteilungsmessungen an Tragflächen kleiner Streckung. Forsch. Geb. Ing.-Wes., vol. 16, no. 3, 1949/50, pp. 85-91.
23. Schoch, David L.: An Investigation of the Flow Characteristics About a Low Aspect Ratio, Sharp Leading-Edge Rectangular Wing. Rep. No. 574 (Contract Nonr 1858(14)), Dep. Aeronaut. Eng., Princeton Univ., Nov. 1961. (Available from DDC as AD 270 111.)

TABLE I. - MODEL DIMENSIONS

Rectangular wings														
AR	b		c _r and c _{ref}		S _{ref}		x _{ref}							
	cm	in.	cm	in.	m ²	ft ²	cm	in.						
0.20	25.40	10	127.00	50	0.322	3.47	31.75	12.5						
.30	30.48	12	101.60	40	.309	3.33	25.40	10.0						
.40	30.48	12	76.20	30	.232	2.50	19.05	7.5						
1.00	50.80	20	50.80	20	.258	2.78	12.70	5.0						
3.00	76.20	30	25.40	10	.193	2.08	6.35	2.5						
Notched rectangular wing														
AR	b		c _r		c _t		c _{ref}		b _n		S _{ref}		x _{ref}	
	cm	in.	cm	in.	cm	in.	cm	in.	cm	in.	m ²	ft ²	cm	in.
1.00	50.80	20	38.94	15.33	55.88	22	51.99	20.47	15.24	6	0.258	2.78	13.00	5.12
Cropped-delta wings with c _r = 25.4 cm (10 in.) and $\Lambda = 63^\circ$ (tested at M = 0.6) (see ref. 18)														
AR	λ	b		c _{ref}		S _{ref}		x _{ref}						
		cm	in.	cm	in.	m ²	ft ²	cm	in.					
1.64	0.10	22.89	9.01	17.09	6.73	0.032	0.344	12.57	4.95					
1.33	.20	20.32	8.00	17.50	6.89	.031	.334	12.27	4.83					
1.08	.30	17.80	7.01	18.11	7.13	.029	.316	11.81	4.65					
.86	.40	15.27	6.01	18.87	7.43	.027	.292	11.25	4.43					
Cropped wings with c _t = 33.22 cm (13.08 in.) and $\Lambda = 63^\circ$ (tested at M = 0.2)														
AR	Ω , deg	b		c _r		c _{ref}		S _{ref}		x _{ref}				
		cm	in.	cm	in.	cm	in.	m ²	ft ²	cm	in.			
0.87	0	50.80	20	83.08	32.71	61.72	24.30	0.295	3.18	36.80	14.49			
.74	-40	50.80	20	104.39	41.10	74.96	29.51	.349	3.76	39.37	15.50			
1.07	40	50.80	20	62.31	24.53	48.92	19.26	.242	2.60	34.67	13.65			
Cropped-arrow wing with c _t = 11.81 cm (4.65 in.) and $\Lambda = 63^\circ$ (tested at M = 0.2)														
AR	Ω , deg	b		c _r		c _{ref}		S _{ref}		x _{ref}				
		cm	in.	cm	in.	cm	in.	m ²	ft ²	cm	in.			
1.92	38.86	50.80	20	41.20	16.22	29.21	11.50	0.135	1.45	27.61	10.87			

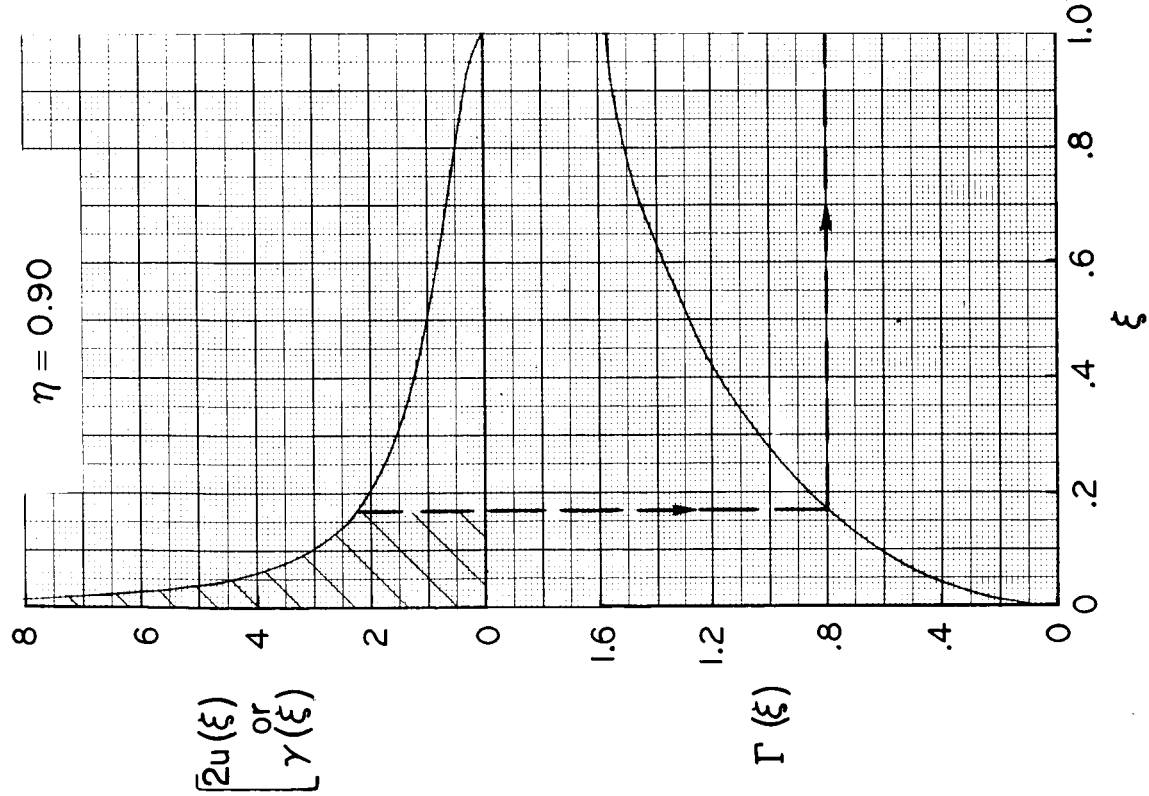
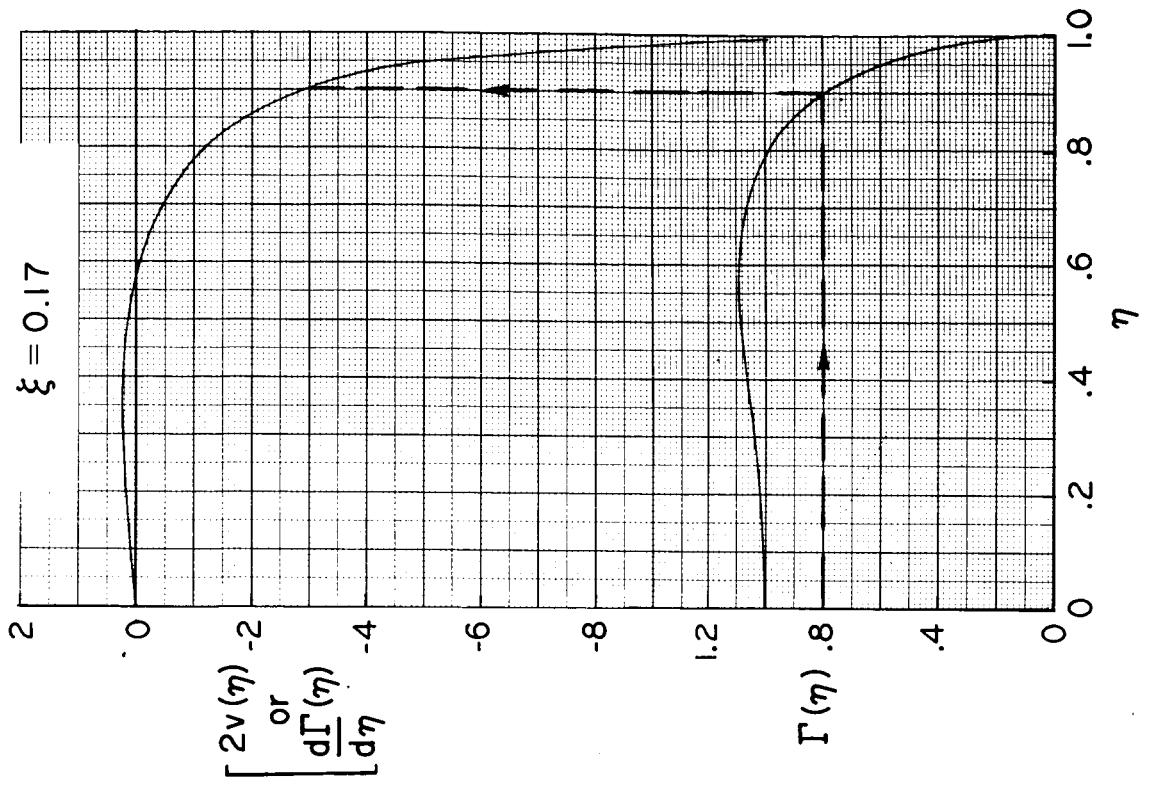


Figure 1.- Potential theory relationship between the backwash and sidewash on a wing with a finite-chord tip.

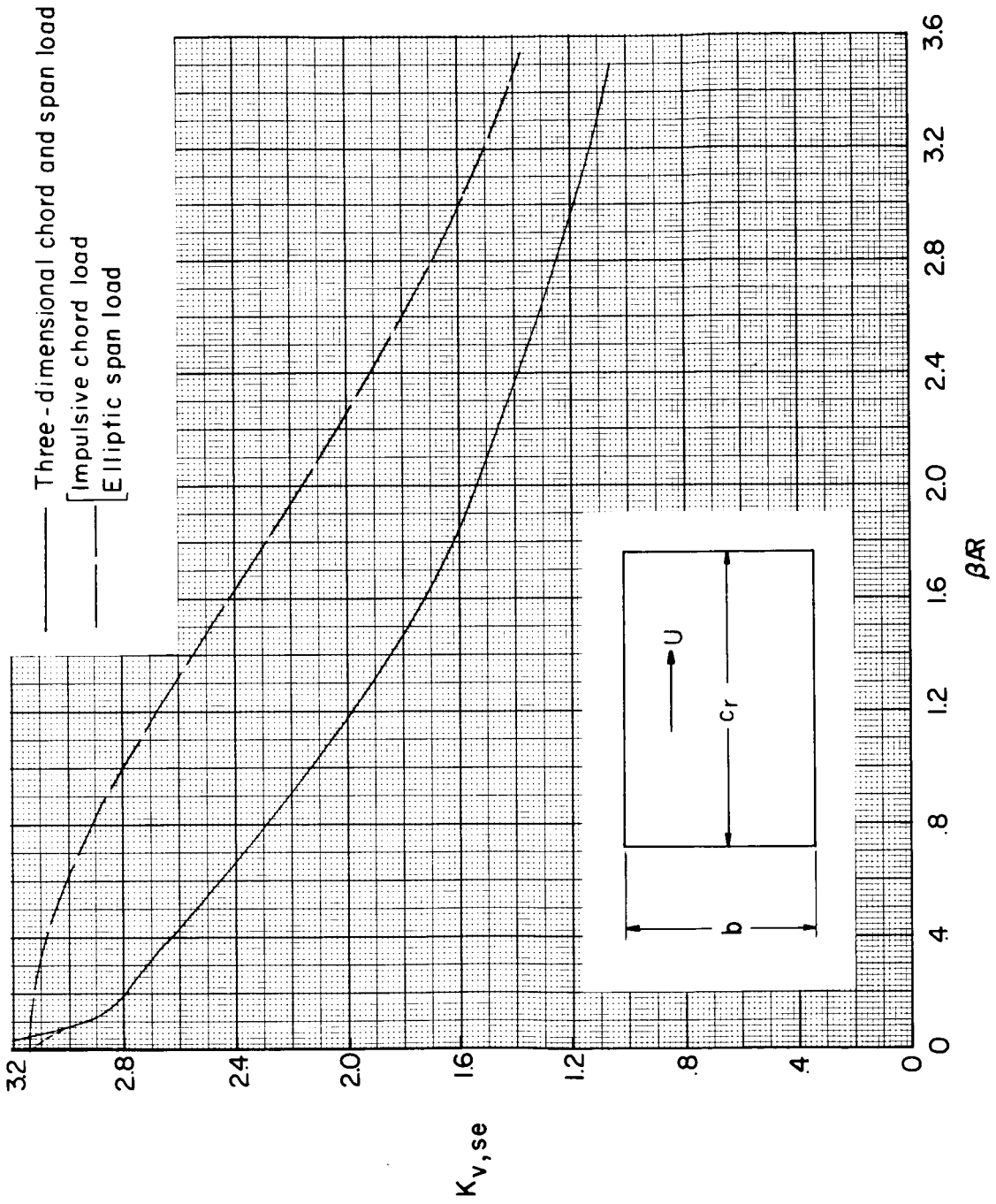


Figure 2.- Effect of chord and span loadings on $K_{v,se}$ of rectangular wings.

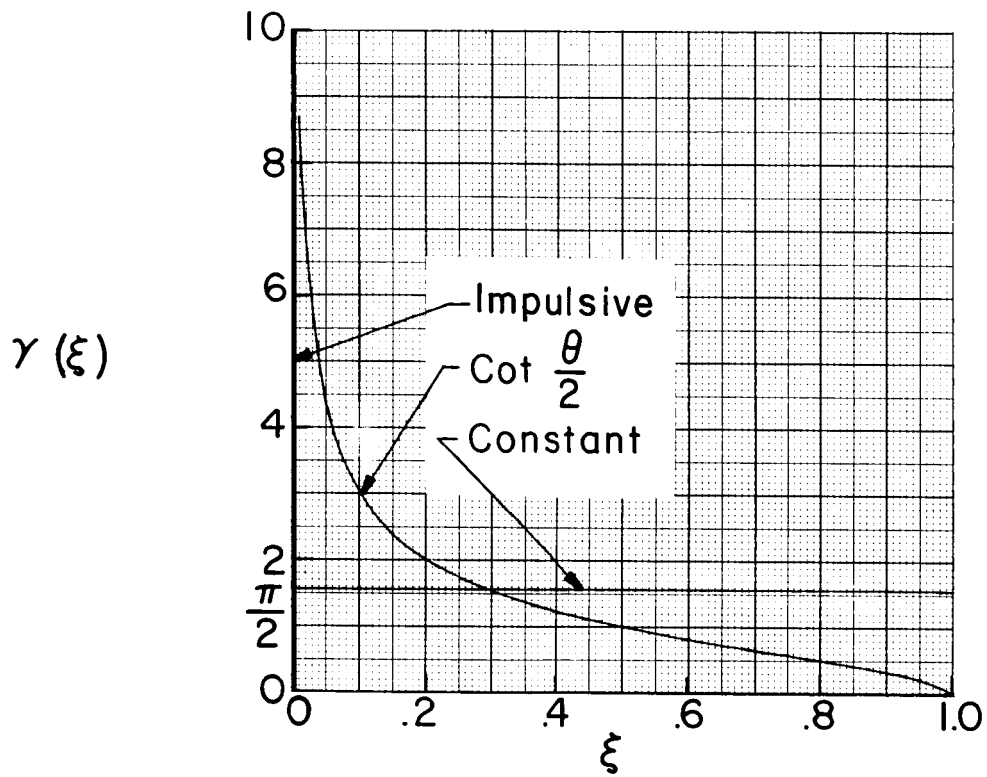


Figure 3.- Different assumed chord-loading distributions in the $R \rightarrow 0$ tip-suction analysis at some η -location.

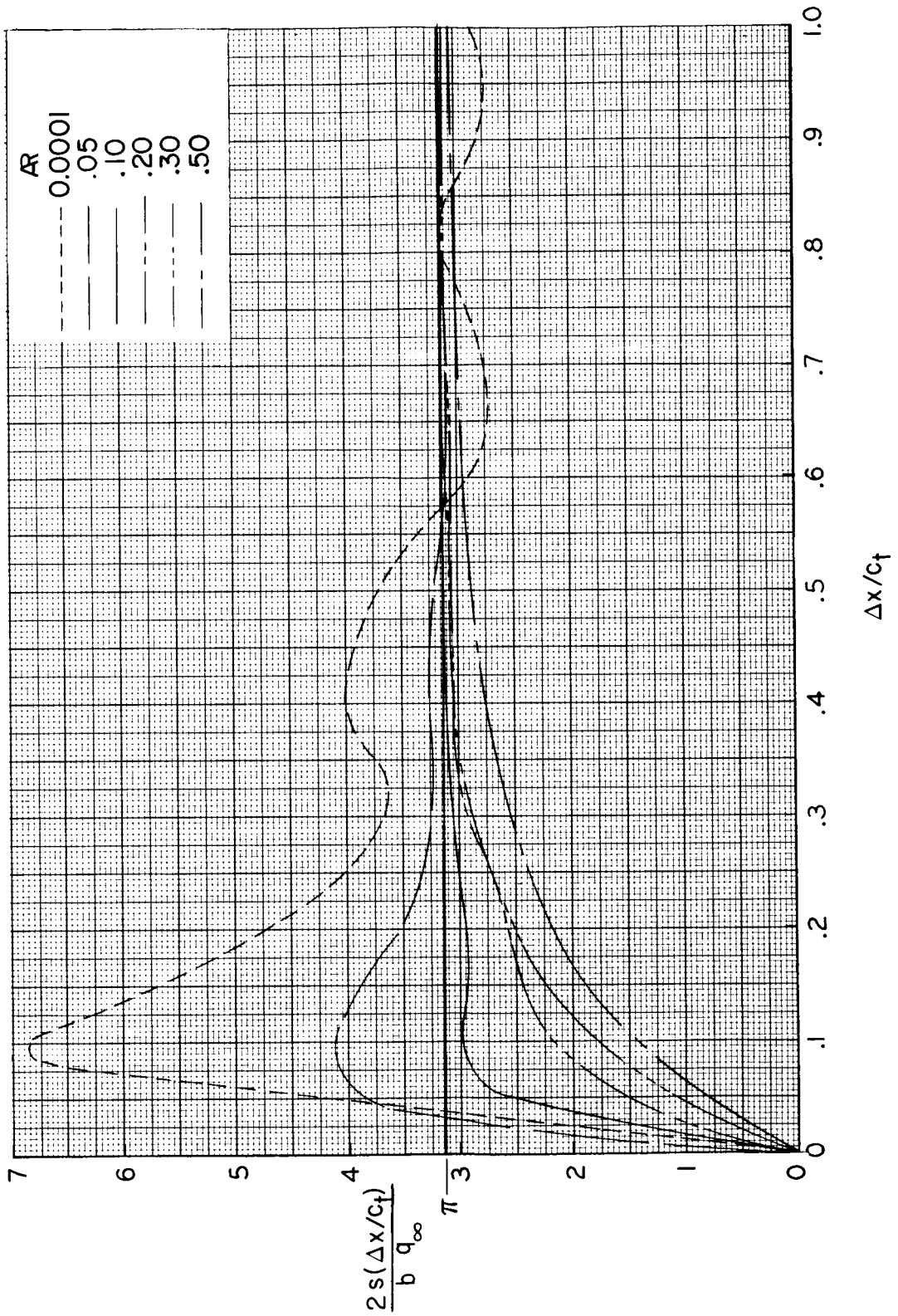


Figure 4.- Effect of aspect ratio on tip-suction distribution of rectangular wings at $M = 0$.

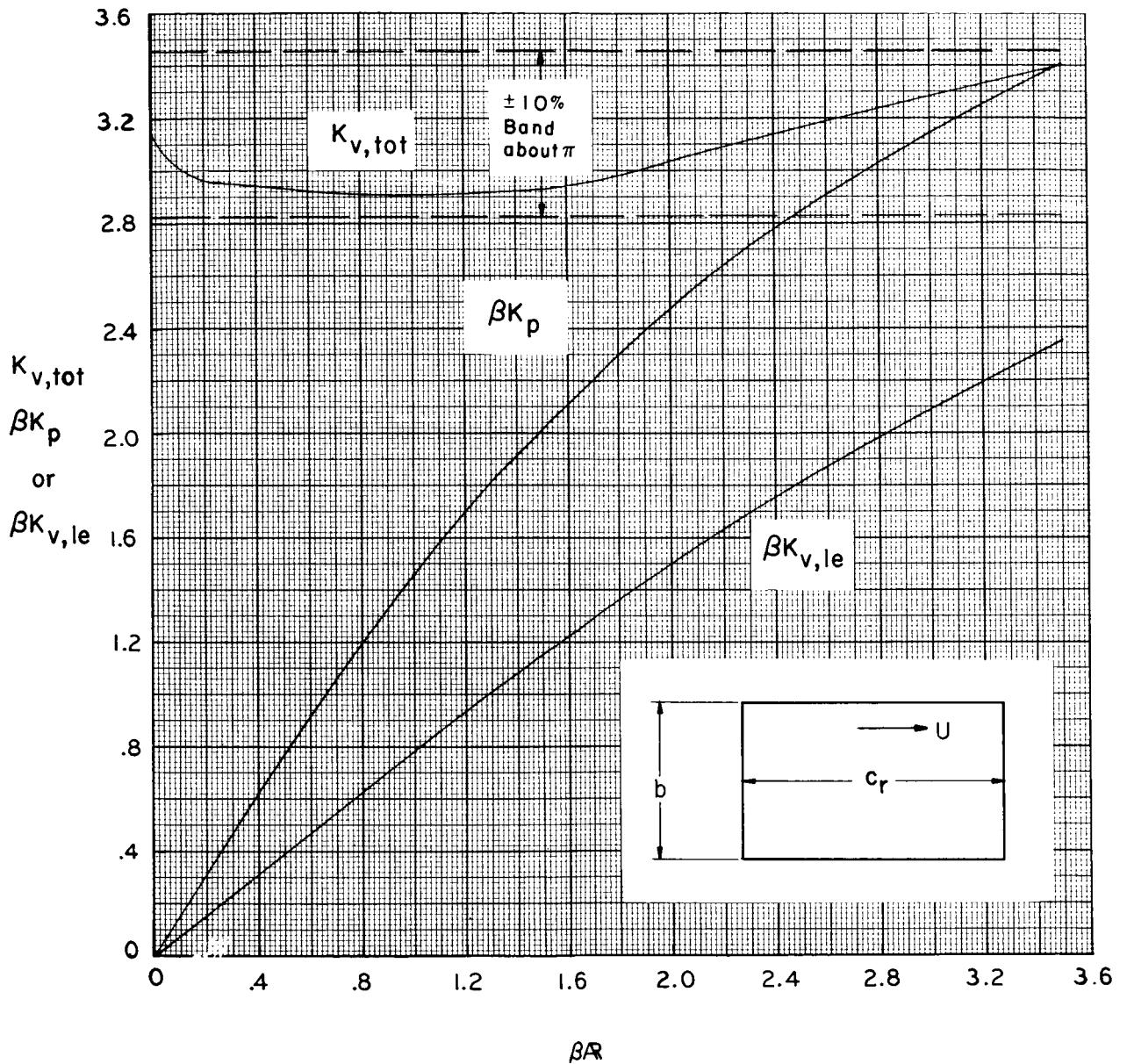


Figure 5.- Variation of βK_p , $\beta K_{v,le}$, and $K_{v,tot}$ with aspect ratio and Mach number for rectangular wings.

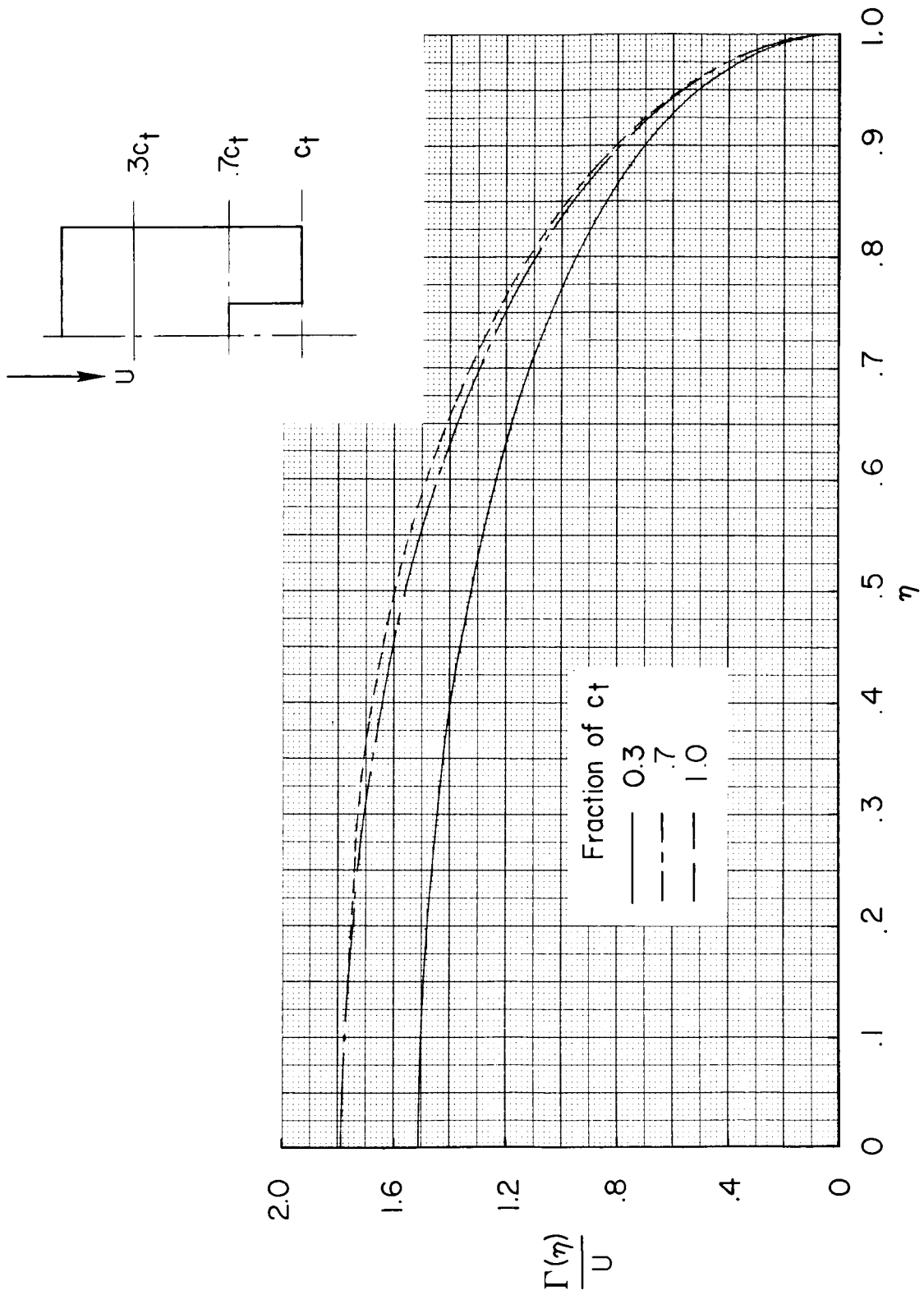


Figure 6.- Effect of fractional chordwise location on accumulated $\Gamma(\eta)/U$ spanwise distribution for a notched wing of $AR = 1.0$ at $M \approx 0$.

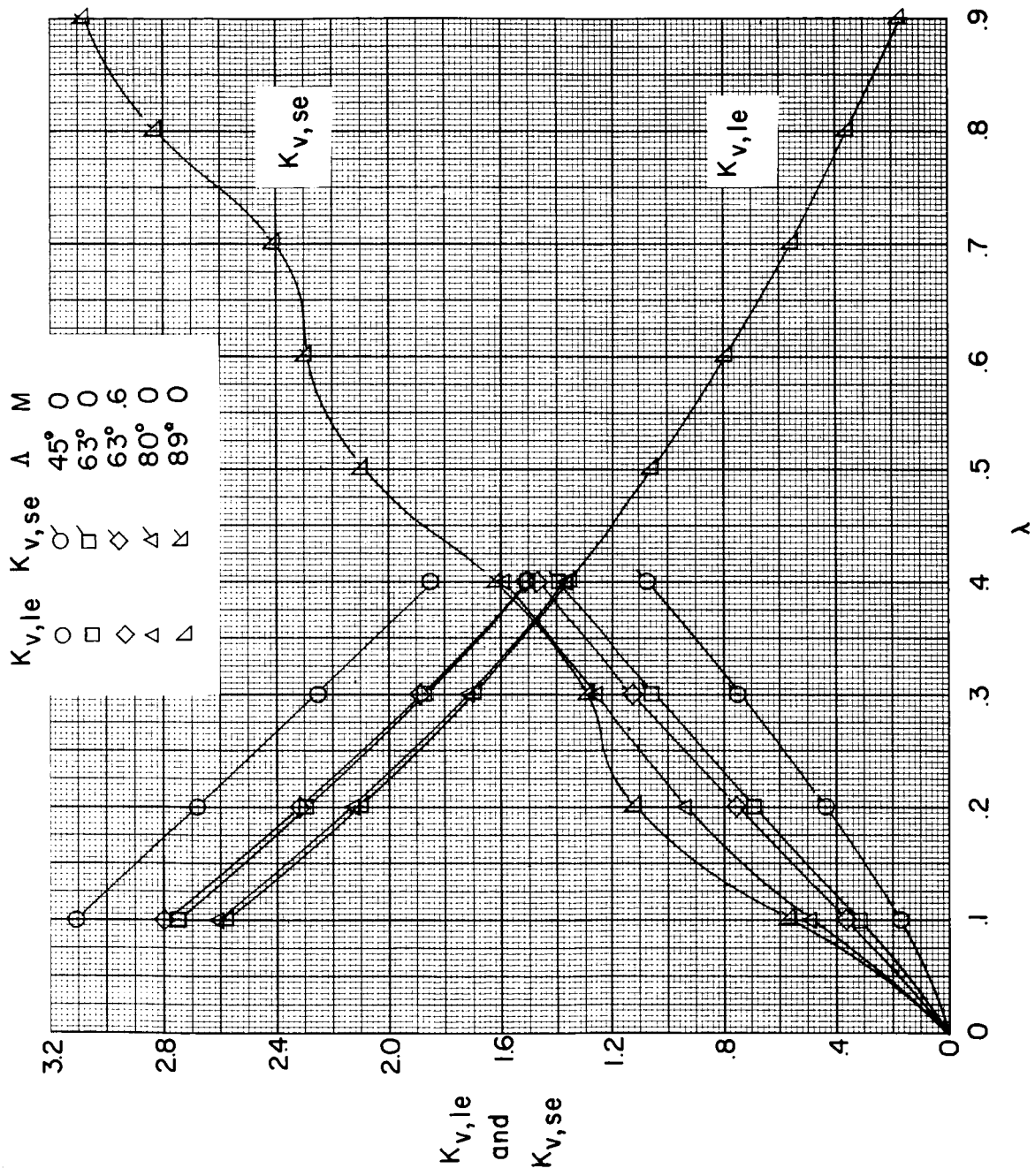


Figure 7.- Effect of leading-edge sweepback and Mach number on $K_{v,le}$ and $K_{v,se}$ for cropped-delta wings.

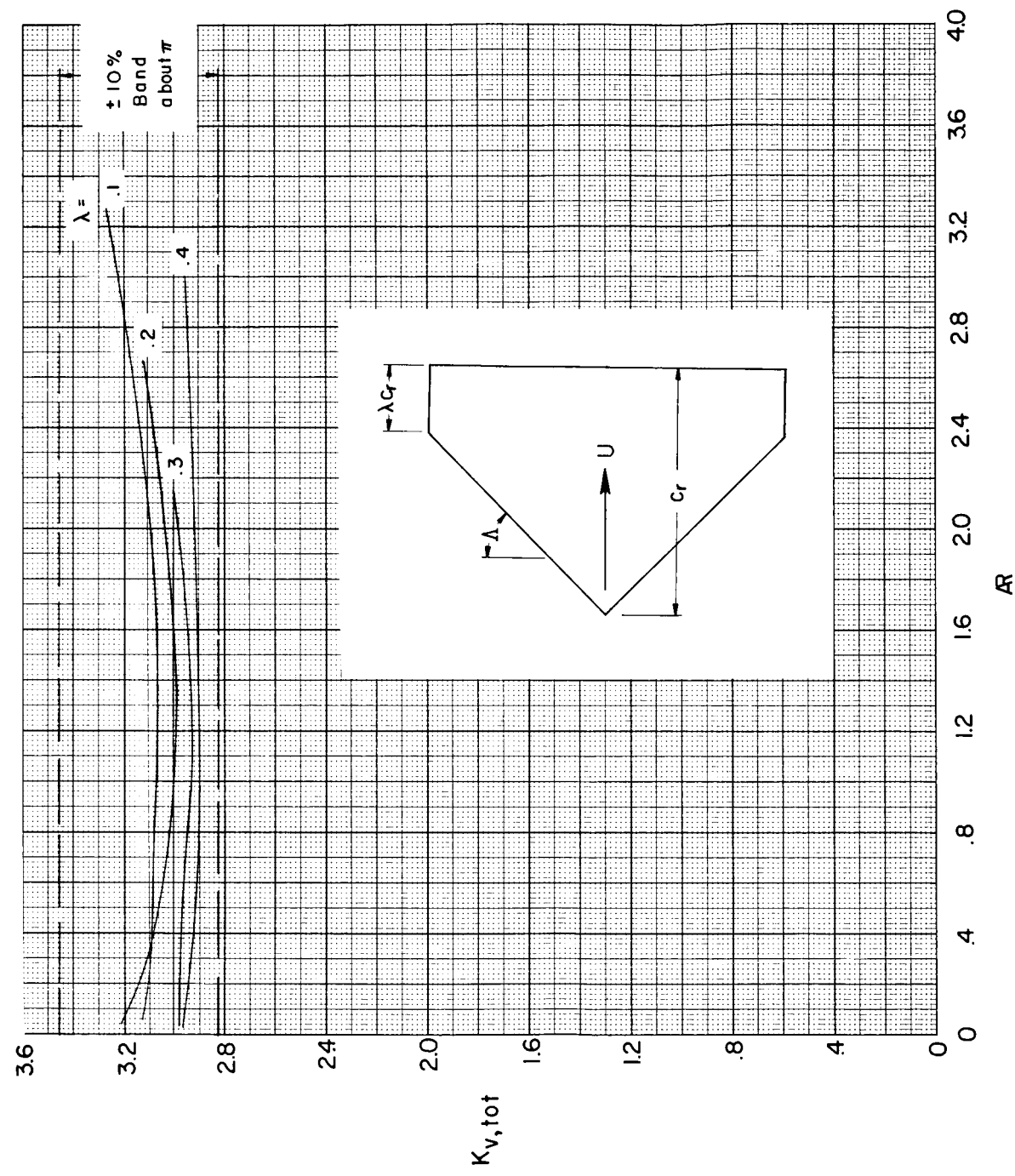


Figure 8.- Effect of taper ratio on $K_{v,tot}$ for cropped-delta wings at $M = 0$.

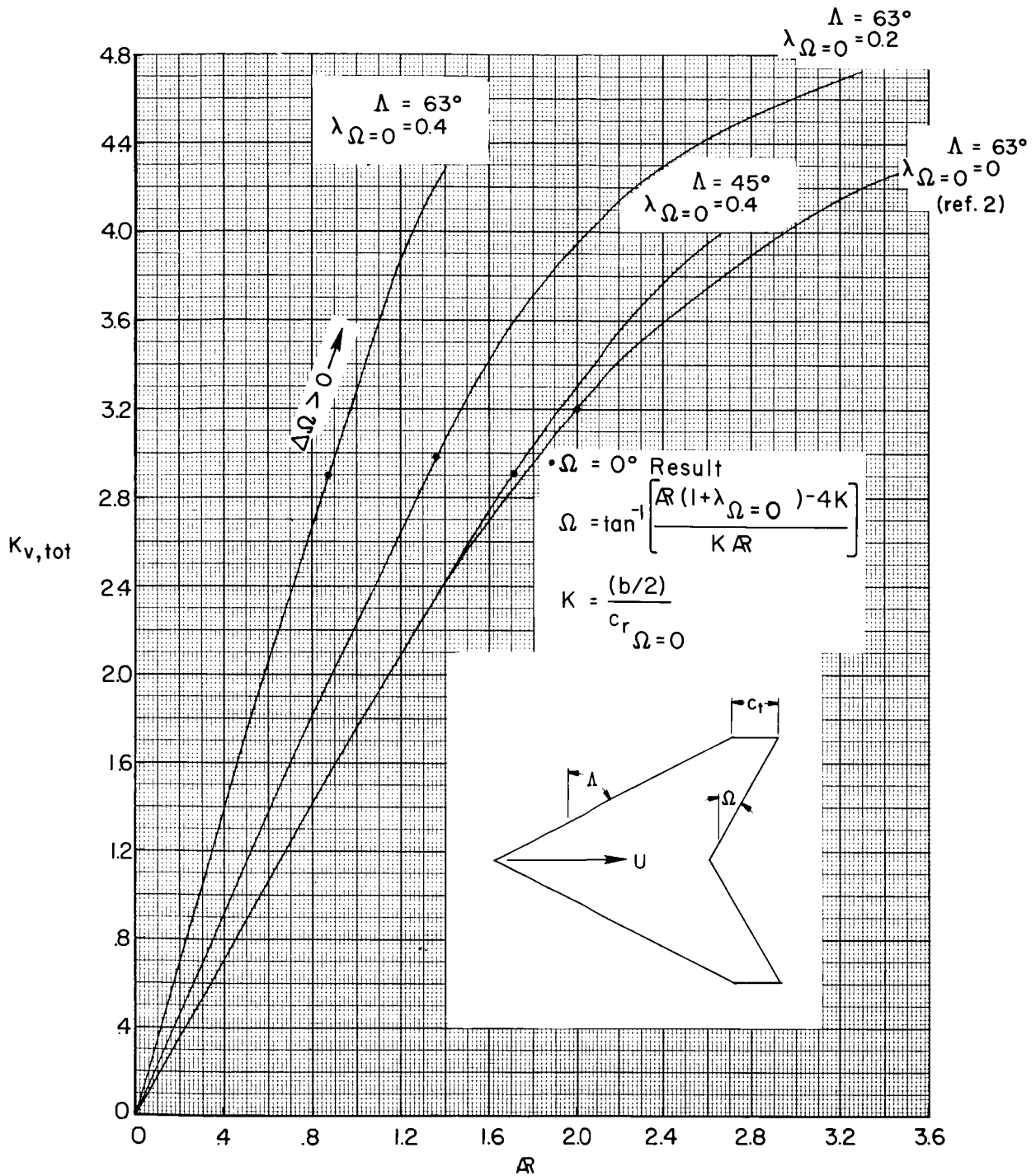
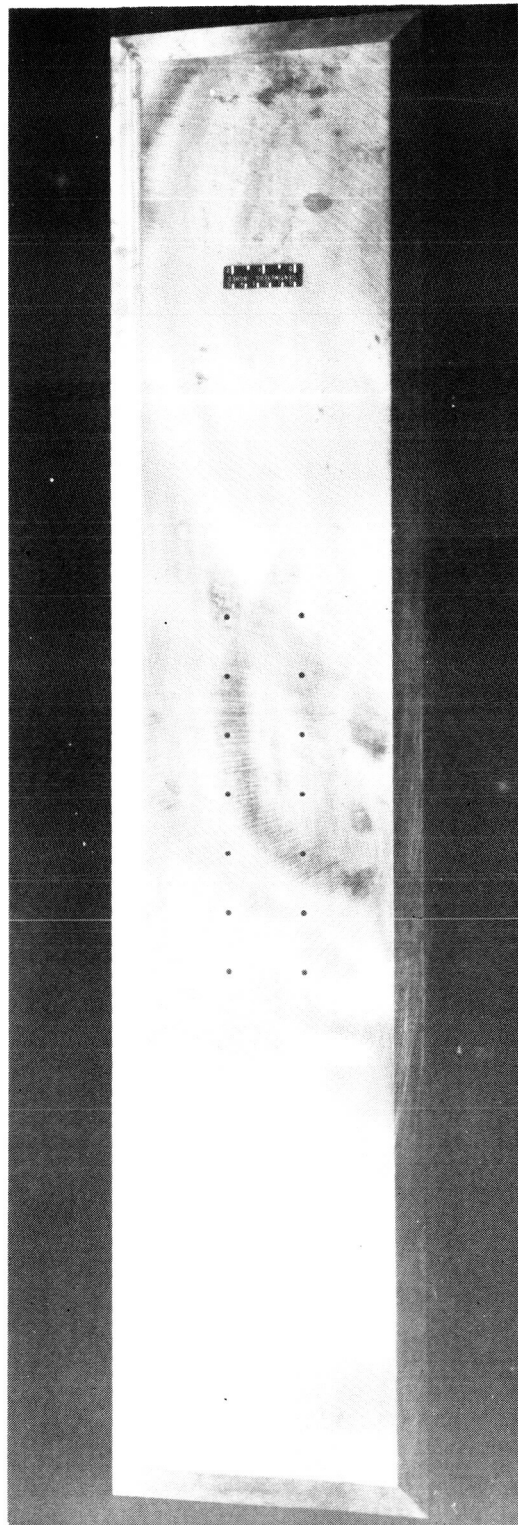


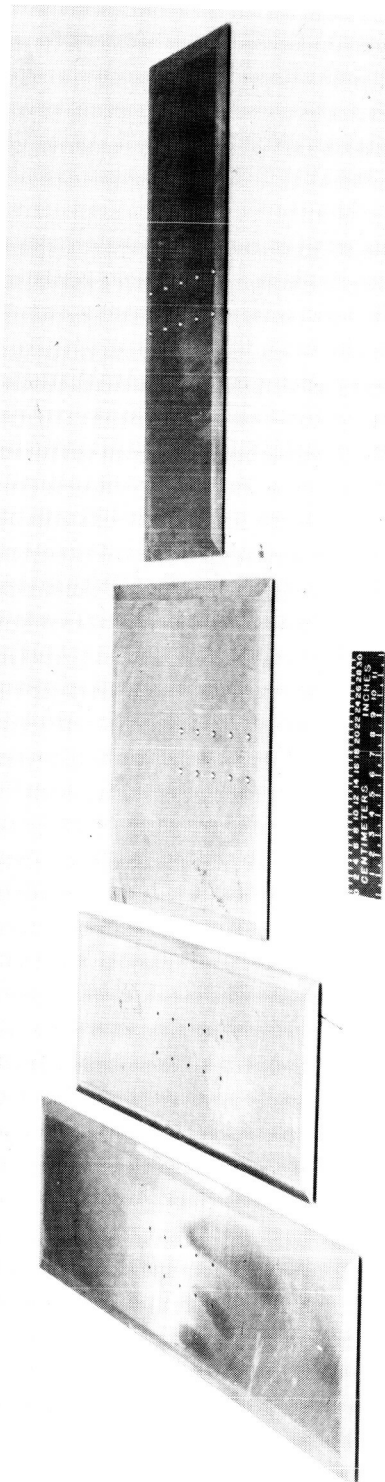
Figure 9.- Effect of leading-edge sweepback and tip chord on $K_{v,tot}$ for selected families of cropped wings at $M = 0$.



L-73-5728

(a) $AR = 0.2$.

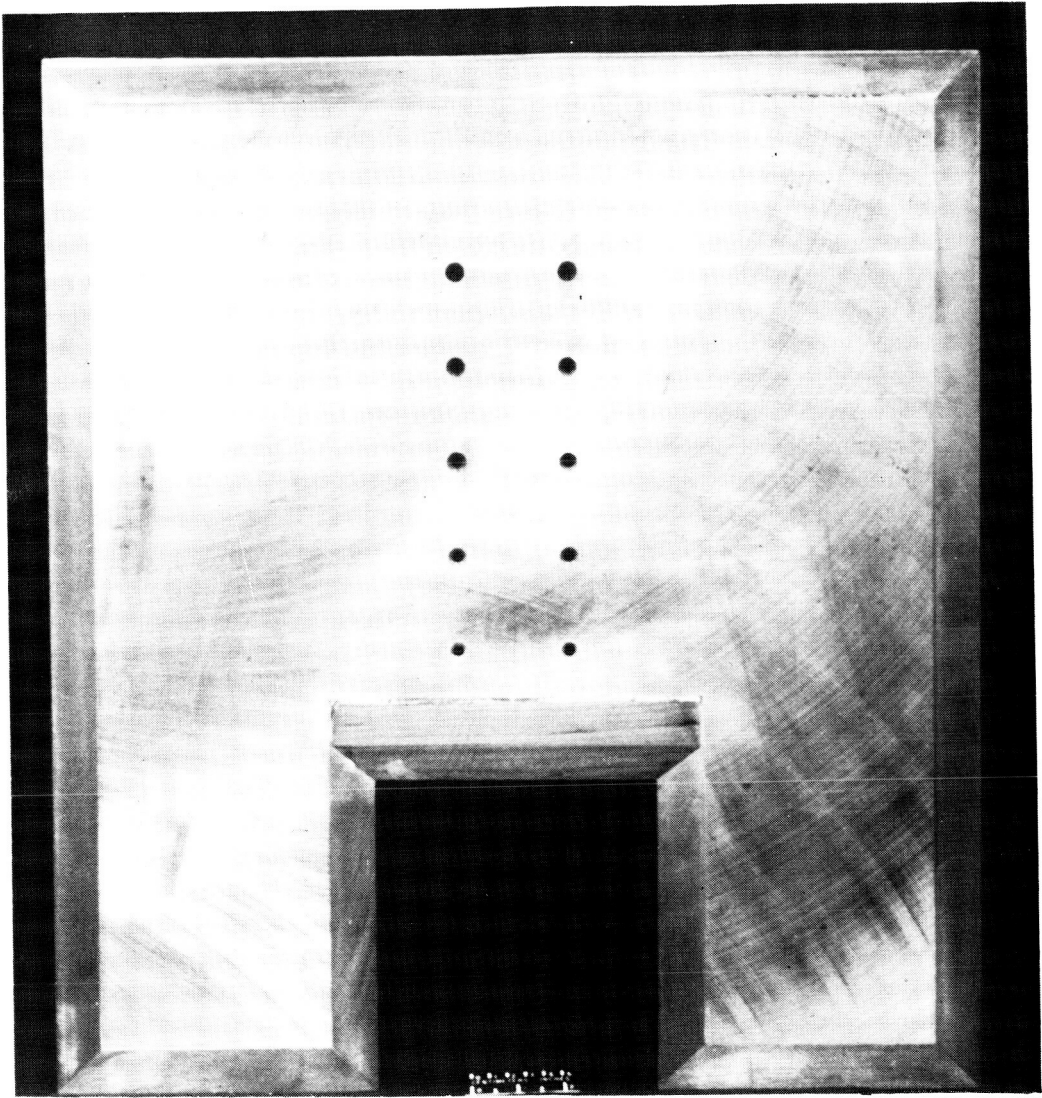
Figure 10.- Photographs of the sharp-edged unswept wing models tested.



L-72-2737

(b) $AR = 0.3$; $AR = 0.4$; $AR = 1.0$; $AR = 3.0$.

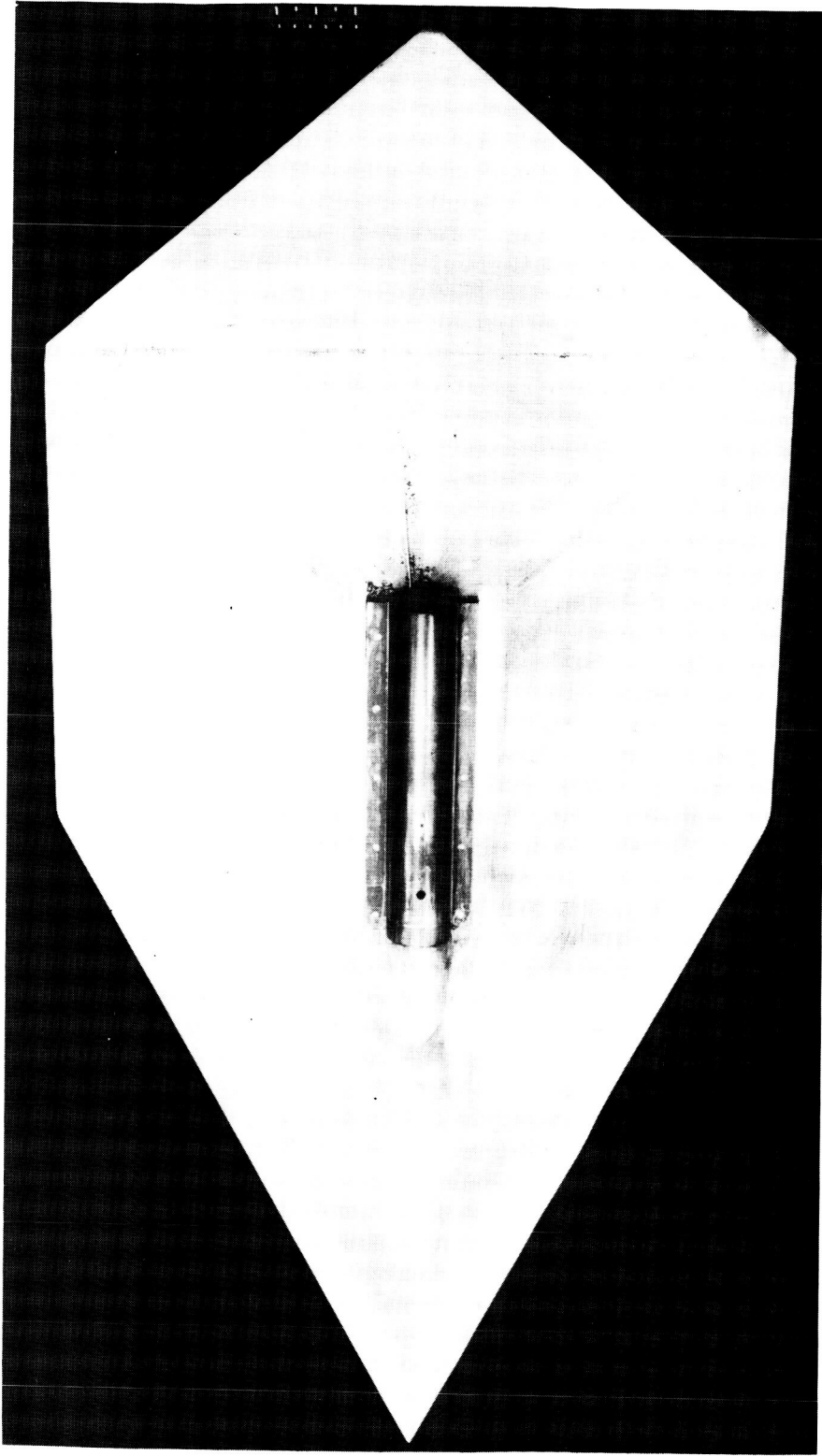
Figure 10.- Continued.



L-73-5568

(c) $\mathcal{AR} = 1.0$; $\lambda = 1.435$.

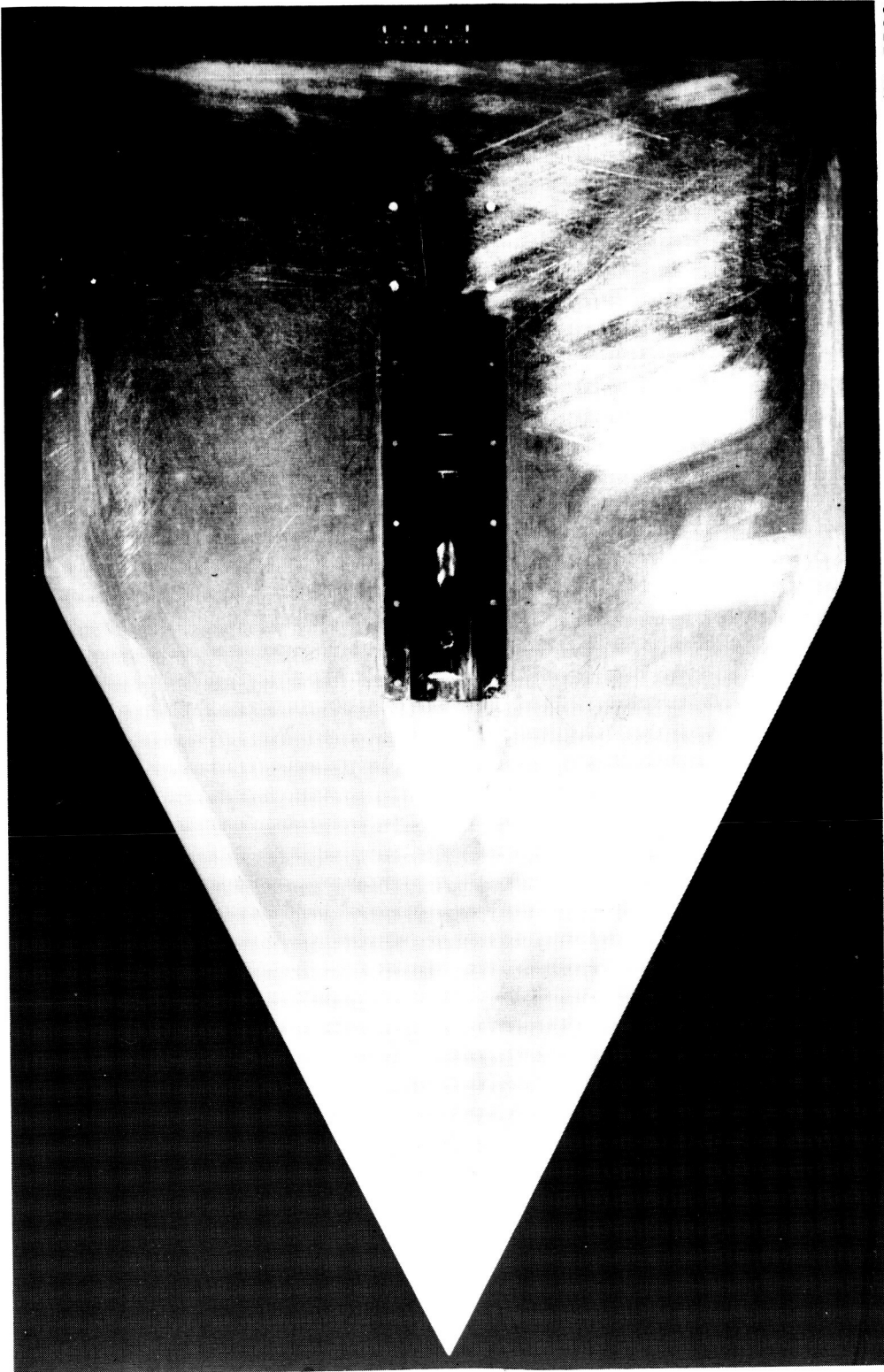
Figure 10.- Concluded.



L-73-5570

(a) Cropped diamond.

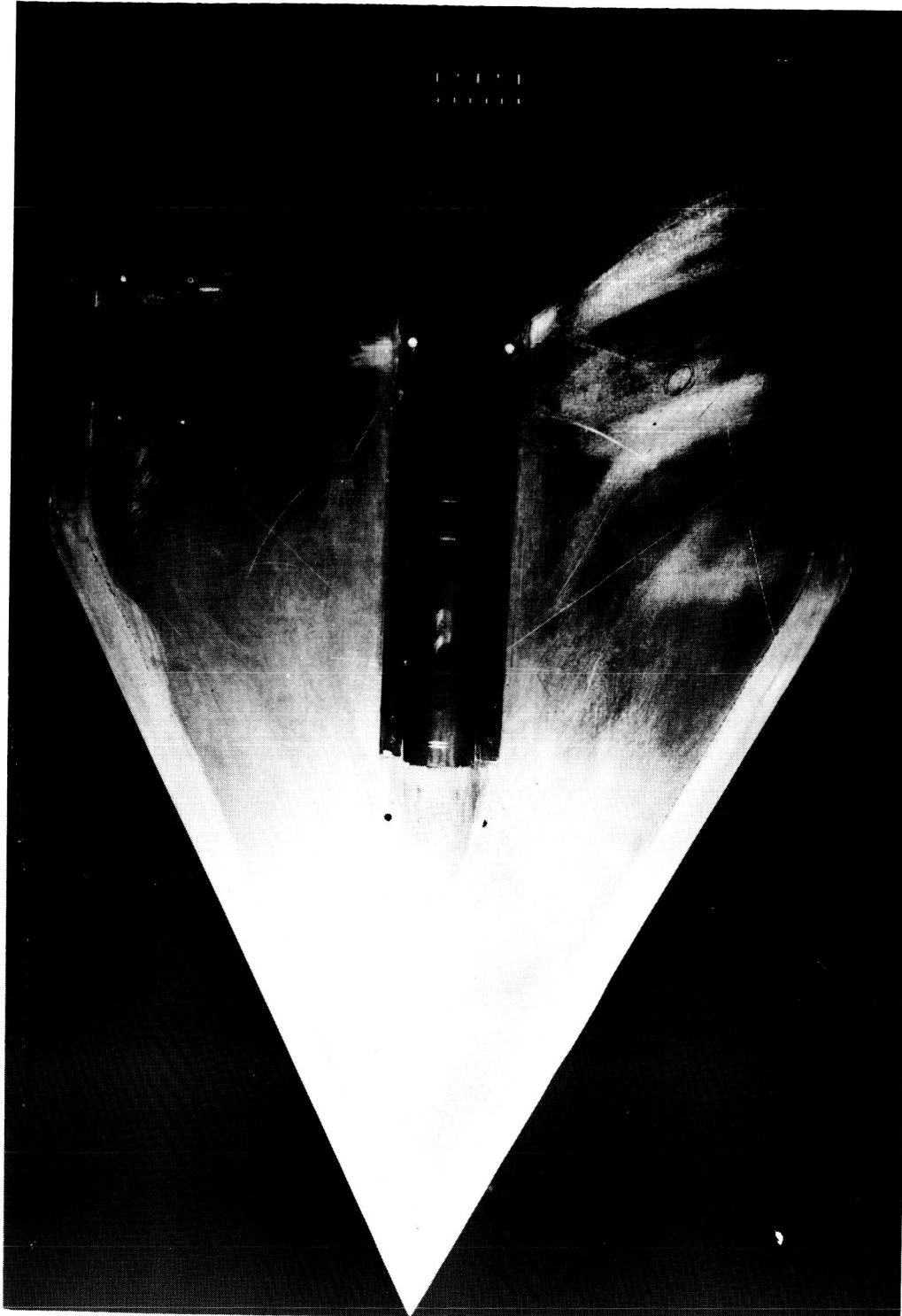
Figure 11.- Photographs of the sharp-edged cropped wing models tested.



L-73-5569

(b) Cropped delta.

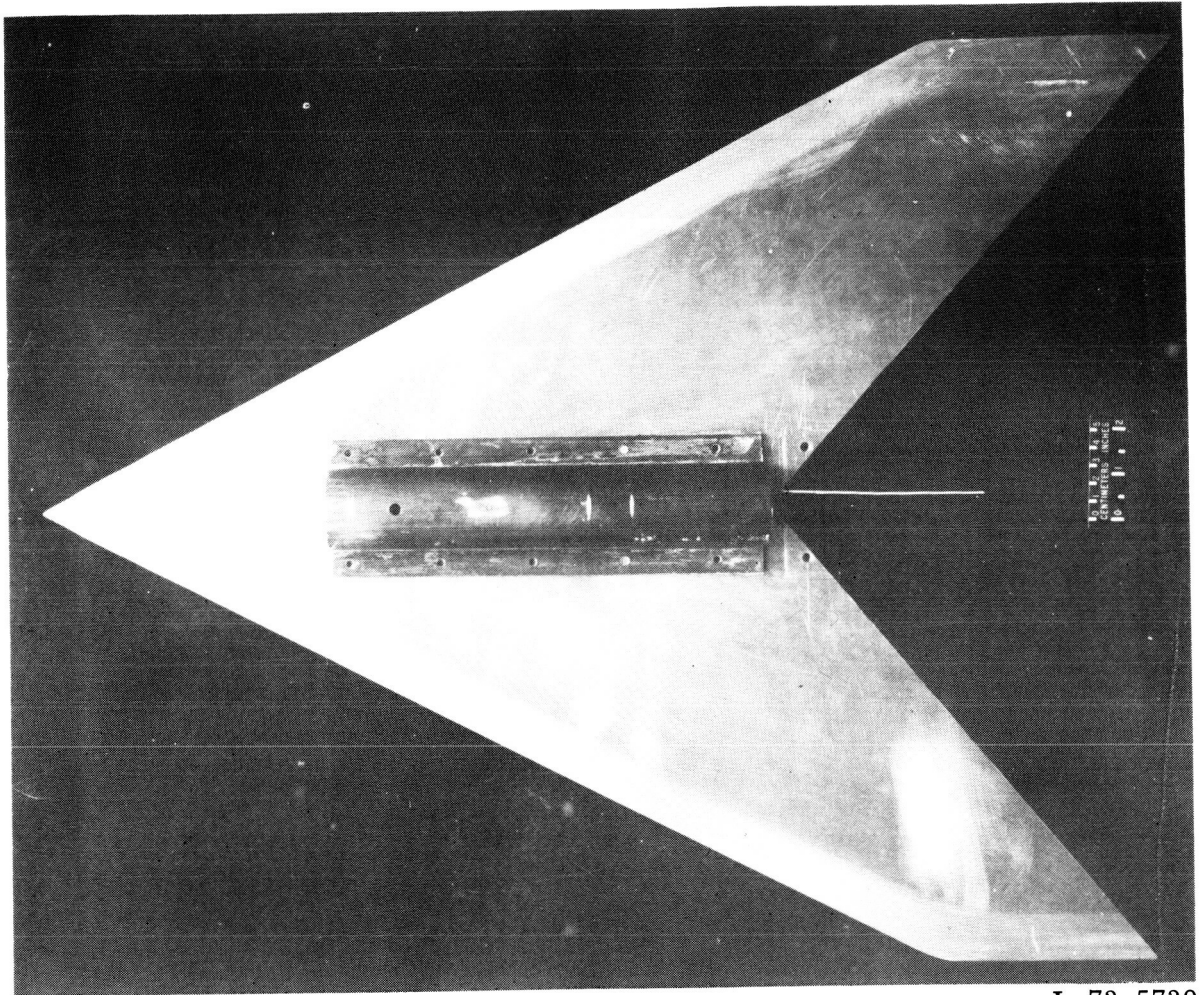
Figure 11. - Continued.



L-73-5727

(c) Cropped arrow (1).

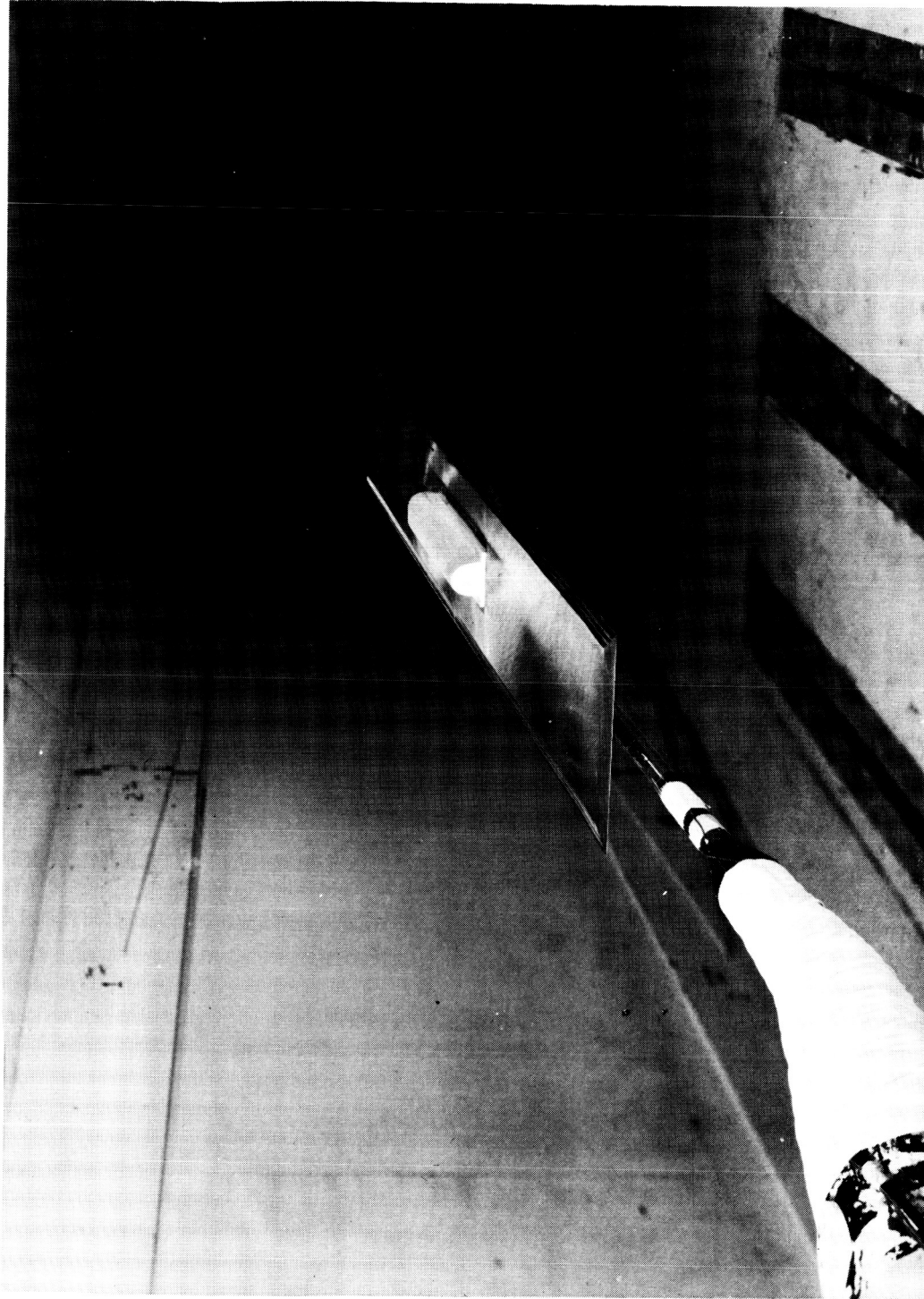
Figure 11.- Continued.



L-73-5730

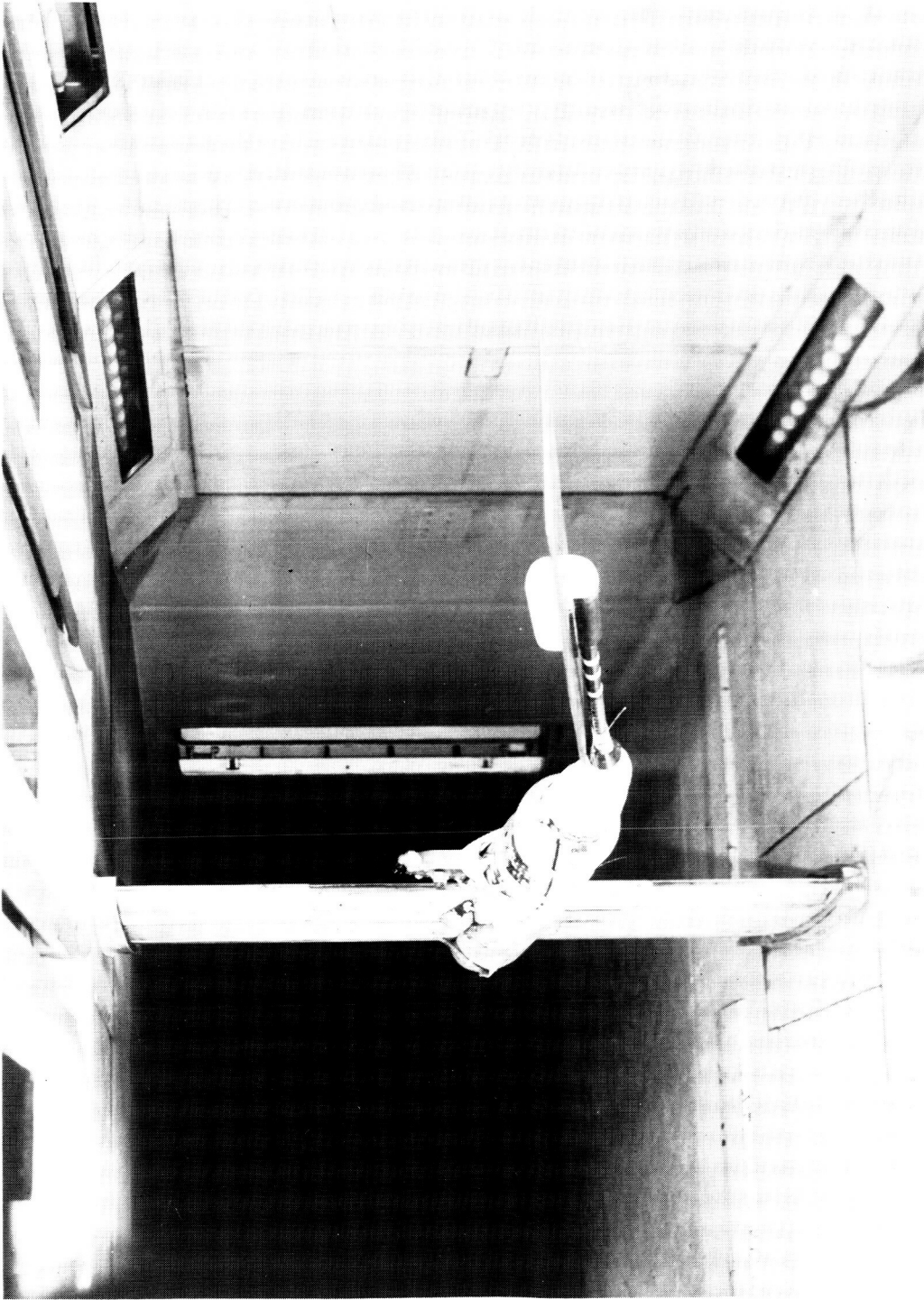
(d) Cropped arrow (2).

Figure 11.- Concluded.



(a) Three-quarter rear view.

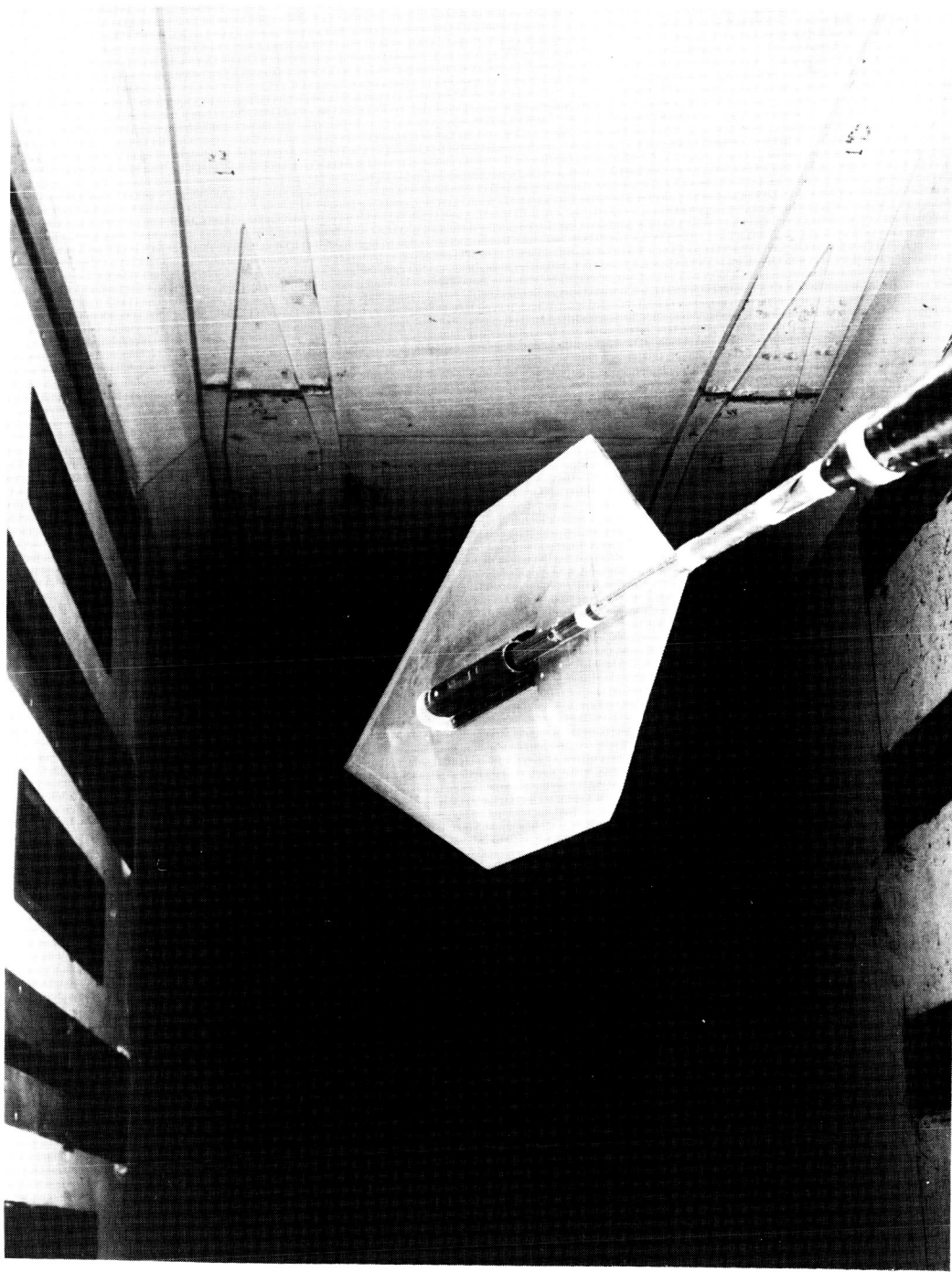
Figure 12. - Typical wind-tunnel setup for a sharp-edged unswept wing.



L-72-2738

(b) Three-quarter front view.

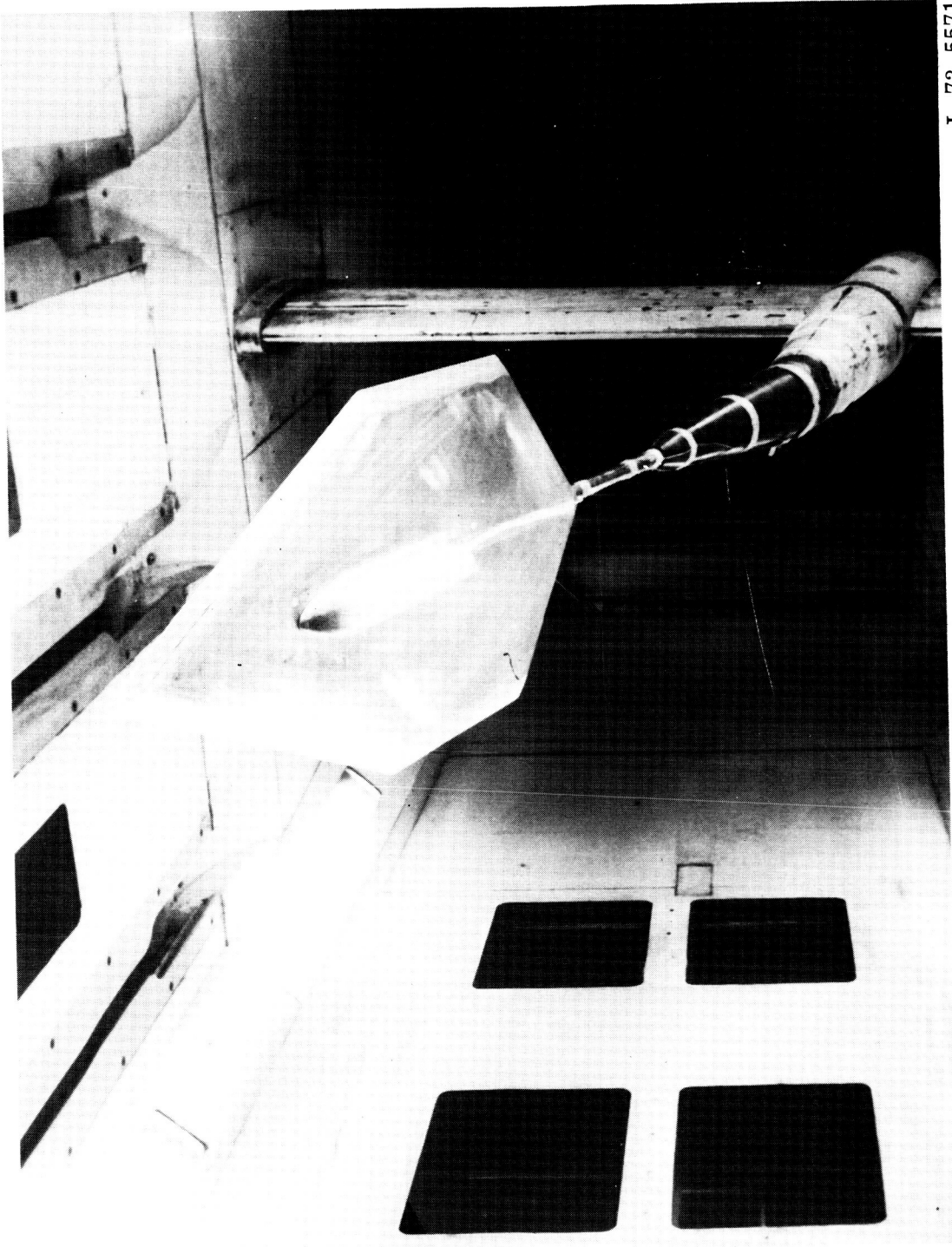
Figure 12. - Concluded.



L-73-5572

(a) Three-quarter rear view.

Figure 13.- Typical wind-tunnel setup for a sharp-edged cropped wing.



L-73-5571

(b) Three-quarter front view.

Figure 13.- Concluded.

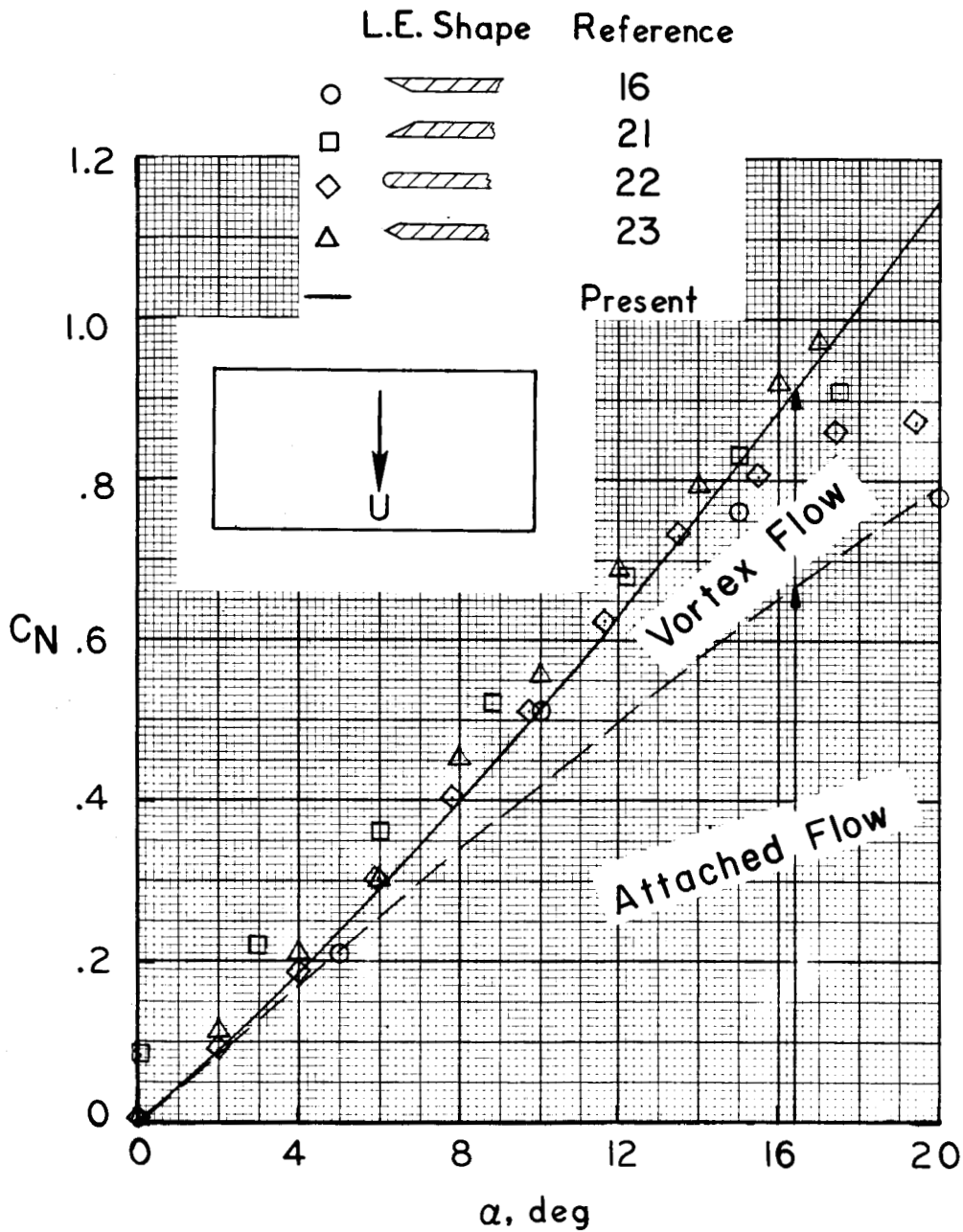


Figure 14.- Effect of edge shaping on C_N for $AR = 2$ rectangular wings at $M \approx 0$.

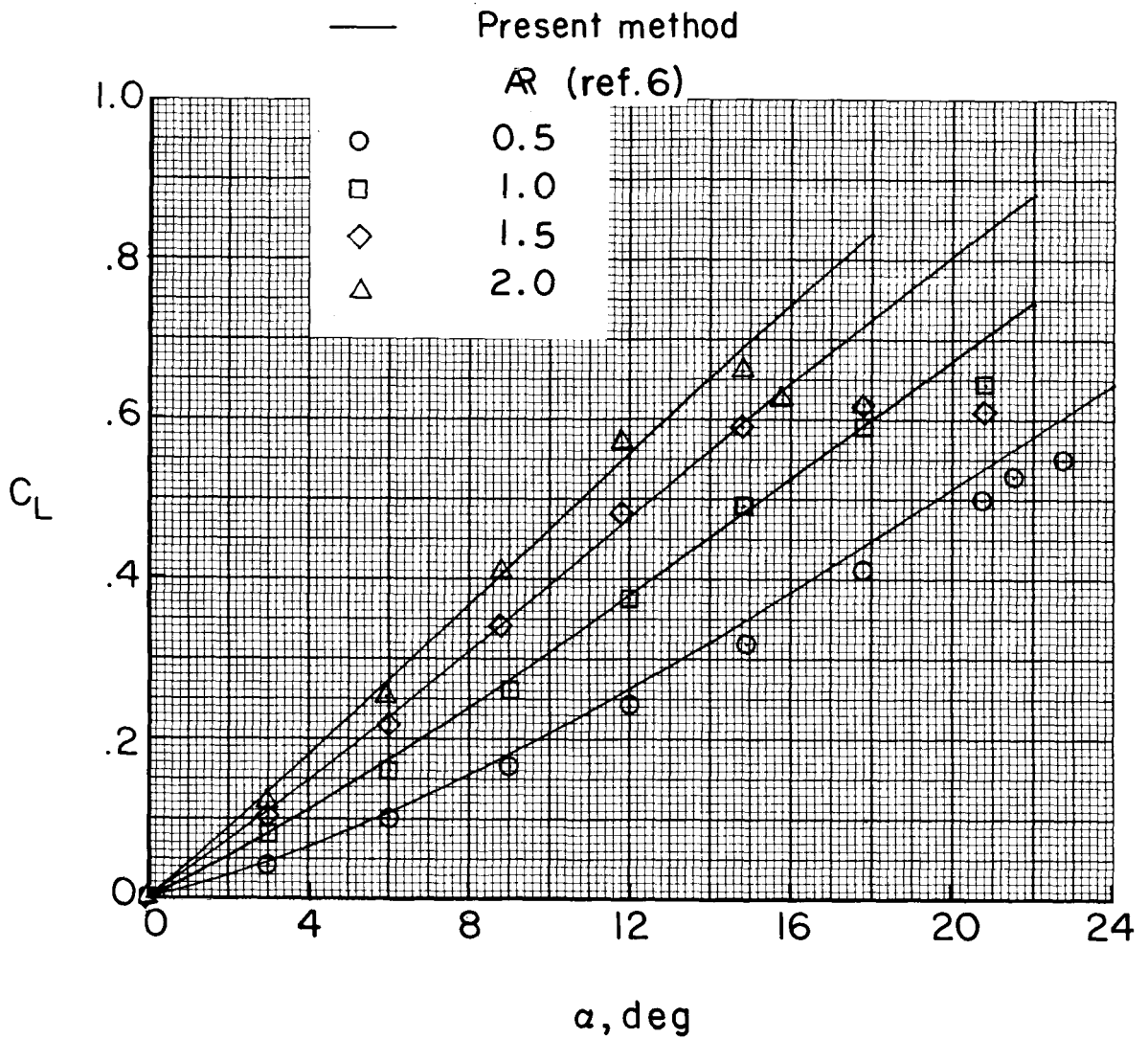
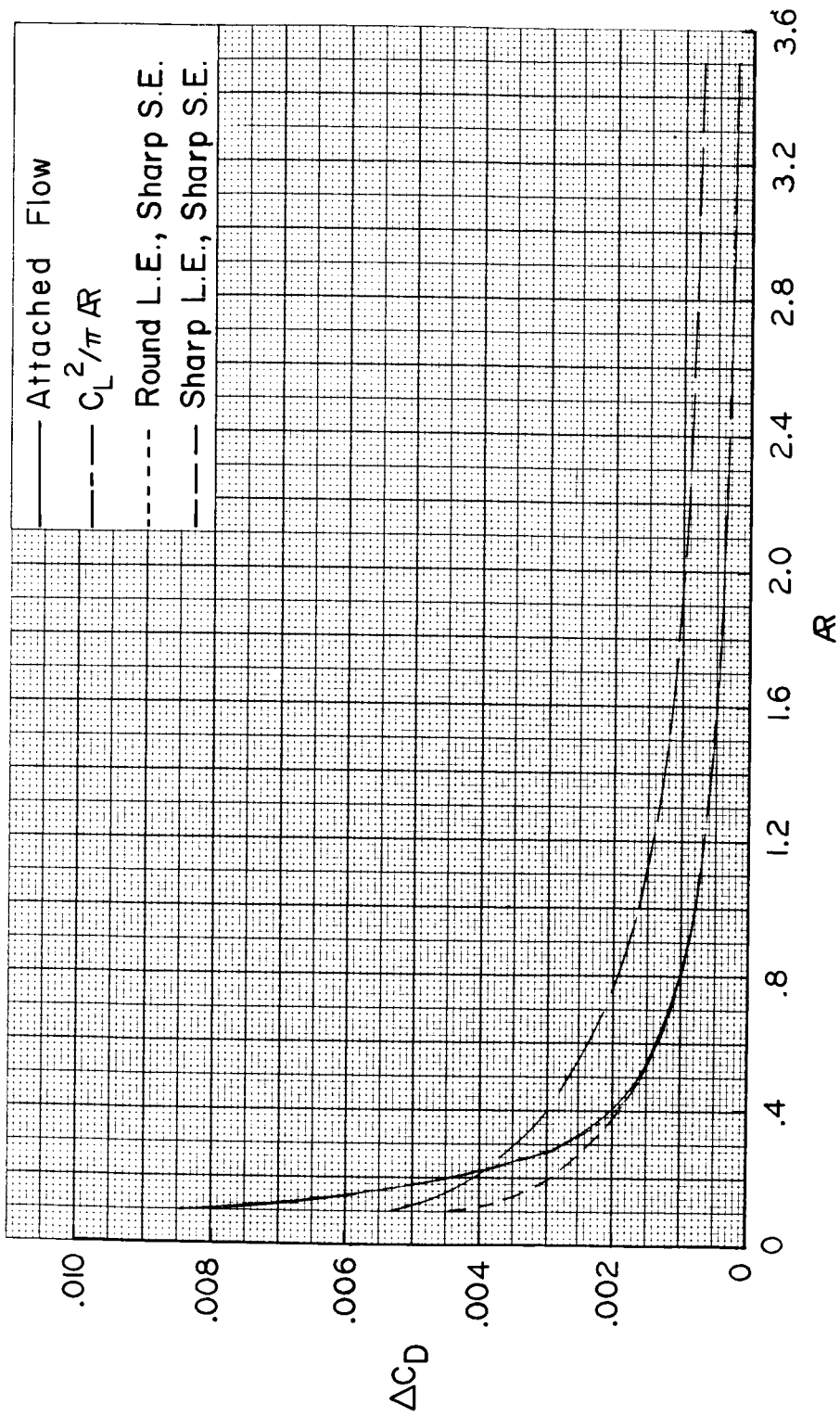
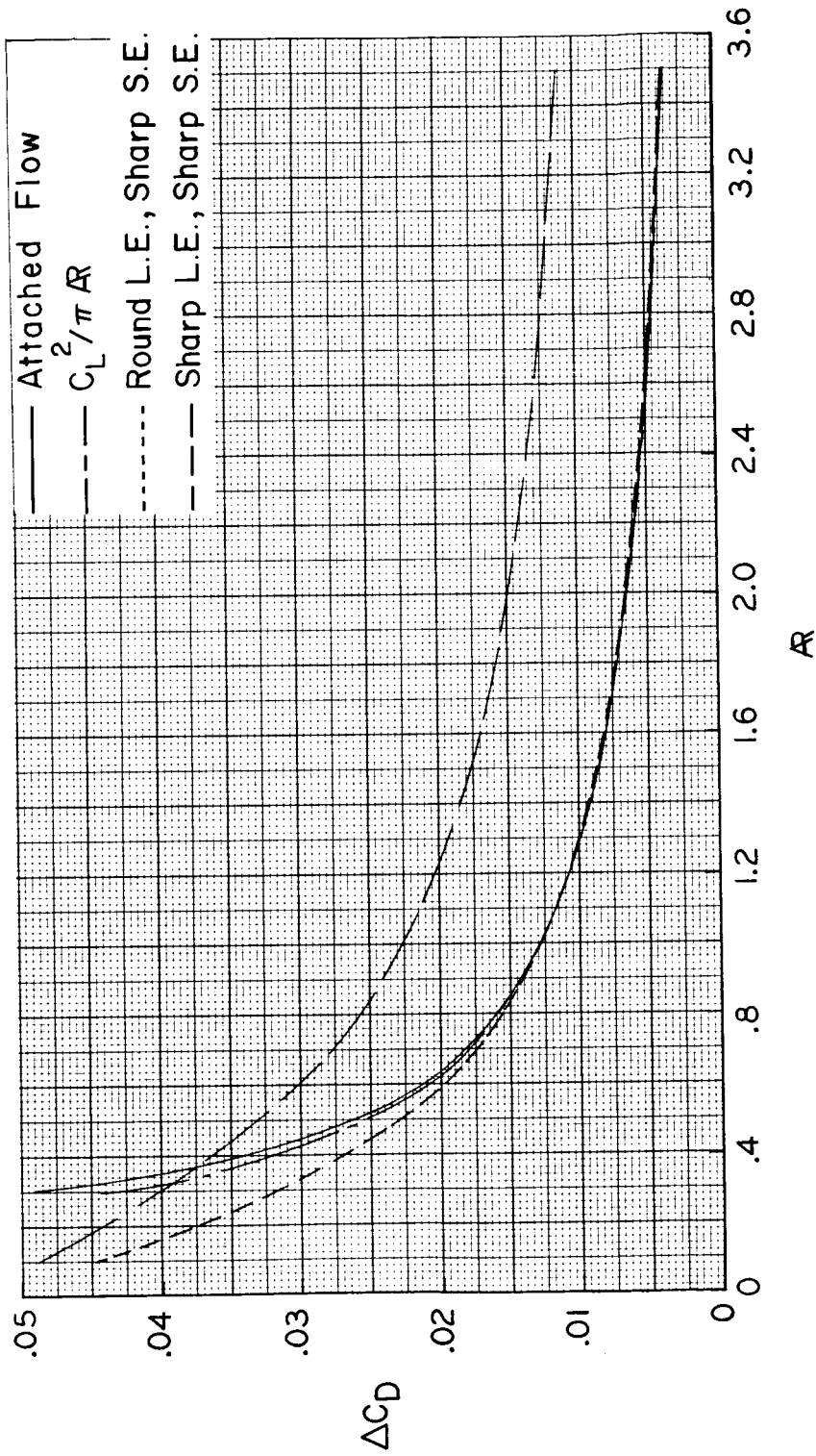


Figure 15.- Effect of aspect ratio on C_L for rectangular wings with round leading edges and vertical sides at $M \approx 0$ (Göttingen 409 airfoil; thickness ratio = 0.126).



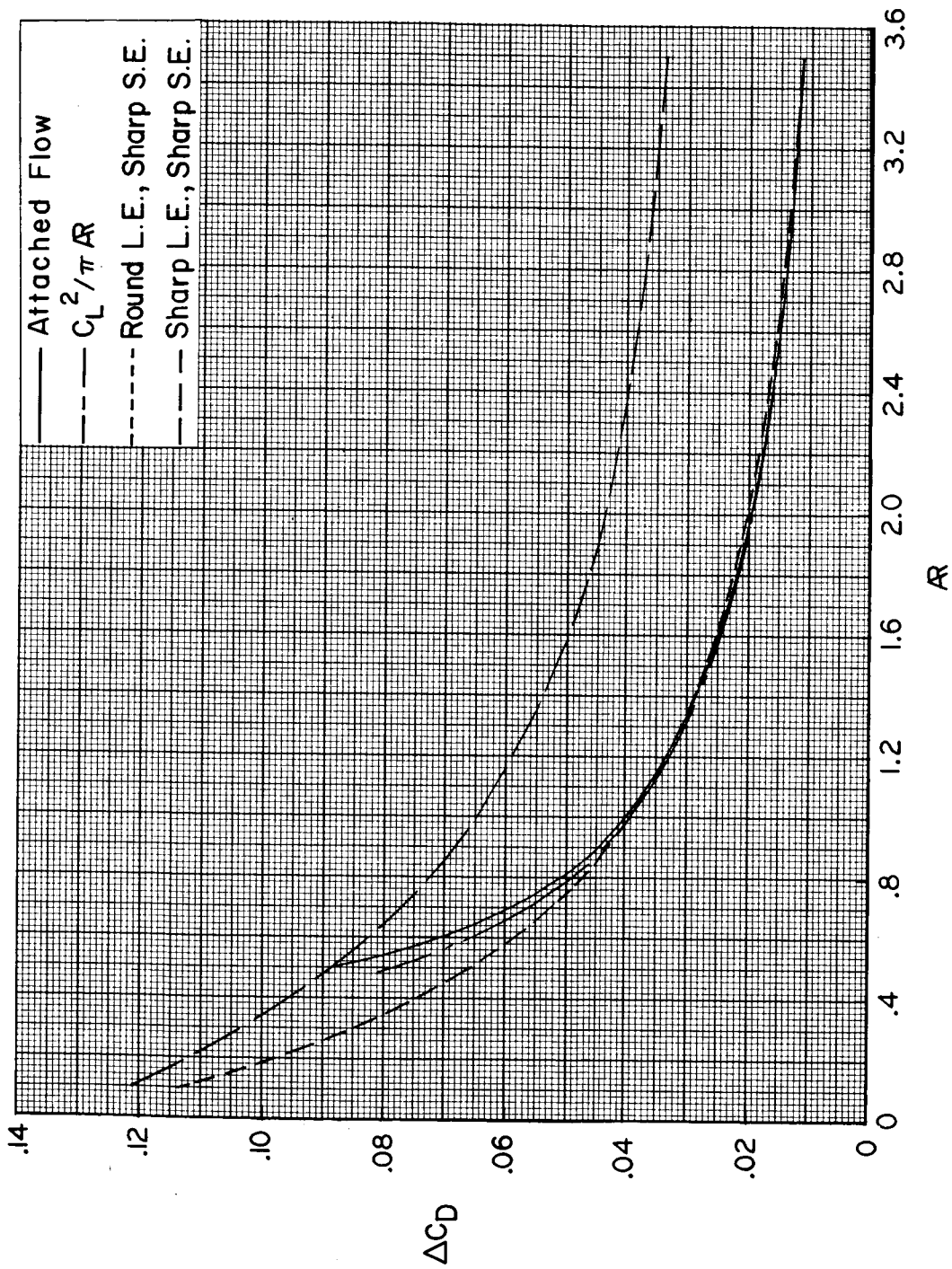
(a) $C_L = 0.05$.

Figure 16.- Drag variation of rectangular wing associated with different edge condition assumptions at $M = 0$.



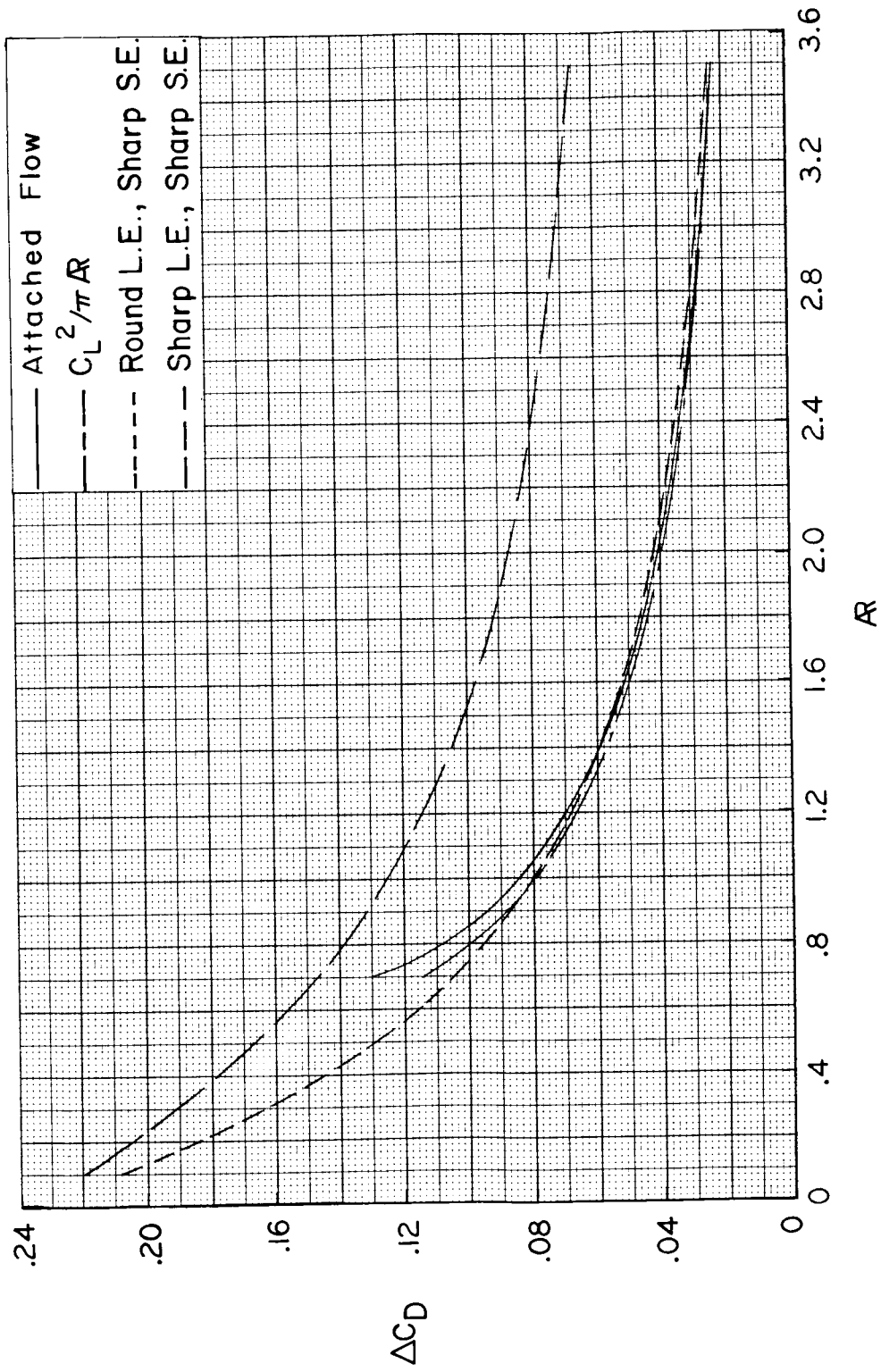
(b) $C_L = 0.20$.

Figure 16. - Continued.



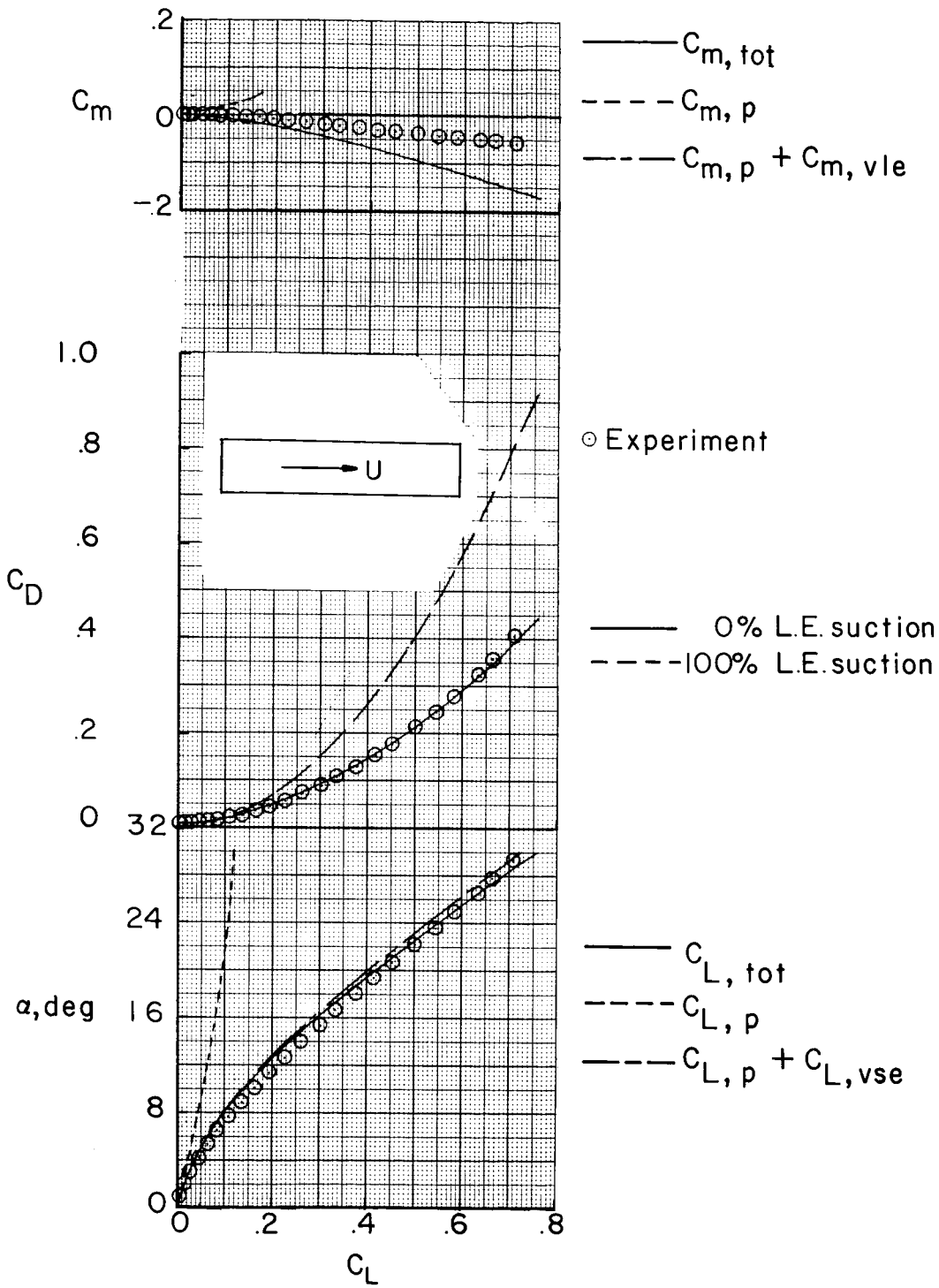
(c) $C_L = 0.35$.

Figure 16.- Continued.



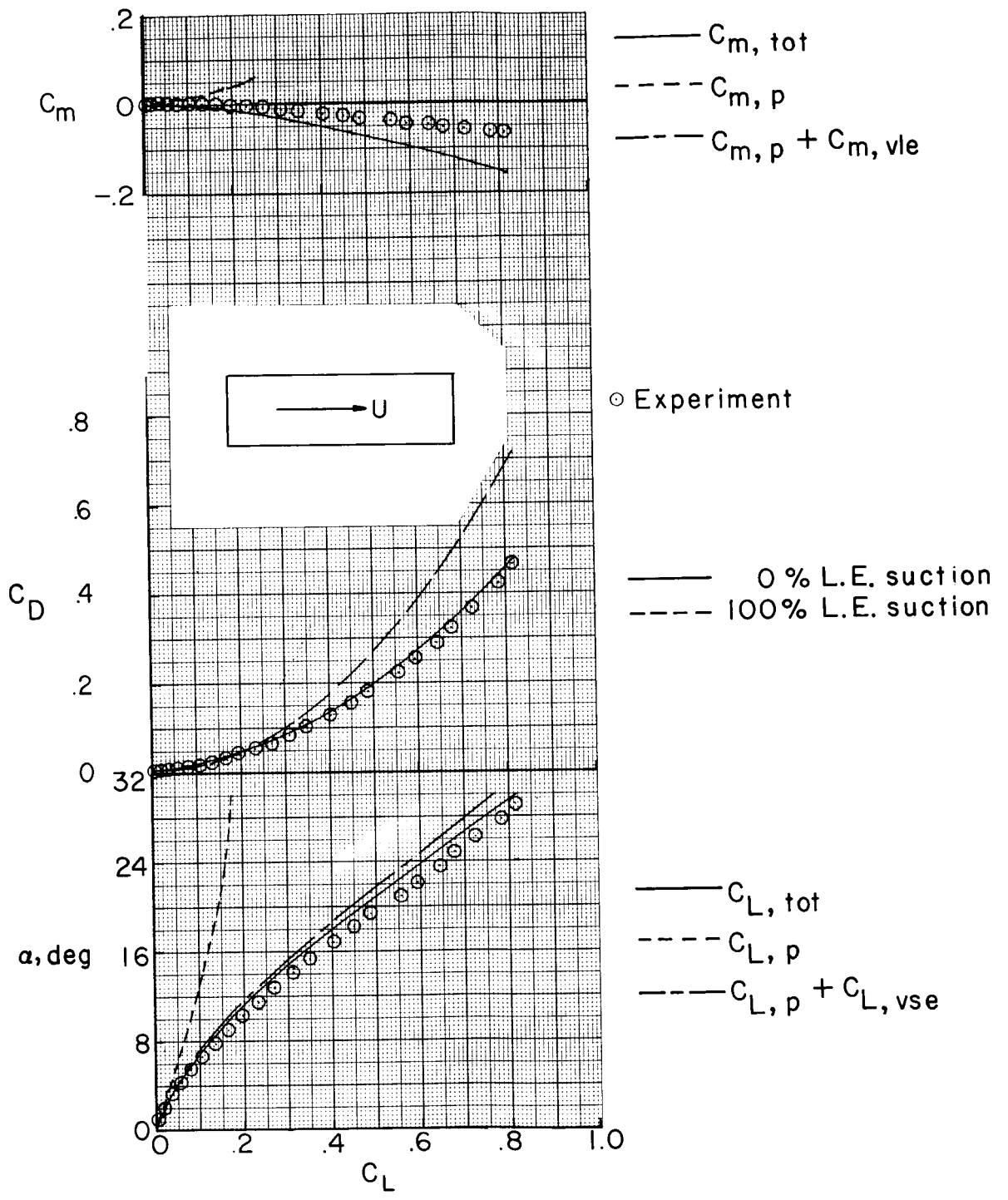
(d) $C_L = 0.50$.

Figure 16.- Concluded.



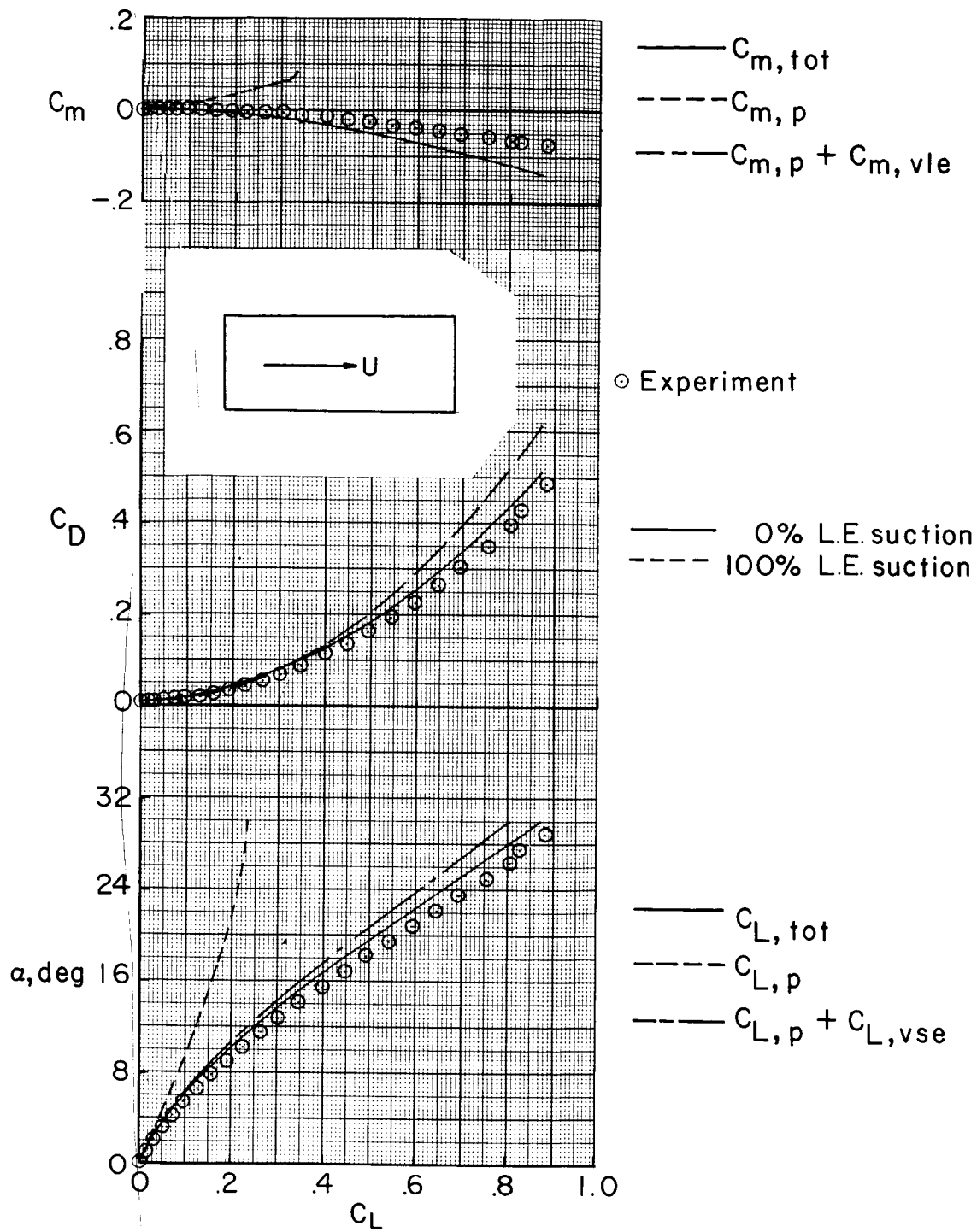
(a) $AR = 0.2$.

Figure 17.- Effect of aspect ratio on some static longitudinal aerodynamic characteristics for sharp-edged rectangular wings at $M = 0.2$.



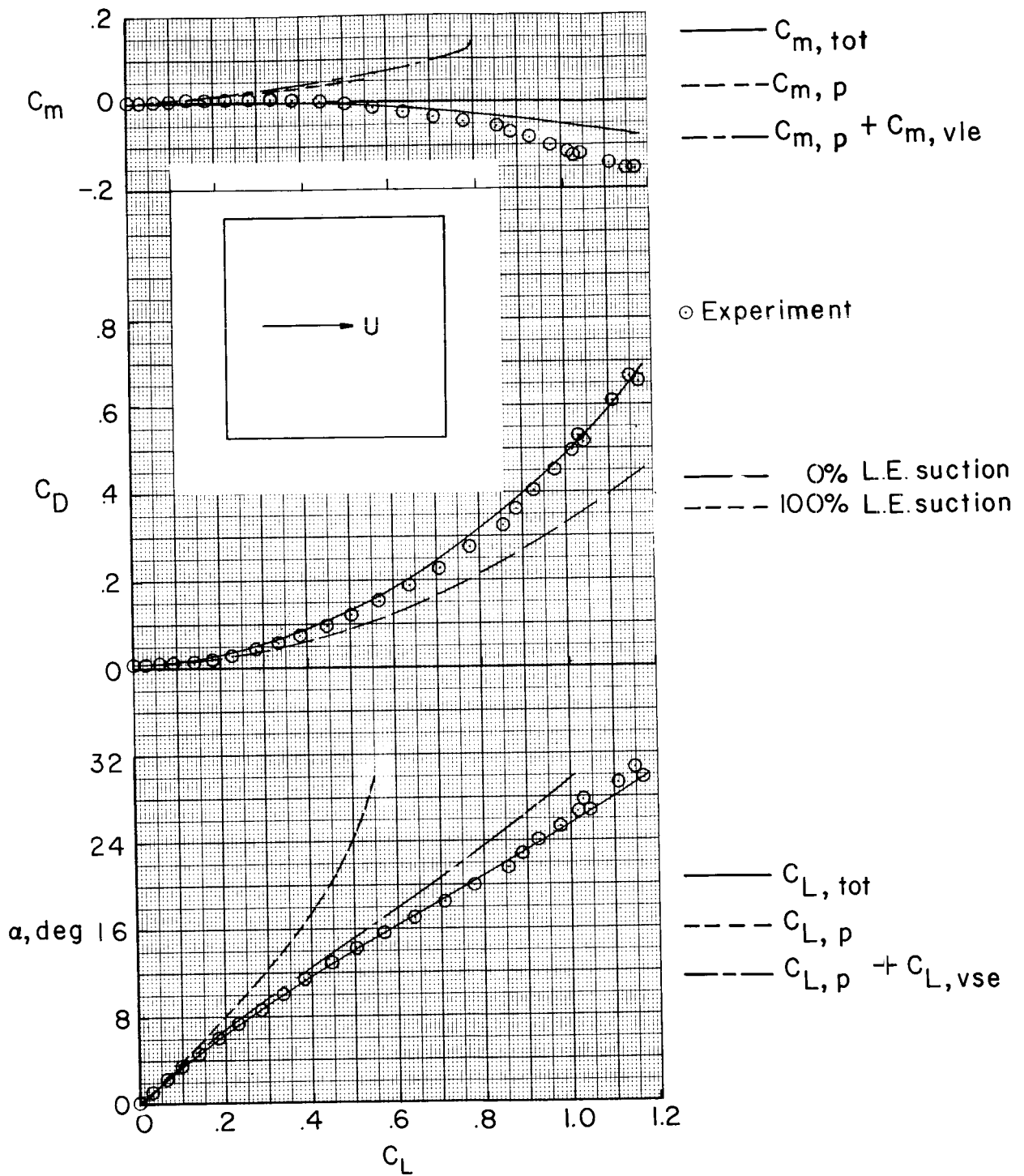
(b) $AR = 0.3$.

Figure 17.- Continued.



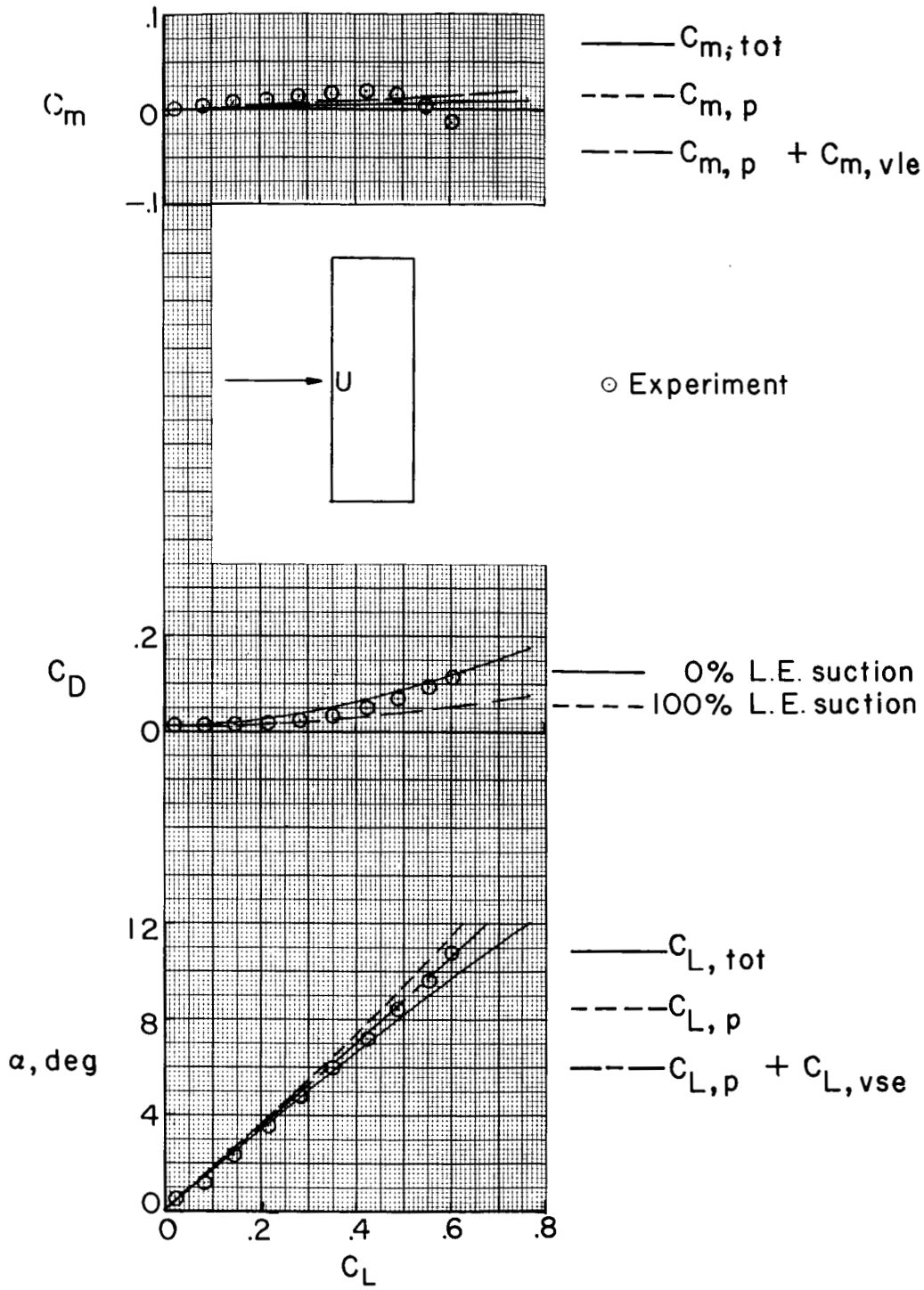
(c) $AR = 0.4$.

Figure 17.- Continued.



(d) $AR = 1.0$.

Figure 17.- Continued.



(e) $Re = 3.0$.

Figure 17.- Concluded.

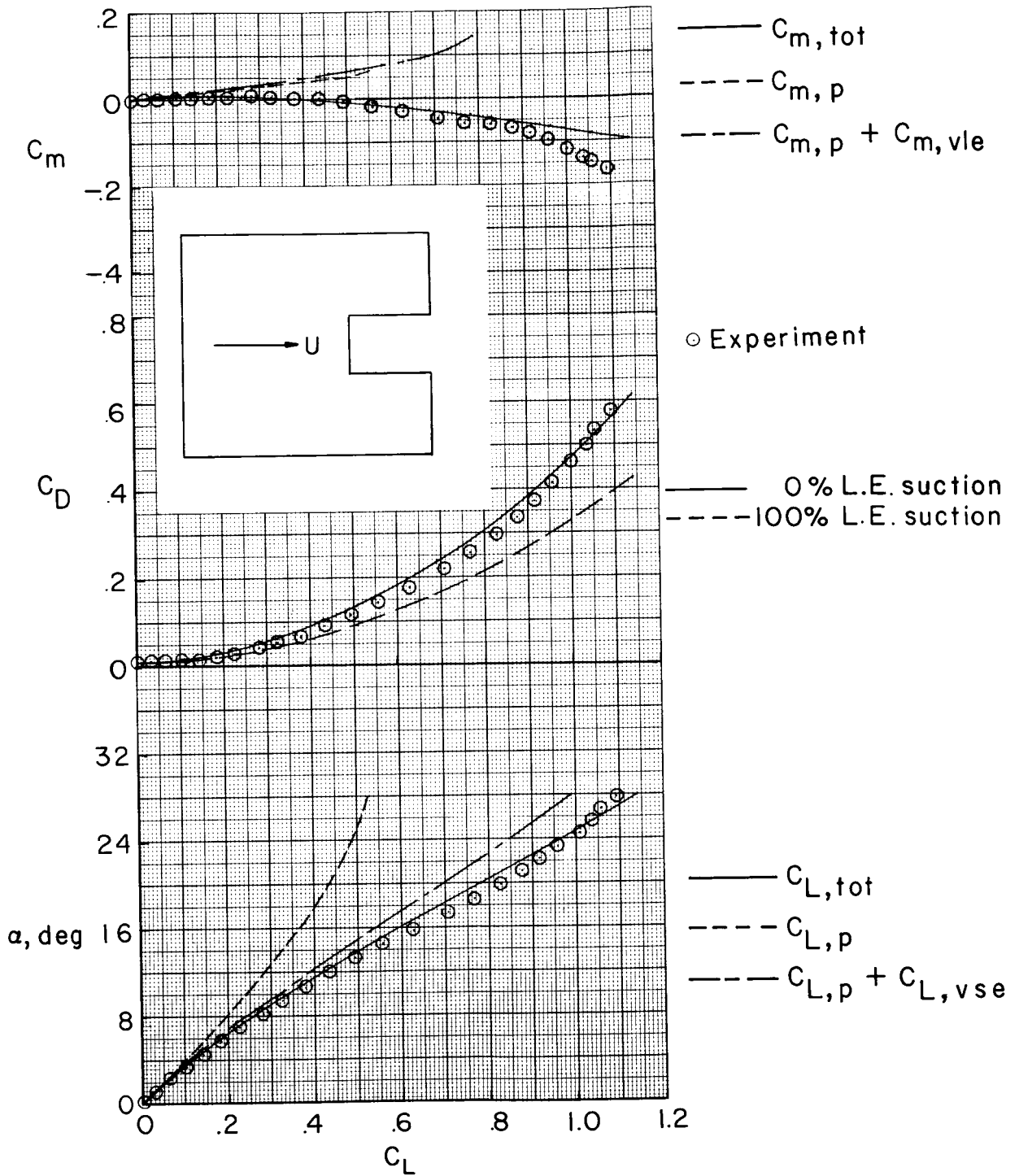
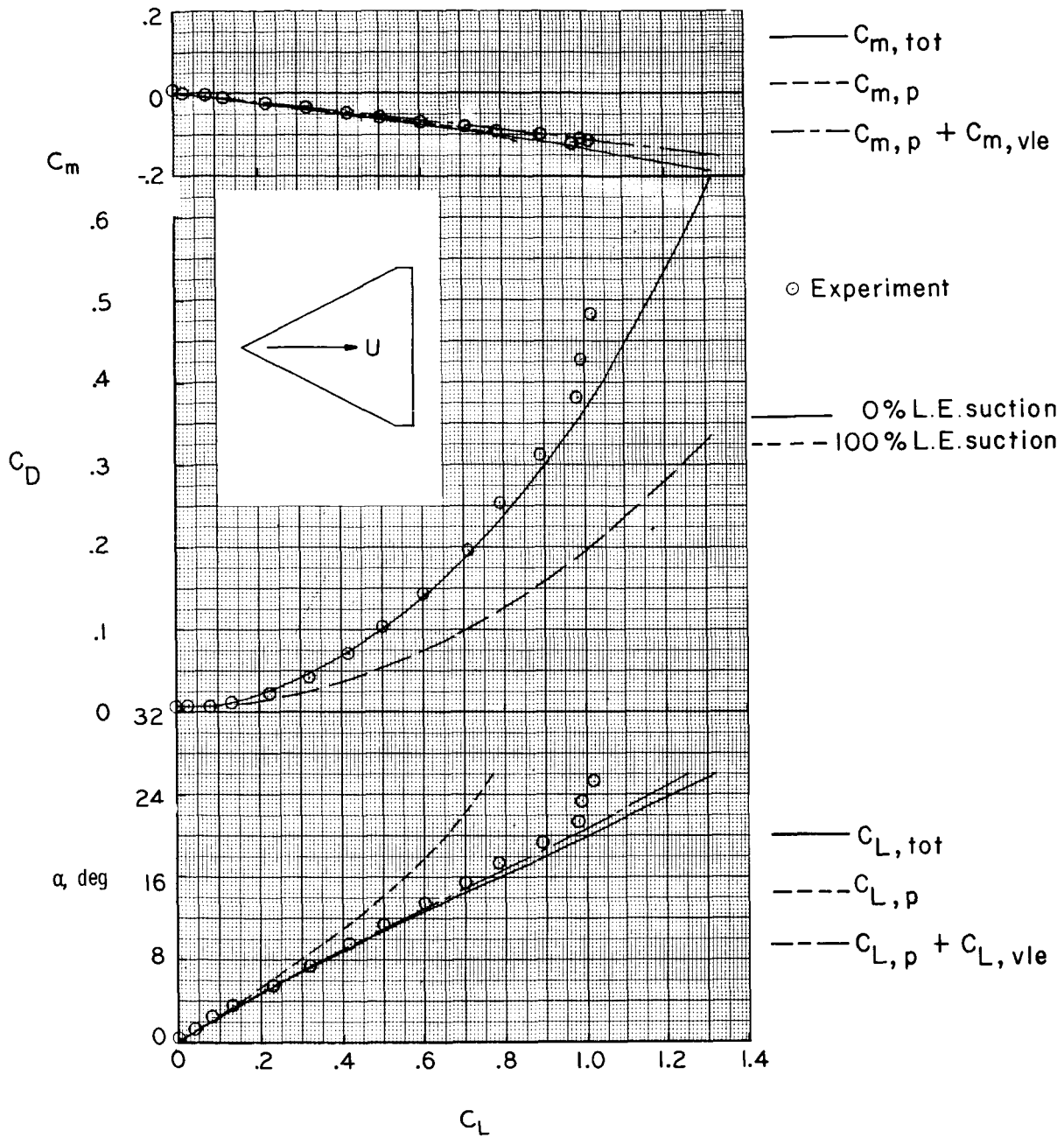
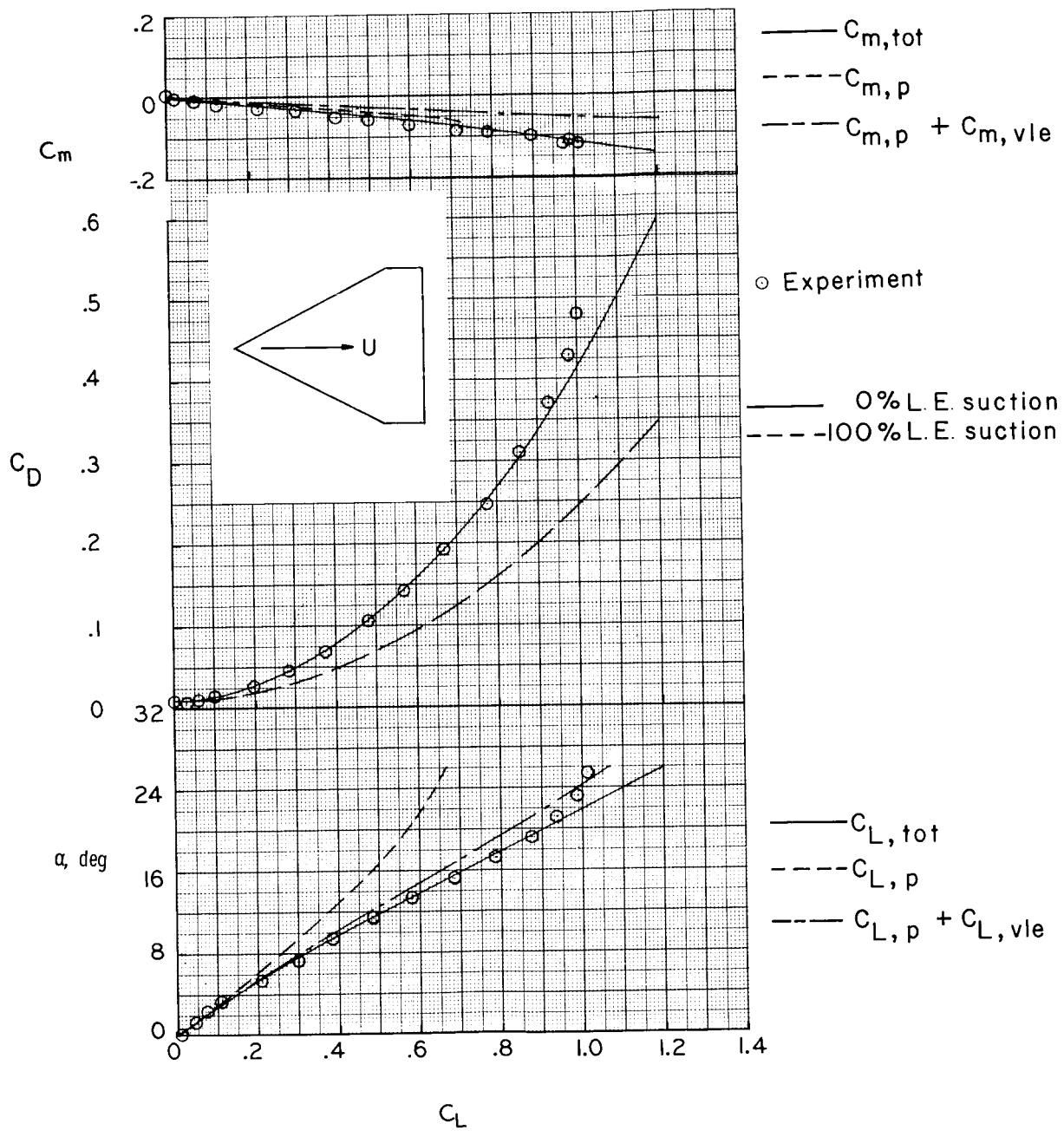


Figure 18.- Some static longitudinal aerodynamic characteristics of a sharp-edged notched rectangular wing. $AR = 1.0$; $M = 0.2$; $\lambda = 1.435$.



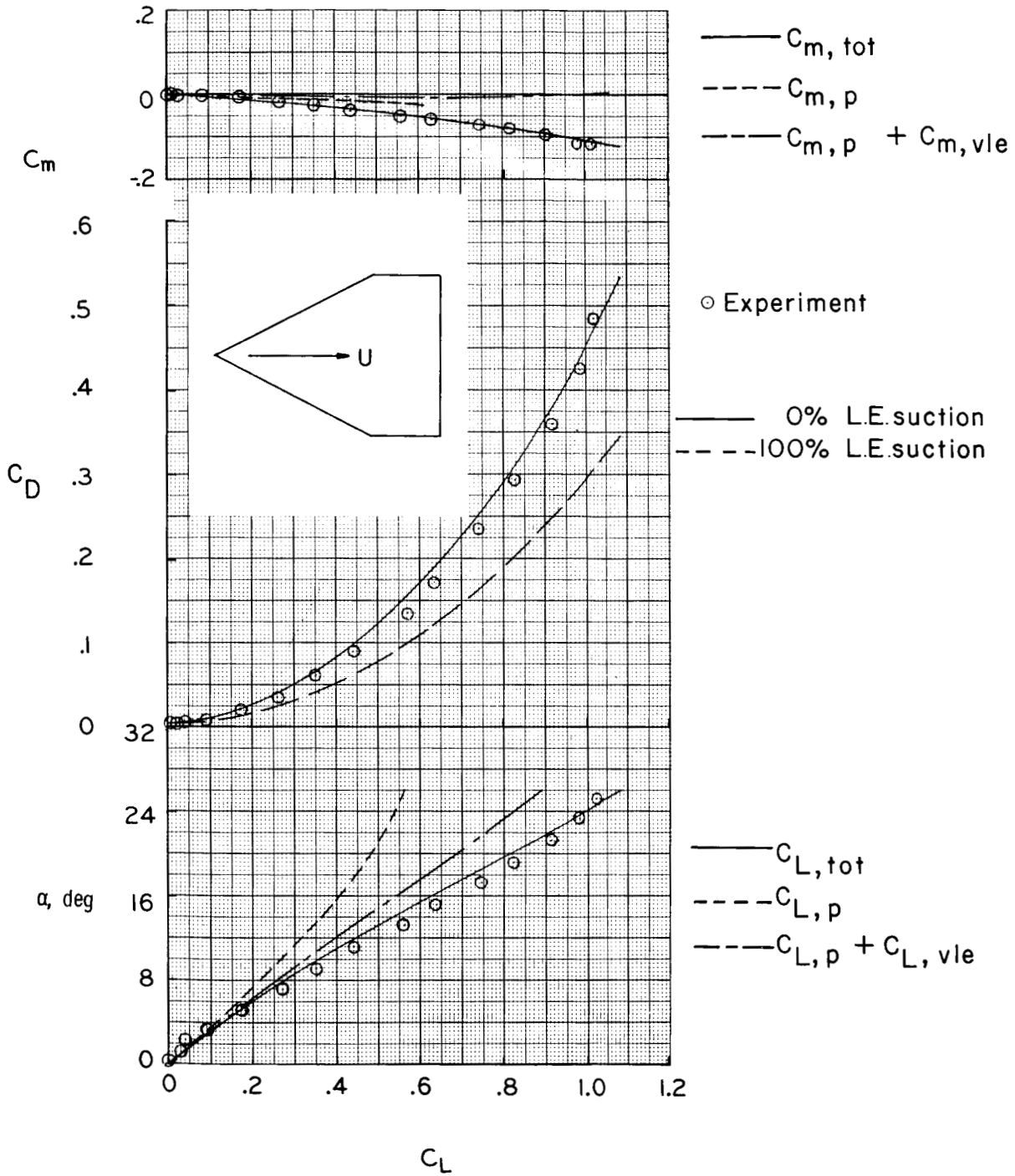
(a) $\lambda = 0.10$.

Figure 19.- Effect of taper ratio on some static longitudinal aerodynamic characteristics for cropped delta wings with $\Lambda = 63^\circ$ and NACA 63A002 airfoils at $M = 0.6$. Experiment obtained from reference 18.



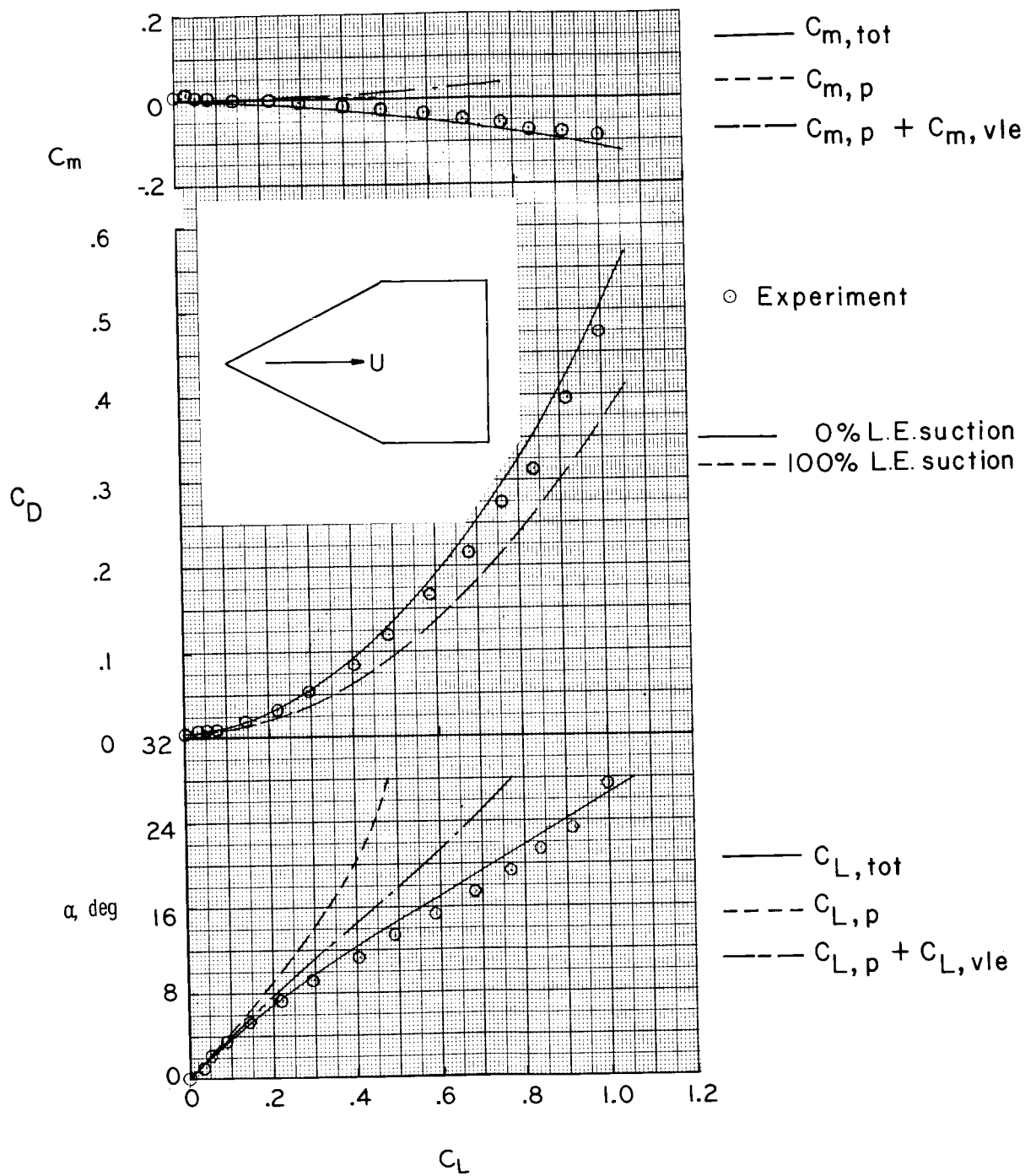
(b) $\lambda = 0.20$.

Figure 19.- Continued.



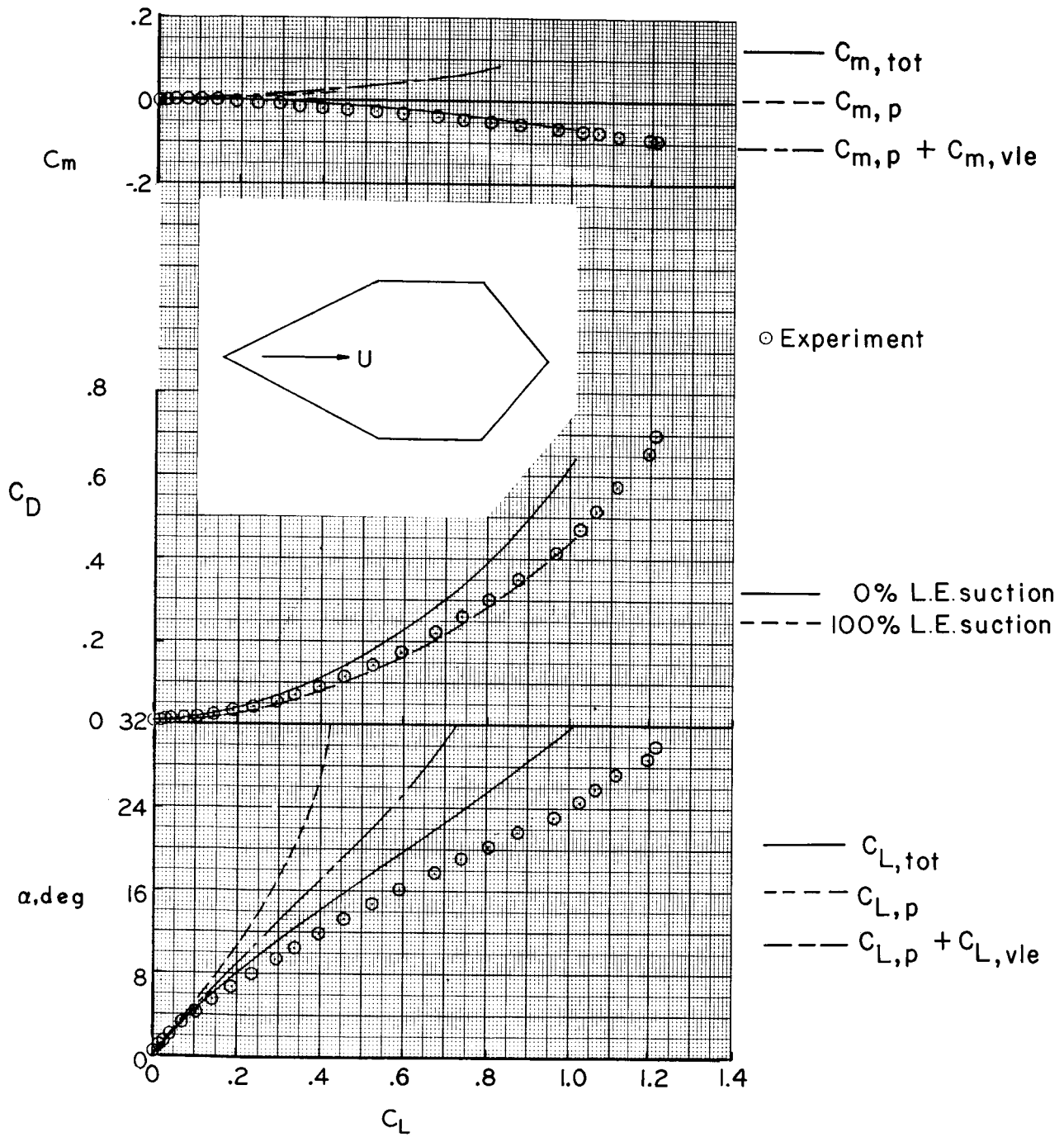
(c) $\lambda = 0.30$.

Figure 19.- Continued.



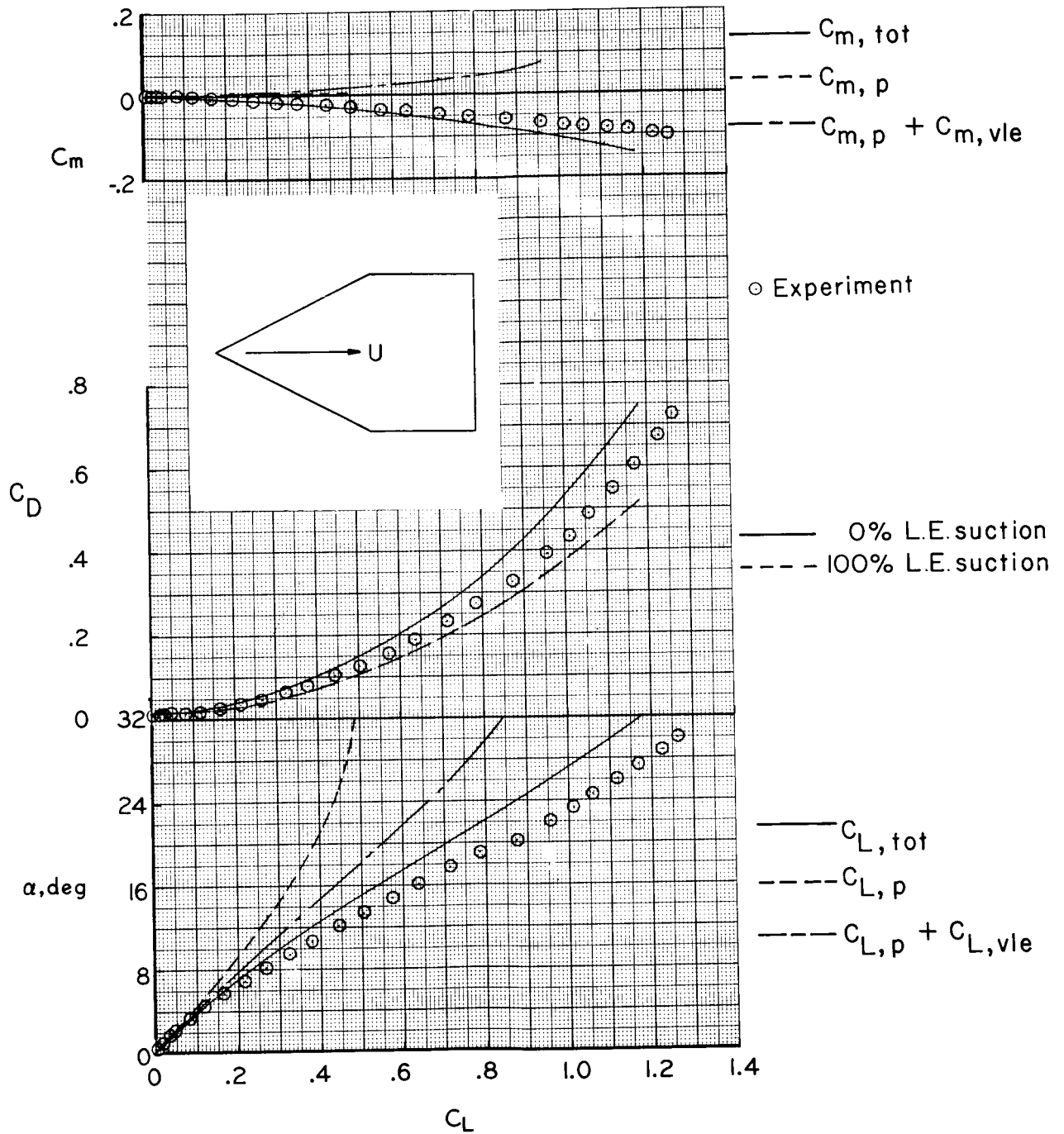
C_L
 (d) $\lambda = 0.40$.

Figure 19.- Concluded.



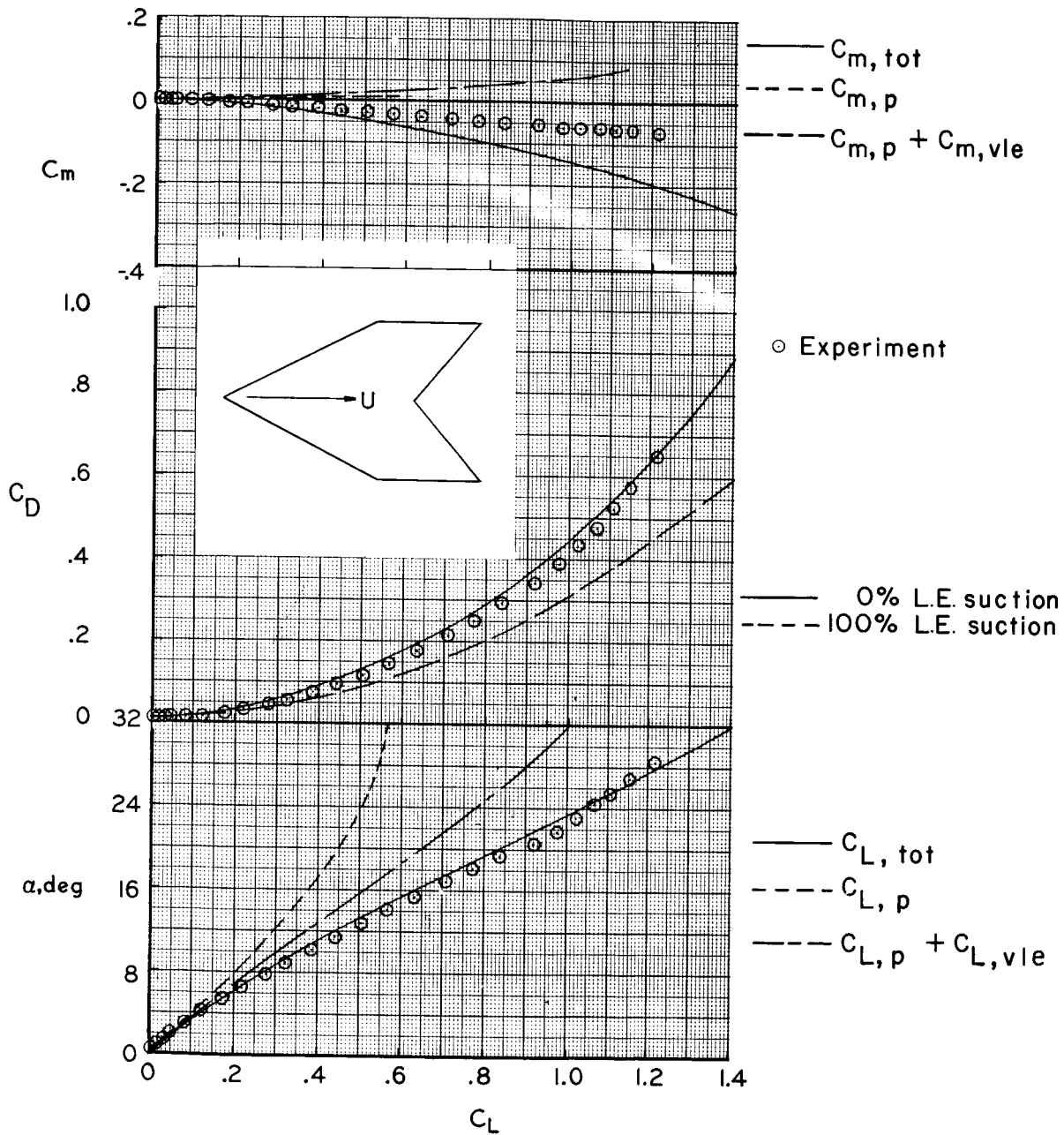
(a) $\Omega = -40^\circ$.

Figure 20.- Effect of trailing-edge sweep on some static longitudinal aerodynamic characteristics for sharp-edged wings with constant tip chord $\lambda_{\Omega=0} = 0.4$, and $\Lambda = 63^\circ$ at $M = 0.2$.



(b) $\Omega = 0^\circ$.

Figure 20. - Continued.



(c) $\Omega = 40^\circ$.

Figure 20.- Concluded.

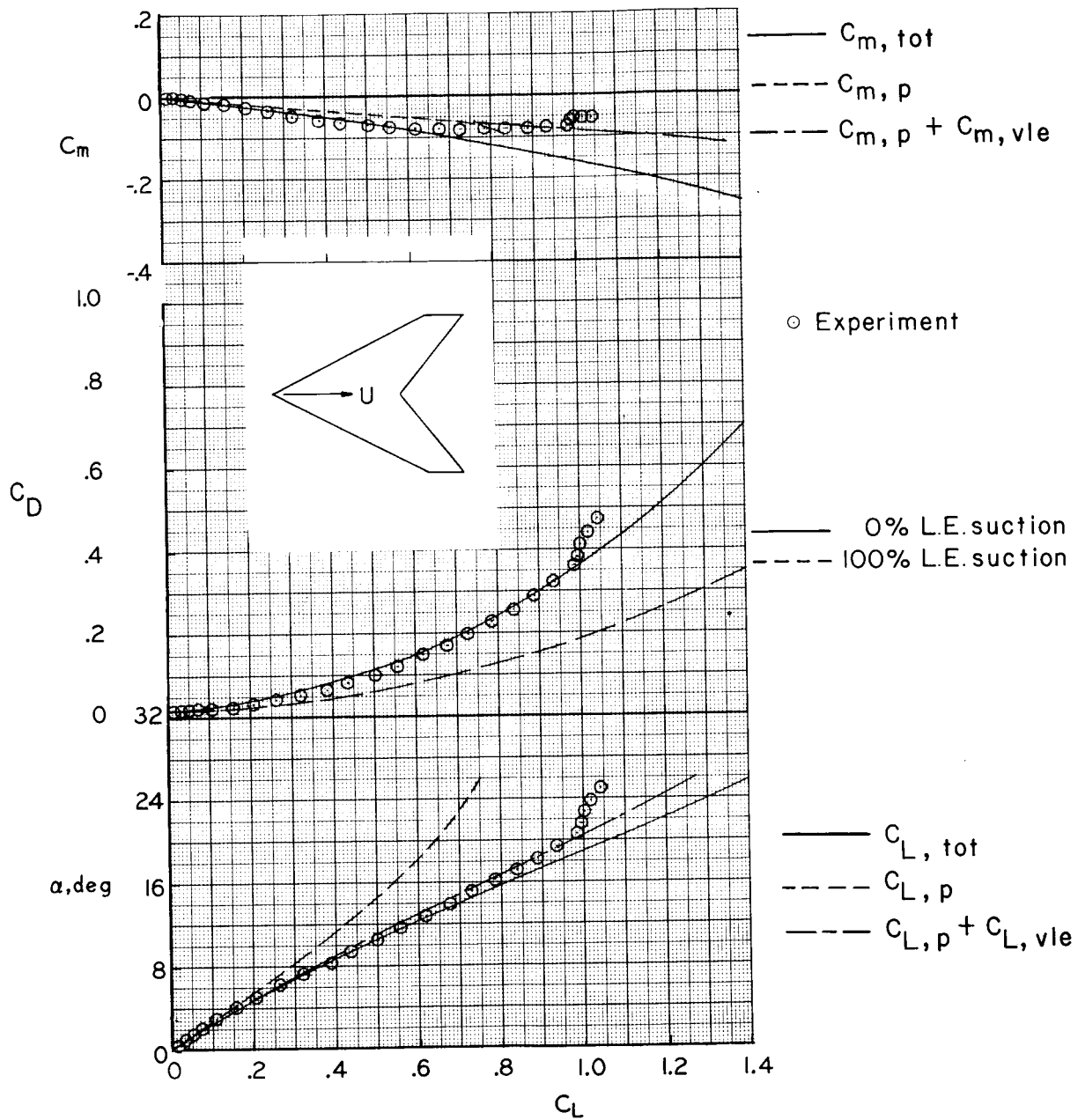


Figure 21.- Some static longitudinal aerodynamic characteristics of a sharp-edged cropped arrow wing having $\lambda_{\Omega=0} = 0.19$, $\Lambda = 63^\circ$, and $\Omega = 38.86^\circ$ at $M = 0.2$.

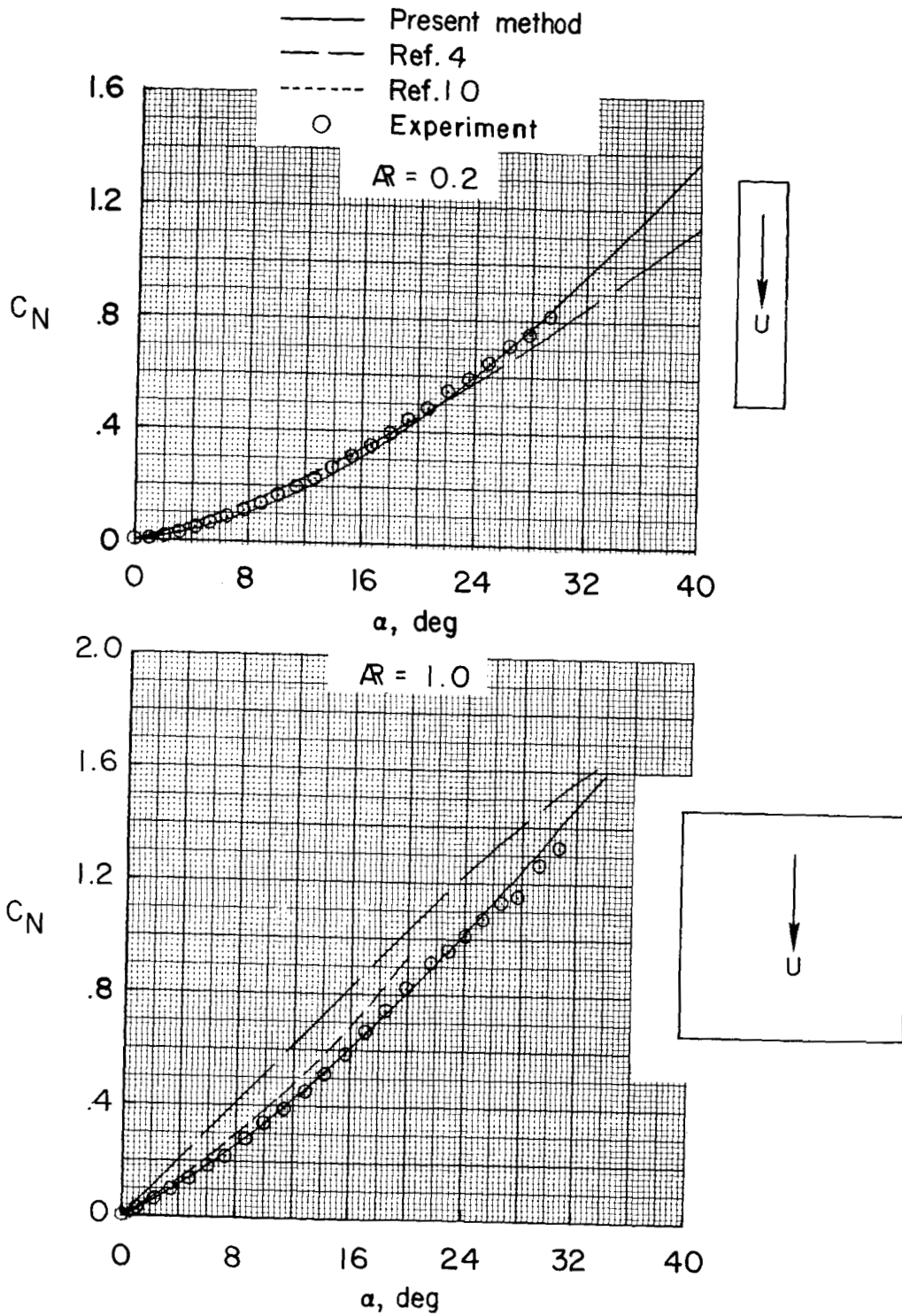


Figure 22.- Effect of aspect ratio on the theoretical and experimental C_N results for two sharp-edged rectangular wings at $M \approx 0$.

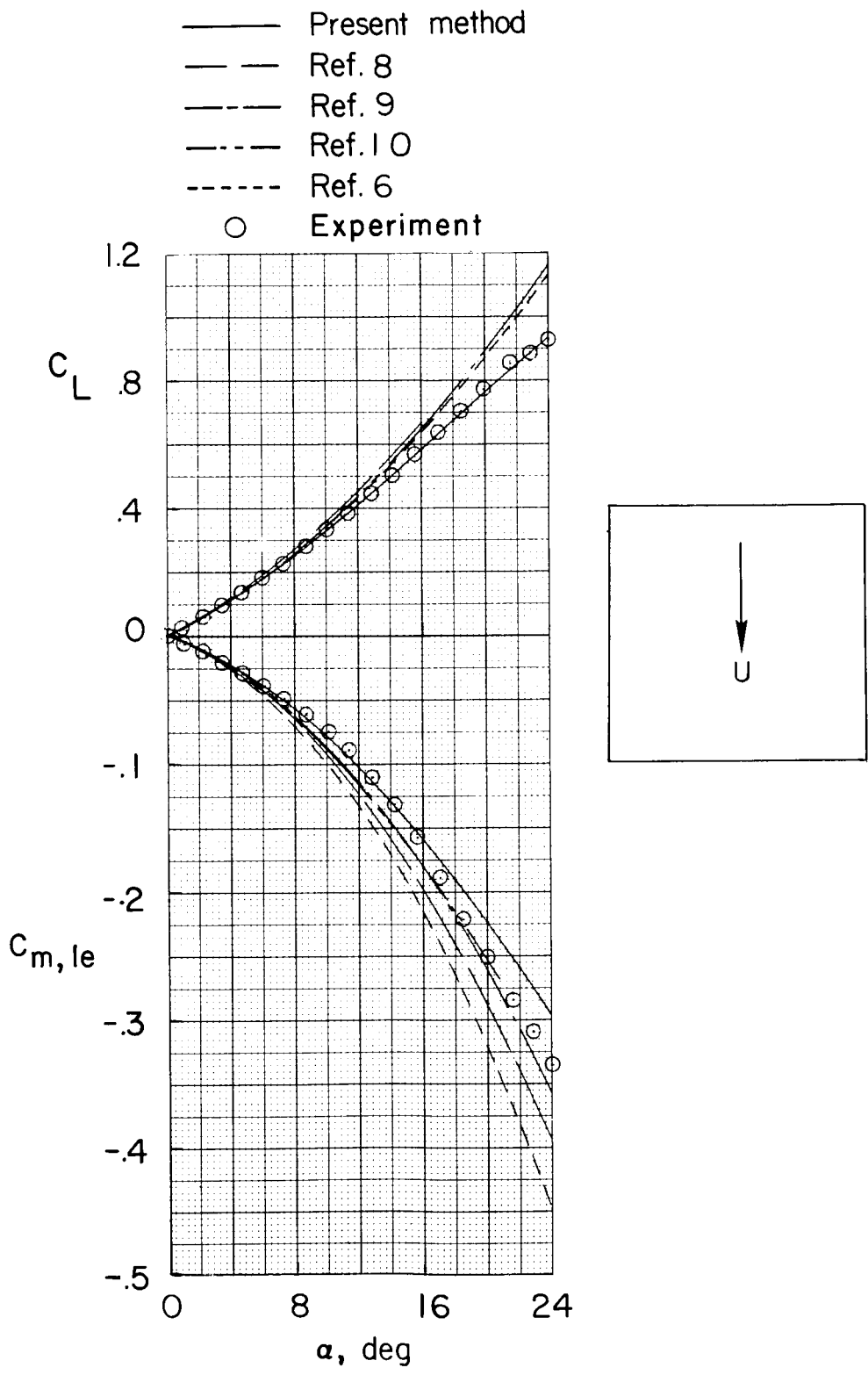


Figure 23.- Theoretical and experimental static longitudinal aerodynamic characteristics for a sharp edged rectangular wing of $AR = 1.0$ at $M \approx 0$.

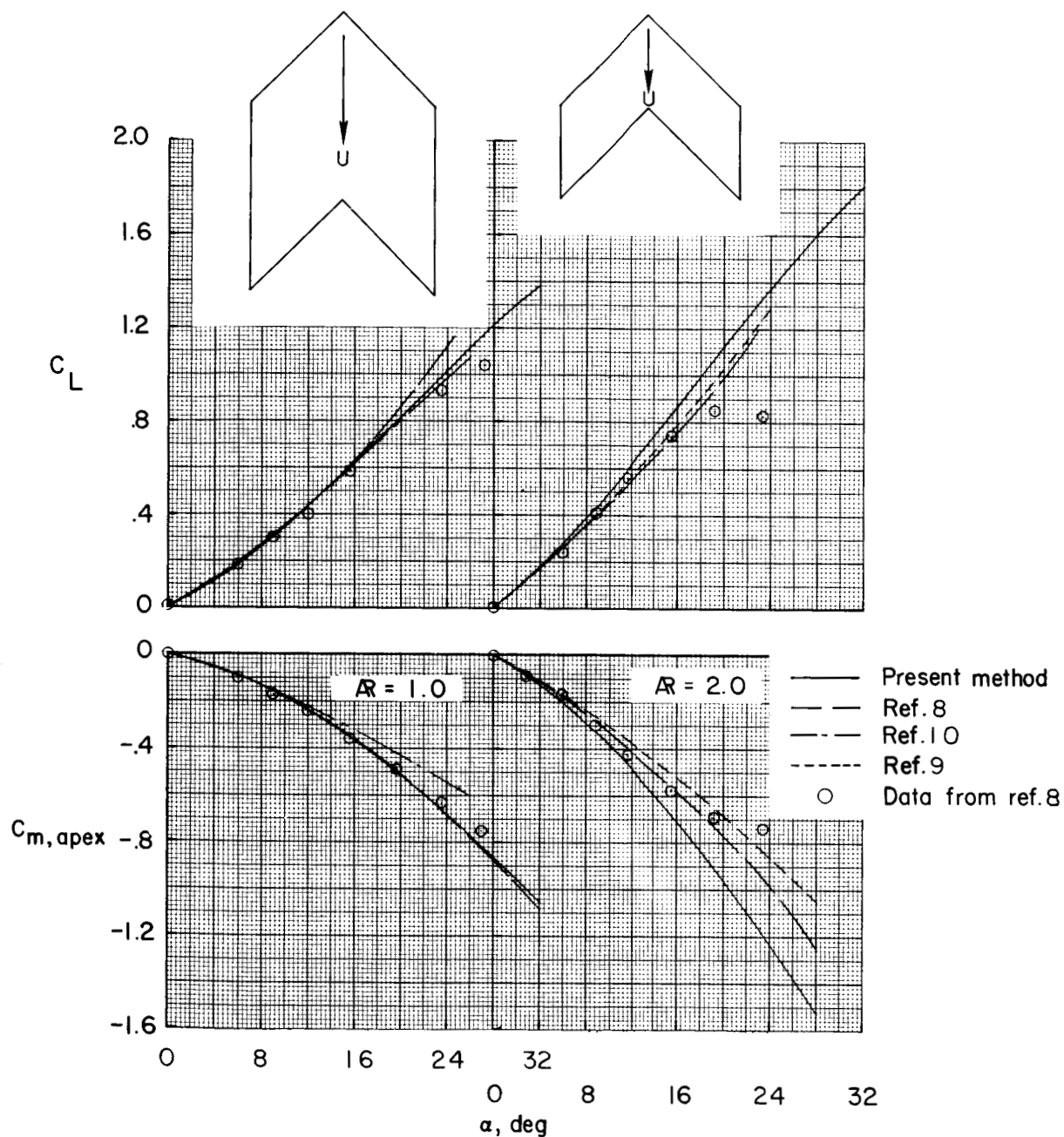


Figure 24.- Effect of aspect ratio on the theoretical and experimental static longitudinal aerodynamic characteristics for two wings. $\Lambda = 45^\circ$; $\lambda = 1.0$; $M \approx 0$.